Solid-State Optical Refrigeration

Markus P. Hehlen[1,*], Mansoor Sheik-Bahae[2], and Richard I. Epstein[2,3]

[1] *Materials Science & Technology Division, Los Alamos National Laboratory, Los Alamos, NM 87545, USA.*

[2] *Department of Physics & Astronomy, University of New Mexico, Albuquerque, NM 87131, USA.*

[3] *ThermoDynamic Films, LLC, Santa Fe, NM 87505, USA.*

For Volume 46 of the *Handbook on the Physics and Chemistry of Rare Earths*

LA-UR-14-20749

* Corresponding author: hehlen@lanl.gov

(505) 665 1737

Contents

1. INTRODUCTION

1.1. Motivation for Cooling Solids with Light

Refrigeration dates back thousands of years in man's quest to store food for extended periods of time. As early as 400 BC, the Persians gathered ice from mountains during winter and stored it in thermally insulated structures (yakhchals), providing refrigeration of foodstuffs during the hot desert summer months (Mahdavinejad and Javanrudi 2012). Ice and snow harvesting was also practiced by the Chinese, Hebrews, Greeks, and Romans. By the 19th century the harvesting, storage, and transportation of ice had been perfected and became a big business. Other historic refrigeration techniques include cooling of water during the night, evaporation of water during the day, and dissolving salts in water. All these early methods were non-cyclic, *i.e.* they required a steady resupply of the refrigerant. The discovery of cyclic refrigeration systems was a major breakthrough. They allowed a working fluid (refrigerant) to absorb and reject heat in a closed system as external work was applied to the refrigerator to drive a thermodynamic cycle. One of the first such systems was a vapor-compression refrigerator described by Oliver Evans in 1805. In 1851, John Gorrie was granted the first US patent on the "improved process for the artificial production of ice" (Gorrie 1851). Today, vapor-compression, vapor-absorption, and gas-cycle refrigerators meet the vast majority of everyday refrigeration needs, and they are critical enablers for a significant portion of the global economy. In the late 19th century, Carl von Linde used the Joule-Thomson effect in a first foray into the cryogenic regime (<123 K) to achieve the liquefaction of air. The ensuing rapid development of cryogenic refrigeration techniques ushered in a new era in physics and condensed matter science that led to many fundamental discoveries such as superconductivity (Heike Kamerlingh Onnes, 1908 (van Delft and Kes 2010)),

superfluidity (independently by Kapista as well as by Allen and Misener, 1937 (Chodos 2006)), and Bose-Einstein condensation (Cornell and Wieman, 1995 (Anderson, Ensher et al. 1995)).

Cryogenic technologies have enabled a wide range of new applications. Detectors based on semiconductors are one important class of devices that benefit from refrigeration. For example, HgCdTe and InSb are used in detectors for long-wave (8-12 μm) and mid-wave (3-5 μm) infrared (IR) light (Rogalski 2011), while high-purity germanium (HPGe) is used for high-resolution gamma-ray spectroscopy (Knoll 2000). In these materials, the incident radiation excites electrons from the valence band to the conduction band and thereby induces an electrical current that can be measured as a signal. However, electrons also can be promoted to the conduction band by random thermal excitations, creating an undesired "dark" current that masks the signal and ultimately limits the performance of the detector. The magnitude of the respective thermal noise is proportional to the square-root of the dark current, *i.e.* $\exp\left(-E_g/2kT\right)$ where T is the temperature in Kelvin, k is the Boltzmann constant, and $E_g = E_c - E_v$ is the band gap energy of the semiconductor defined as the energy difference between the bottom of the conduction band (E_c) and the top of the valence band (E_v). To operate as IR detectors, such materials must have relatively small band gaps (0.15 eV for HgCdTe, 0.23 eV for InSb, and 0.73 eV for Ge) and, as a result, thermal excitation of electrons to the conduction band is a likely process at ambient temperatures (note that $kT = 0.0259$ eV at 300 K). Such detectors therefore have to be cooled to cryogenic temperatures to sufficiently reduce the thermal noise and correspondingly increase the detector sensitivity (Rogalski 2005). Cryogenic refrigeration of semiconductor devices can be particularly challenging in applications that have tight constraints for size, weight, and power, such as in portable, airborne, and space-based detector systems.

Liquid helium has been used as a refrigerant on spacecraft because it has a total enthalpy per mass ratio that is only surpassed by hydrogen, which is usually avoided because of its flammability (Green 2003). Subliming solid cryogens such as methane, ethylene, carbon dioxide, or ammonia can provide cooling to the 60–150 K range. The main drawbacks of such stored cryogen systems however are their complexity, weight, the finite supply of refrigerant, and the associated limited useful lifetime which rarely exceeds one year in space applications (Nast, Barnes et al. 1976). Thermoelectric coolers (TECs) overcome the lifetime constraints of stored cryogens. They are based on the Peltier effect in which a temperature change is achieved when an electrical current flows through a junction of two different materials. However, the lowest temperatures even of advanced multi-stage TECs are limited to ~175 K, which is still well above the desired operating temperature for many semiconductor detectors. This currently leaves mechanical coolers as the only available long-duration cryogenic technology, with the most common types being Stirling, Brayton, Gifford-McMahon, Joule-Thomson, and pulse tube refrigerators. They allow for cooling to <10 K, can have multi-year reliability, and offer multi-Watt cooling power (Zagarola, Breedlove et al. 2009). The main disadvantages arise from the moving parts that are present in all these mechanical devices. They impose inherent reliability limitations and are the source of vibrations that impart microphonic noise to the detector and the associated electronics. These vibrations cause capacitive changes in the electrical connections between the HPGe and the pre-amplifier that degrade the signal resolution in gamma-ray spectrometers (Gilmore and Hemingway 1998). In optical cameras, mechanical vibrations can cause the image to blur and limit the resolution (Veprik, Babitsky et al. 2009). Significant advances in enhancing reliability (Zagarola, Breedlove et al. 2009), reducing vibrations (Veprik, Babitsky et al. 2009), and digital signal filtering (Schultz, Keyser et al. 2007) have been achieved

over the past decades. Nevertheless, microphonic noise remains the major factor limiting the resolution of detectors in many applications. Optical refrigeration can also be used to counteract heat generation in lasers. Bowman *et al* proposed that net heat generation could be eliminated in a solid-state laser by balancing the radiated power from stimulated and spontaneous emission and the absorbed power (Bowman and Mungan 2000, Bowman, Jenking et al. 2002, Bowman, O'Connor et al. 2010). This would reduce thermal gradients that cause strains in the laser material and distortion of optical waves and thus enable higher average output powers than currently possible.

In 1995, Epstein *et al* observed the cooling of a solid by a laser for the first time (Epstein, Buchwald et al. 1995). The effect was based on the principle of anti-Stokes fluorescence and produced a mere 0.3 Kelvin per Watt of laser power temperature drop of the glass sample near room temperature. Since then, the fundamental aspects of this phenomenon have been studied extensively, and both laser-cooling materials and optical cryocooler devices have been developed. In 2010, optical refrigeration into the cryogenic regime using an ytterbium-doped fluoride crystal ($YLiF_4$:Yb^{3+}) (Seletskiy, Melgaard et al. 2010) was first achieved, and a temperature of 114 K was reached starting from 300 K (Melgaard, Seletskiy et al. 2013). The most recent report is on cooling to 93 K of a 10 mol% Yb^{3+}-doped $YLiF_4$ crystal (Melgaard, Seletskiy et al. 2014). Optical refrigeration to liquid nitrogen temperatures (<77 K) appears within reach in the near future as both the materials and the device architecture are being optimized. Anti-Stokes fluorescence cooling is a solid-state, all-optical process and therefore inherently free of mechanical vibrations. This property makes it a highly attractive method for the refrigeration of materials and devices that are susceptible to microphonic noise. In this Chapter we will review the principles of solid-state optical refrigeration (Sect. 2), the associated

experimental techniques (Sect. 3), the relevant material properties (Sect. 4), the materials studied to date (Sect. 5), and the engineering aspects of optical cryocoolers (Sect. 5). We will conclude with an outlook on the remaining challenges and on the application potential of this new cooling technology (Sect. 6).

1.2. Definition of Solid-State Optical Refrigeration

The term “laser cooling” is used for several distinct phenomena. It is therefore worthwhile to define it precisely for the context of the present article. In general, “laser cooling” describes the cooling of a physical system upon interacting with laser light. The role of the laser light is to reduce the amount of energy contained in a particular degree of freedom. In gases at low temperatures (<10 K) for example, the energy is primarily contained in translational degrees of freedom. Such a system can be laser-cooled by the Doppler effect (Hänsch and Schawlow 1975, Cohen-Tannoudji and Phillips 1990). When a laser is tuned to the low-frequency side of an atomic absorption, the atoms in the gas will more strongly absorb when they move towards the light source than when they move away from it. Each time an atom absorbs a photon moving towards it, it loses momentum equal to that of the photon. When the excited atom subsequently relaxes by spontaneous emission, the emitted photon is in a random direction, and, on the average, does not change the atoms momentum. Arranging two counter-propagating laser beams and performing many such absorption-emission cycles reduces the momentum in the direction of the laser propagation axis. Three orthogonal sets of counter-propagating laser beams create an optical molasses that cools the ensemble of atoms in the gas, in the best case, down to the

Doppler cooling limit. Chu, Cohen-Tannoudji, and Philips were awarded the 1997 Nobel Prize in Physics for developing the methods to cool and trap atoms with laser light.

While Doppler cooling and related techniques can cool and trap small numbers of atoms in dilute gases to low temperatures, they are not suited to cool the bulk quantities of material that are needed for the refrigeration of macroscopic objects. To do so, one has to turn to the vibrational degrees of freedom. Translational motion is largely absent in solids, and their thermal energy is primarily contained in vibrations, *i.e.* the oscillations of atoms about fixed equilibrium positions. The elastic excitations of vibrations in a solid are referred to as phonons which are further classified as acoustic phonons and, in crystals consisting of more than one type of atom, optical phonons. Acoustic phonons are wave-like collective motions of atoms along the same direction (*e.g.* sound waves), while optical phonons encompass localized motions of different atoms in opposing directions. The opposing motion of cations and anions associated with optical phonon modes can induce electric dipoles that can then interact with the electric component of the incident electro-magnetic wave, hence the name “optical” phonon. The resulting electron-phonon coupling allows laser light to interact with the vibrational degrees of freedom in a solid (Kim and Kaviany 2009), making laser-cooling of solids possible in certain cases as we shall see in the following. In the present context, the term “laser cooling” shall describe the laser-induced reduction of energy contained in the *vibrational* degrees of freedom of a solid.

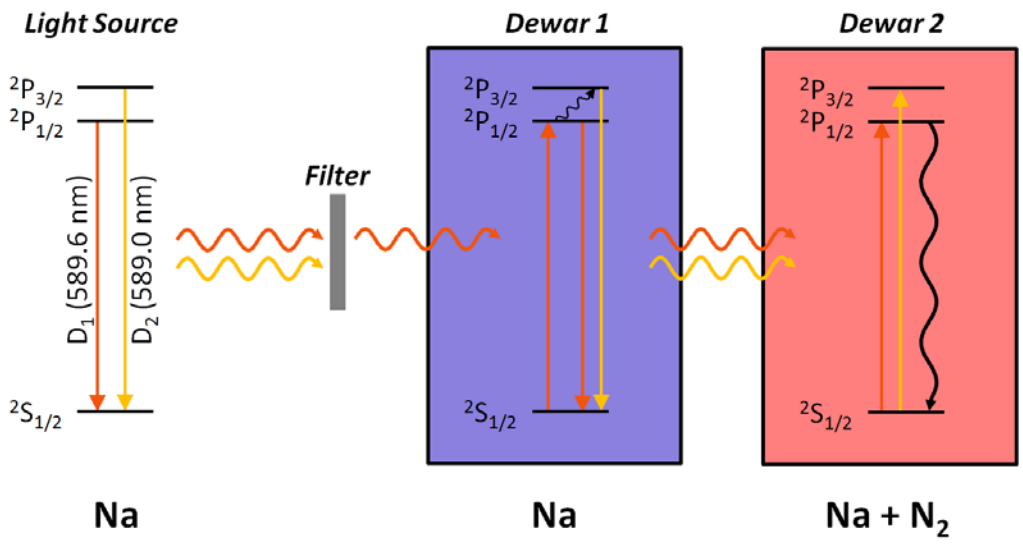

Figure 1: Gedankenexperiment described by Pringsheim in 1929 (Pringsheim 1929). A filtered sodium vapor lamp is used as a spectrally narrow light source to excite the $^2S_{1/2} \rightarrow {}^2P_{1/2}$ electronic transition of sodium atoms in Dewar 1. Inelastic collisions in the gas promote some sodium atoms from the $^2P_{1/2}$ to the $^2P_{3/2}$ excited state (wiggly arrow), causing both resonant ($^2P_{1/2} \rightarrow {}^2S_{1/2}$) and anti-Stokes ($^2P_{3/2} \rightarrow {}^2S_{1/2}$) fluorescence. Dewar 1 cools as a result of the transfer of translational energy of the gas to electromagnetic energy. The fluorescence emitted by Dewar 1 is absorbed by sodium vapor in Dewar 2, in which nitrogen has been added to quench the ^2P fluorescence. Dewar 2 heats up as a result of the transfer of electromagnetic to translational energy of the gas.

1.3. History of Optical Refrigeration

For the vast majority of luminescent materials, the emission spectrum is shifted to *lower* energy with respect to the absorption spectrum of the corresponding electronic transition. The associated energy difference is referred to as the Stokes shift, named after the Irish physicist Sir George G.

Stokes (1819–1903). This energy difference between the excitation source and the fluorescence is converted into vibrational and/or translational energy within the medium, causing the well-known heating of solids and gases upon excitation with light. In the 1920s it was observed, however, that some phosphors doped with transition metals emitted light of *higher* energy than the excitation source, an effect that was termed "anti-Stokes fluorescence". Lenard, Schmidt, and Tomascheck proposed in 1928 that anti-Stokes fluorescence had to be accompanied by emission of longer-wavelength light such as not to produce a quantum efficiency greater than unity and not to violate the second law of thermodynamics (Lenard, Schmidt et al. 1928). This argument was challenged by Peter Pringsheim in 1929, who was working at the Physical Institute of the University of Berlin at the time (Pringsheim 1929). He described a Gedankenexperiment in which he used a filtered sodium vapor lamp as a spectrally narrow light source to excite sodium vapor in Dewar 1 to the $^2P_{1/2}$ electronic excited state (see Figure 1). Inelastic collisions in the gas cause some excited Na atoms to be further excited to the $^2P_{3/2}$ excited state, which is only 17.3 cm^{-1} ($0.08kT$ at 300 K) above $^2P_{1/2}$. Both excited states then relax radiatively to the ground state by resonant ($^2P_{1/2}\rightarrow{}^2S_{1/2}$) and anti-Stokes ($^2P_{3/2}\rightarrow{}^2S_{1/2}$) fluorescence. As a result, the Na gas in Dewar 1 cools because its mean emission wavelength is slightly shorter than the excitation wavelength, with the energy difference corresponding to the energy that has been transferred from the translational degrees of freedom to electromagnetic radiation. The emission from Dewar 1 is then absorbed by sodium gas in Dewar 2, in which the ^2P emission has been completely quenched by the addition of nitrogen. As a result, Dewar 2 heats up because of the transfer of electromagnetic energy to the translational degrees of freedom of the gas. Pringsheim pointed out that, while Dewar 1 by itself may violate the second law of thermodynamics, the system as a whole did not. His argument was the first to postulate that one part of a physical

system could be cooled by light. However it was not fully accepted until 1946, when Landau presented a consistent description that included the entropy of the radiation field based on Bose-statistics applied to a "photon gas" (Landau 1946, Ruan, Rand et al. 2007). He showed that the entropy of the radiation field is a function of both the solid angle of the propagating light and the frequency bandwidth of the light. Hence, a laser with high directionality and narrow spectral bandwidth represents a low-entropy radiation field. In contrast, luminescence isotropically emitted by a sample and comprising a range of emission frequencies represents a higher-entropy radiation field. The process of optical refrigeration therefore converts low-entropy laser light into higher-entropy anti-Stokes fluorescence, in agreement with the second law of thermodynamics.

It was realized early that a high quantum efficiency was a prerequisite for realizing cooling of a system by laser light. For example, the Dewar 1 in Figure 1 can only achieve net cooling if the two excited states $^2P_{1/2}$ and $^2P_{3/2}$ predominantly decay by radiative relaxation (resonant and anti-Stokes fluorescence) rather than by non-radiative decay (like in Dewar 2). Non-radiative relaxation transfers the entire excitation energy into the translational/vibrational degrees of the freedom and thus causes significant heating. This is particularly detrimental because the energy of the excited state is typically much larger than the energy gained by anti-Stokes fluorescence (on the order of kT). In 1981, Djeu *et al* achieved the first net cooling by anti-Stokes luminescence in CO_2 gas at 250–300 ^oC (Djeu and Whitney 1981). They pumped the (100)$\rightarrow$(001) excited-state absorption with a CO_2 laser at 10.6 μm to produce anti-Stokes luminescence from the (001)$\rightarrow$(000) transition at 4.3 μm. Net laser-induced cooling or heating was observed as negative or positive changes in the total gas pressure. The inferred temperature drop was ~1 K.

Kastler pointed out in 1950 that lanthanide ions doped into transparent solids could be effective fluorescent coolers because they possess excited states with high quantum efficiencies (Kastler 1950). A first experimental attempt to achieve laser cooling of a solid was undertaken by Kushida and Geusic of Bell Telephone Laboratories in 1968 (Kushida and Geusic 1968). They used the 1064 nm light of a Nd^{3+}-doped $Y_3Al_5O_{12}$ (YAG:Nd) laser to excite another Nd^{3+}-doped YAG crystal that was placed inside the laser cavity. Laser excitation of Nd^{3+} at 1064 nm produced some anti-Stokes luminescence at 946 nm. As shown in Figure 2, they measured the sample temperature as a function of laser power first for an *undoped* YAG reference crystal. They observed a linear increase in temperature with increasing laser power even though the undoped YAG crystal should have had no absorption at 1064 nm. They concluded that their crystals contained impurities (suspected to be mostly Dy^{3+}) that were excited by the 1064 nm laser and that decayed non-radiatively, causing internal heating. In comparison however, the Nd^{3+}-doped YAG crystal exhibited *less* heating than the undoped crystal, which provided direct evidence for the presence of additional laser-induced cooling by anti-Stokes luminescence from Nd^{3+}. The difference of the two experiments (dashed line in Figure 2) indicates a laser-induced cooling effect of up to ~0.7 K at a pump power of 200 W. While no net cooling of the bulk crystal was achieved in this experiment, this early work correctly recognized and explicitly stressed the importance of high sample purity for achieving a net refrigeration effect.

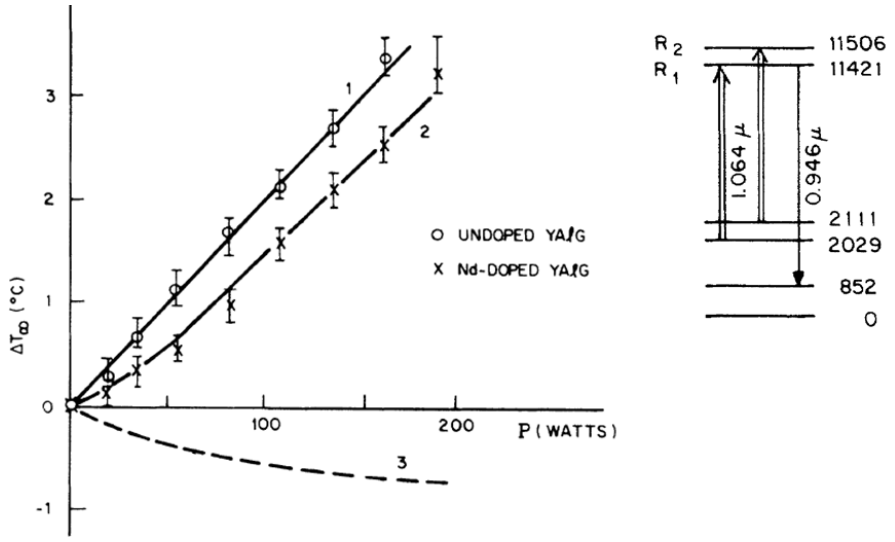

Figure 2: Observation of laser-induced cooling in a Nd^{3+}-doped $Y_3Al_5O_{12}$ (YAG) crystal (Kushida and Geusic 1968). The sample was excited by a YAG:Nd laser at 1064 nm and produced anti-Stokes luminescence at 946 nm. A YAG crystal doped with Nd^{3+} (crosses) showed less heating than an undoped YAG crystal (open circles). While no net cooling of the bulk was achieved, the difference of the two measurements (dashed line) provided first experimental evidence for the presence of laser cooling in a solid. *Reprinted (Figs. 2 and 3) with permission from T. Kushida and J.E. Geusic, Phys. Rev. Lett., Vol. 21, pp. 1172-1175, 1968. Copyright (2014) by the American Physical Society.*

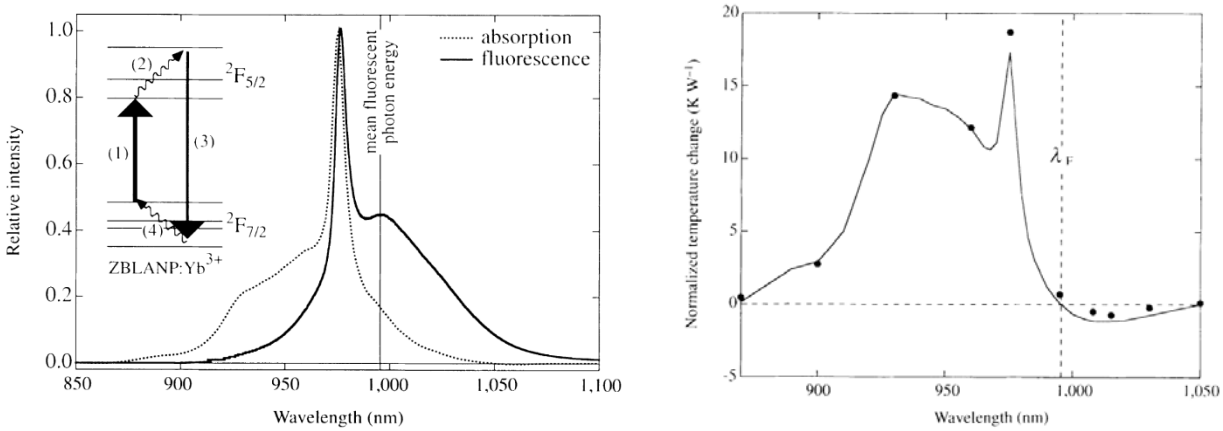

Figure 3: *Left:* Absorption (dotted line) and fluorescence (solid line) spectrum of the $^2F_{7/2} \leftrightarrow {}^2F_{5/2}$ transition (inset) of Yb^{3+} in the fluoride glass ZBLANP at room temperature. The vertical line indicates the mean fluorescence wavelength ($\tilde{\lambda}_F$) at ~995 nm. *Right:* Temperature change (normalized to laser power) of ZBLANP:Yb^{3+} at different pump laser wavelengths. Net bulk cooling of up to 0.3 K/W was observed when the pump wavelength exceeded $\tilde{\lambda}_F$. *Reprinted by permission from Macmillan Publishers Ltd: Nature, R. I. Epstein et al, Vol. 377, pp. 500–503, Copyright 1995.*

The year 1995 marked a milestone in solid-state optical refrigeration when Epstein *et al* at Los Alamos National Laboratory (LANL) were able to observe net laser cooling of a bulk Yb^{3+}-doped fluoride glass for the first time (Epstein, Buchwald et al. 1995). At that time, fluoride glasses such as ZBLANP (an acronym for the glass composition ZrF_4–BaF_2–LaF_3–AlF_3–NaF–PbF_2) were being developed for use in long-haul fiber-optic telecommunications. Fluoride glasses have low optical attenuation in the near-infrared spectral region and thus offered the possibility of repeater-less transoceanic fiber-optic telecom links. Low-loss fluoride fiber

preforms of high purity were produced commercially for subsequent drawing into optical fibers. The sample used by Epstein *et al* was a fiber preform of ZBLANP doped with 1 wt% Yb^{3+}. It was cut to $2.5 \times 2.5 \times 6.9$ mm^3 size and prepared with optical-quality surfaces. They used two identical samples placed next to each other. One of the samples was excited in the 870–1050 nm wavelength range of the $^2F_{7/2} \rightarrow {}^2F_{5/2}$ absorption of Yb^{3+} using a tunable titanium-sapphire laser. The temperature difference between the pumped and un-pumped samples was measured using a calibrated InSb thermal camera that detected thermal emission in the 3–5 μm range. As shown in Figure 3, the pumped ZBLANP:Yb^{3+} glass showed net bulk cooling of up to 0.3 K/W when the laser wavelength was greater than the mean fluorescence wavelength ($\tilde{\lambda}_F$), *i.e.* when the regime of net anti-Stokes fluorescence was realized.

The Epstein team at LANL focused their early efforts on Yb^{3+}-doped ZBLANP glass, and they developed the various experimental techniques along with higher-power lasers and pumping geometries. By 1999, LANL researchers had cooled a fiber sample of ZBLANP:Yb by 65 K to 236 K (Gosnell 1999), fueling the promise of optical refrigeration of solids to cryogenic temperatures (see Figure 4). The potential for higher cooling efficiencies in Tm^{3+} compared to Yb^{3+} set the theme for the 2000–2005 time period during which Tm^{3+}-doped ZBLANP glass and BaY_2F_8 crystals were studied. By 2003, ZBLANP:Tm^{3+} had been cooled by 19 K to 281 K (Hoyt, Hasselbeck et al. 2003). While a higher intrinsic cooling efficiency in Tm^{3+} was experimentally confirmed, the net cooling did not surpass earlier results achieved with Yb^{3+} primarily because the experimenters did not have high-power laser sources near the 2 μm pump wavelength. Research on Yb^{3+}-doped glasses continued in parallel and culminated in cooling of a ZBLANP:Yb^{3+} glass to 208 K in 2005 (Thiede, Distel et al. 2005). This result remains the lowest temperature achieved to date using a glass host. By this time, the preparation of sample surfaces

and the design of the cooling chamber had been optimized, and high-power lasers (up to 11 W) at the optimum pump wavelength of 1026 nm for ZBLANP:Yb^{3+} had been developed. It was believed that the cooling performance was primarily limited by impurities in the ZBLANP glass. Impurities such as transition-metal ions can absorb laser light and, rather than emitting anti-Stokes fluorescence and contributing to cooling, they decay non-radiatively and cause parasitic heating within the sample. Various efforts were undertaken to reduce transition-metal impurities in fluoride glasses, including electrochemical purification of the ZBLANP melt (Bao, Newman et al. 1995, Fajardo, Sigel Jr et al. 1997) and chelate-assisted solvent-extraction purification of precursor materials (Patterson, Stark et al. 2011). However, they did not provide a significant improvement of the net cooling performance, and the cryogenic regime remained elusive.

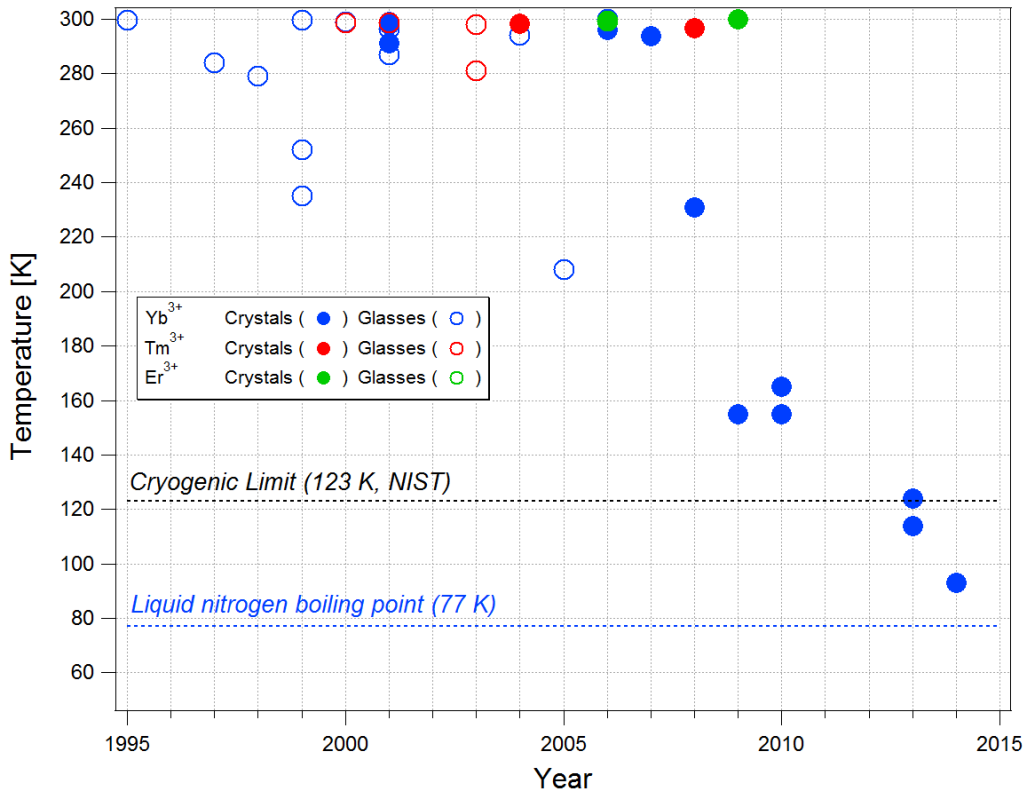

Figure 4: History of solid-state optical refrigeration. The experimental results shown here are taken from studies that observed *net* laser-induced bulk cooling in glasses (open circles) or crystals (solid circles) doped with lanthanide ions. To date, net laser cooling has been achieved in solids doped with Yb^{3+} (blue), Tm^{3+} (red), and Er^{3+} (green). Also indicated is the cryogenic limit of 123 K as defined by the National Institute of Standards and Technology (NIST, black dashed line) and the boiling point of liquid nitrogen at 77 K (blue dashed line).

A profound change in focus began in 2005 when Bigotta *et al* observed laser cooling in a BaY_2F_8 fluoride crystal doped with 2.5% Yb^{3+} and measured a 4 K temperature drop upon exciting the crystal with 3 W at 1025 nm in a single-pass configuration (Bigotta, Parisi et al. 2006). While Yb^{3+}-doped YAG and Y_2SiO_5 crystals (Epstein, Brown et al. 2001) as well as a

Tm^{3+}-doped BaY_2F_8 crystal (Patterson, Hasselbeck et al. 2004) had been studied before with similar results, Yb^{3+}-doped fluoride crystals would prove to open the way for laser cooling to the cryogenic regime. Bigotta *et al* presented a subsequent study of Yb^{3+}-doped BaY_2F_8 and $YLiF_4$ (YLF) crystals that slightly improved on their earlier cooling results and provided detailed spectroscopic information (Bigotta, Di Lieto et al. 2007). Their results were soon followed by a series of record-breaking laser cooling results obtained by Sheik-Bahae's group at the University of New Mexico using Yb^{3+}-doped YLF crystals (Seletskiy, Hasselbeck et al. 2008, Seletskiy, Melgaard et al. 2009, Seletskiy, Melgaard et al. 2010, Seletskiy, Melgaard et al. 2010, Melgaard, Seletskiy et al. 2013, Melgaard, Seletskiy et al. 2013). In 2013, Melgaard *et al* placed a 10 mol% Yb^{3+}-doped YLF crystal in a multi-pass cavity contained in a tightly-fitting low-thermal-emissivity cavity and pumped the crystal with 45 W at 1020 nm. They achieved laser cooling to 114 K (see Figure 5) (Melgaard, Seletskiy et al. 2013), surpassing the performance of all earlier studies with glassy samples and advancing the field into the cryogenic regime (<123 K). The latest report by this group has shown cooling of YLF:10%Yb^{3+} to 93 K starting from 271 K, advancing the field into the sub-100 K range for the first time (Melgaard, Seletskiy et al. 2014).

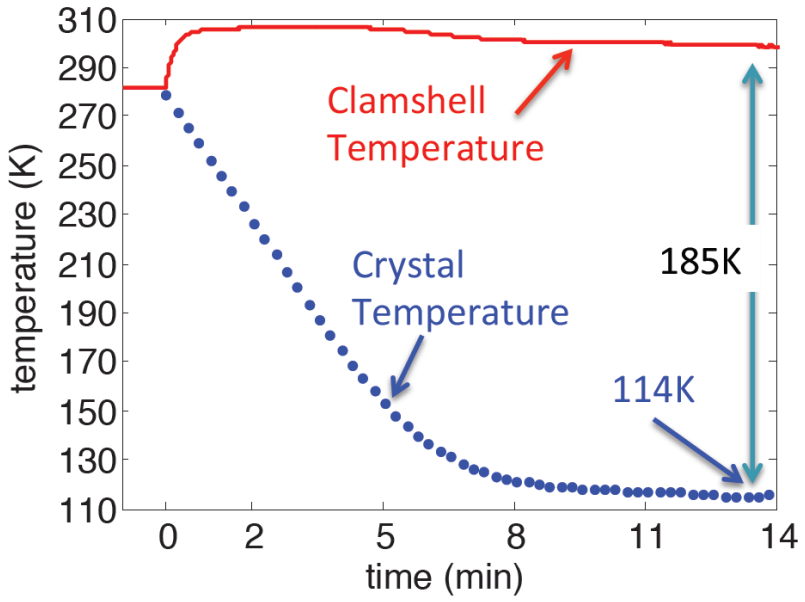

Figure 5: Cooling of a 10 mol% Yb^{3+}-doped YLF crystal. The 45 W pump laser operating at 1020 nm was turned on at t=0. *Reprinted from S. D. Melgaard, D. V. Seletskiy, A. Di Lieto, M. Tonelli, M. Sheik-Bahae, "Optical refrigeration progress: cooling below NIST cryogenic temperature of 123K", Proc. SPIE 8638 (2013) 863804-1, with permission from SPIE.*

Interestingly, the purity of these record-breaking YLF:Yb^{3+} samples did not significantly improve over that of earlier ZBLAN-based fluoride glasses. Rather, the primary advance was enabled by the much lower magnitude of inhomogeneous broadening of crystal-field transitions in the crystal hosts. In a glass, the absence of long-range structural order leads to a distribution of coordination geometries and thus crystal-field strengths around the Yb^{3+} ions. This causes an associated spread in the spectral width of the electronic transitions. In contrast, the highly ordered structure of crystals minimizes this broadening and concentrates the absorption cross section of the ensemble of Yb^{3+} ions into a much narrower spectral range. This is illustrated in Figure 6, where the long-wavelength side of the $^2F_{7/2} \rightarrow {}^2F_{5/2}$ absorption is shown for Yb^{3+} in

ZBLAN glass (red lines) and YLF crystal (blue lines) at three different temperatures. The lower inhomogeneous broadening of the crystal-field transitions in the crystal results in a significantly greater peak absorption cross section at 1020 nm, particularly at low temperatures. The higher peak absorption cross section in crystals allows for correspondingly more efficient absorption of the pump light by Yb^{3+} ions and thus cooling to lower temperatures compared to glasses. The following Sections provide a detailed review of the principles of solid-state laser cooling, the basic material choices and tradeoffs, the experimental techniques, the achievements with various laser-cooling materials, and the device design considerations.

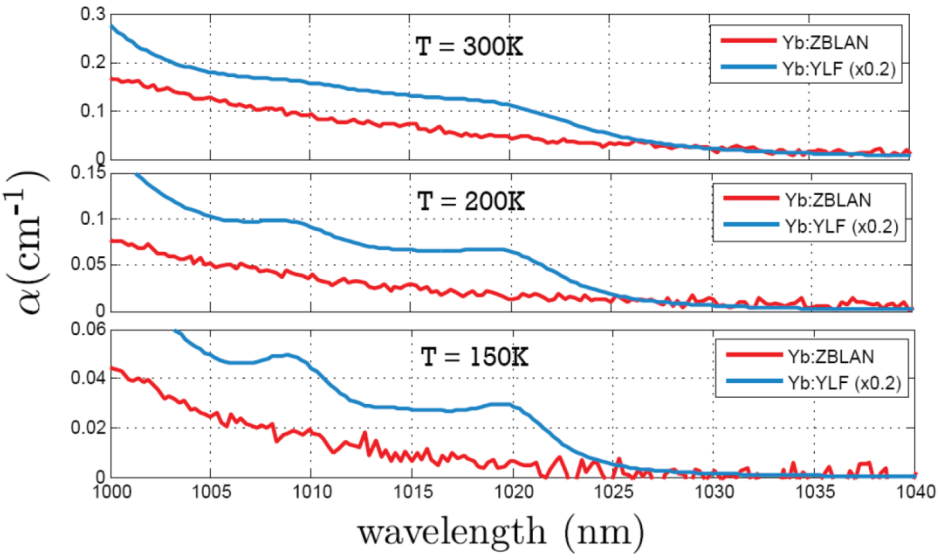

Figure 6: Comparison of the long-wavelength side of the $^2F_{7/2} \rightarrow {}^2F_{5/2}$ absorption in Yb^{3+} doped into ZBLAN glass (red traces) and $YLiF_4$ crystal (YLF, blue traces) at different temperatures normalized to 1 mol% Yb^{3+} doping (Melgaard 2013). The peak absorption coefficient at the 1020 nm pump wavelength is significantly greater in the crystal compared to the glass, most importantly at low temperatures. *Reprinted by permission from the University of New Mexico.*

Semiconductors are another class of materials with potential for optical refrigeration. Over the past 18 years, numerous theoretical and experimental studies have been published. Materials such as III-V GaAs heterostructures and AlGaAs quantum wells grown by metal-organic chemical vapor deposition (MOCVD) and molecular beam epitaxy (MBE) have been studied extensively. Laser cooling of semiconductors however has proven to be quite elusive. Challenges include the stringent purity requirements for achieving low background absorption, surface recombination effects, a quantum efficiency that depends on carrier density, and inefficient extraction of the luminescence from the high-refractive index semiconductor substrates. In 2013, Zhang *et al* reported the first net cooling of a semiconductor (Li, Zhang et al. 2013, Zhang, Li et al. 2013). They used chemical-vapor deposition to fabricate CdS nanobelts with thicknesses ranging from 40–240 nm and lengths of tens of μm. The CdS nanobelts were then suspended across inverted square-pyramid shaped holes etched into a SiO_2/Si substrate and excited with different lines of an argon ion laser. They achieved 40 K of net cooling of a 110 nm thick CdS nanobelt starting from 290 K when pumping a 514 nm. Semiconductor laser cooling shall be excluded from the present article, and the reader is referred to recent reviews on this topic (Sheik-Bahae and Epstein 2007, Epstein and Sheik-Bahae 2009).

2. PRINCIPLES OF SOLID-STATE OPTICAL REFRIGERATION

2.1. Electronic States of Lanthanide Ions

The most successful solid-state optical refrigeration results to date have been achieved with solids doped with tripositive lanthanide (Ln^{3+}) ions. The 4*f* shell is only partially filled along the series from Ce^{3+} to Yb^{3+}, giving rise to electron configurations ranging from $[Xe]4f^1$ to $[Xe]4f^{13}$, respectively. Electrostatic (Coulomb) interactions between the 4*f* electrons and spin-orbit interactions are of comparable magnitude (10^3–10^4 cm^{-1}) and are dominant in the lanthanides. They produce a set of electronic states (multiplets) that is characteristic for each $[Xe]4f^n$ electron configuration (Dieke and Crosswhite 1963, Hehlen, Brik et al. 2013). The multiplets are designated with $^{2S+1}L_J$ term symbols, where S, L, and J are the total spin angular momentum, total orbital angular momentum, and total angular momentum, respectively. In an Ln^{3+}-doped insulator, the coordination of anions around the Ln^{3+} cation produces an electrostatic field that lowers the spherical symmetry of the idealized "free ion" case and therefore causes an energy splitting of the $^{2S+1}L_J$ multiplets. The magnitude of this crystal-field interaction is much smaller (10^1–10^2 cm^{-1}) than Coulomb and spin-orbit interactions because the 4*f* electrons are shielded quite effectively from the surroundings by the outer 5*s* and 5*p* orbitals. As a result, Ln^{3+} ions maintain much of their "free ion" character even when they are placed into a solid. A now famous energy-level diagram of $^{2S+1}L_J$ multiplets up 40000 cm^{-1} was first presented Dieke and Crosswhite in 1963 (Dieke and Crosswhite 1963), and a full calculation of all $^{2S+1}L_J$ energy levels was recently reported by Peijzel *et al* (Peijzel, Meijerink et al. 2005). Figure 7 shows the $^{2S+1}L_J$ multiplets up 20000 cm^{-1} for select Ln^{3+} ions that are relevant for solid-state laser cooling.

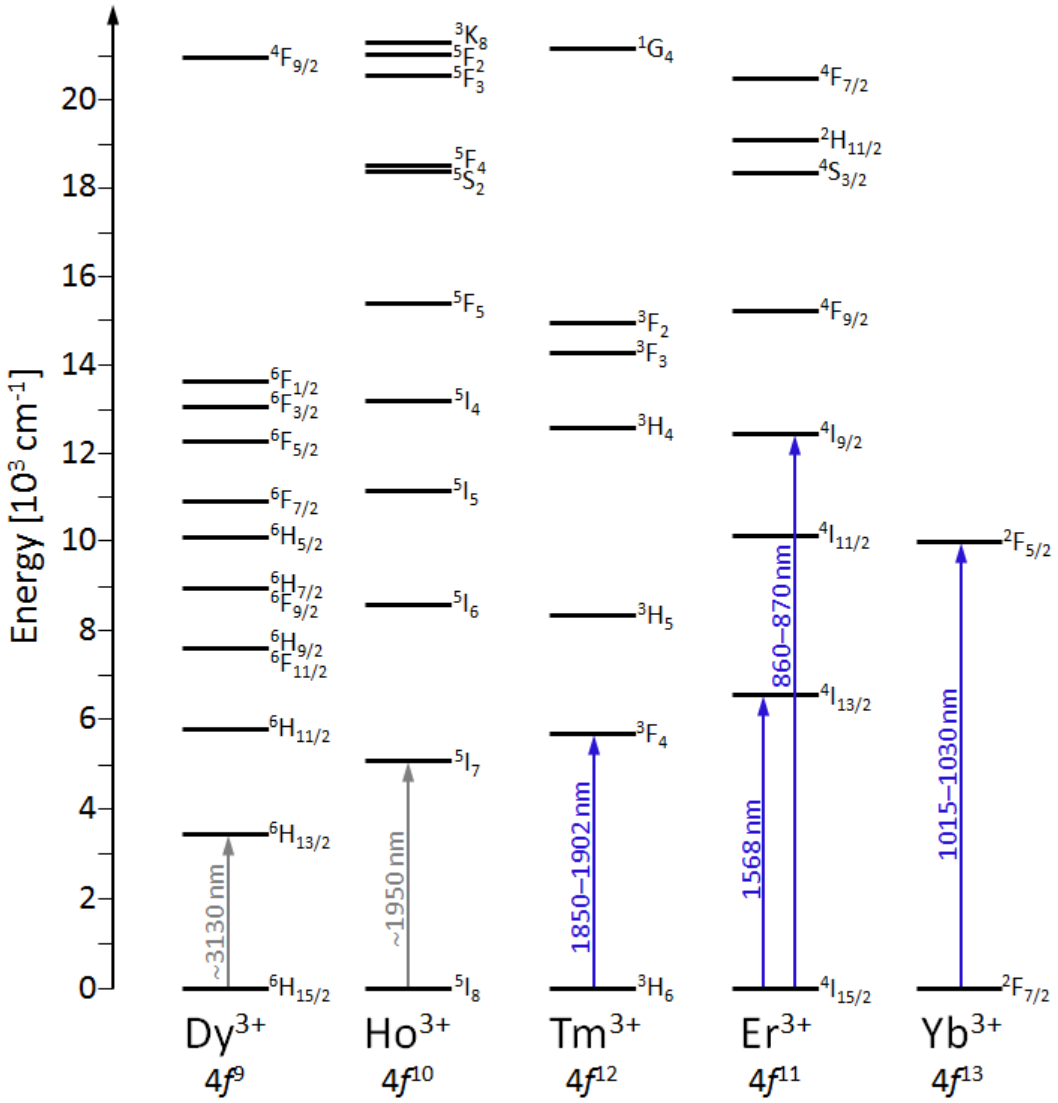

Figure 7: Partial energy level diagram for the $^{2S+1}L_J$ multiplets of select Ln^{3+} ions relevant for solid-state laser cooling. The ions are ordered with increasing energy of the first excited state. The blue arrows for Tm^{3+}, Er^{3+}, and Yb^{3+} indicate the pump wavelengths of transition that have been used successfully for net laser cooling. The gray arrows for Dy^{3+} and Ho^{3+} give approximate pump wavelengths for future experiments.

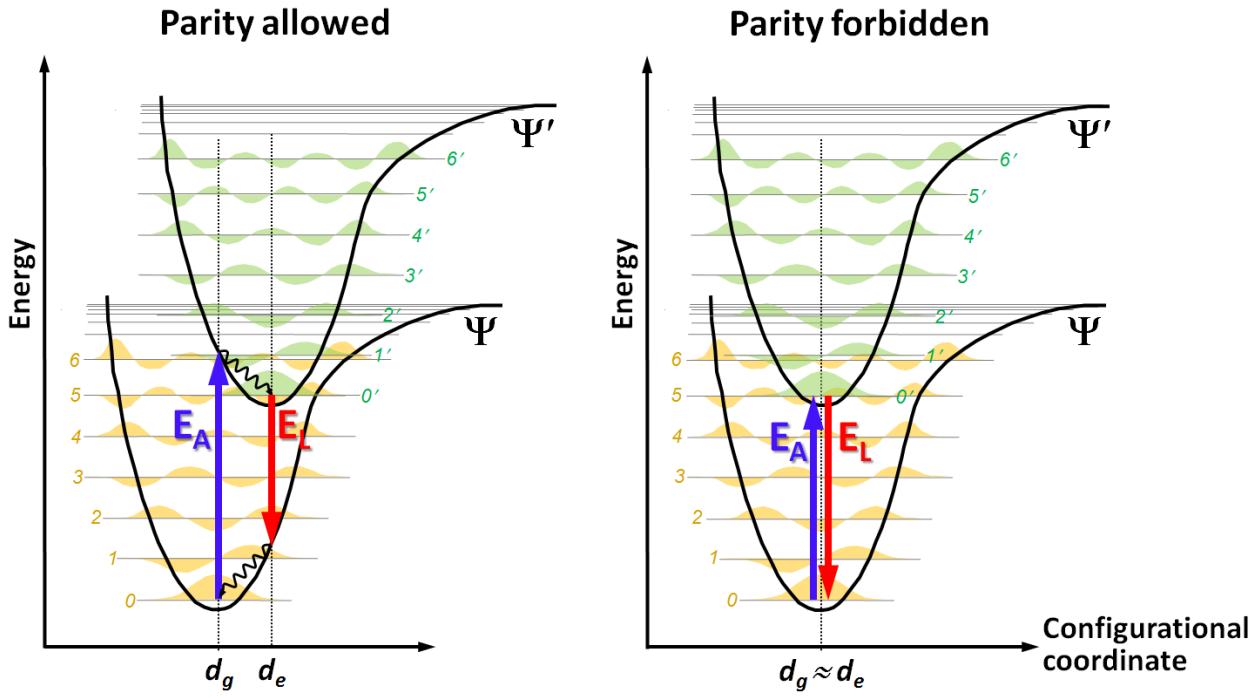

Figure 8: Illustration of excitation (at energy E_A) and relaxation (at energy E_L) for a parity allowed (left) and a parity forbidden (right) electronic transition between a ground (Ψ) and excited (Ψ') state. Non-radiative relaxation processes are indicated as wiggly arrows. The potential energy of the electronic states (black lines) are shown as a function of a configurational coordinate (*i.e.* one of the normal modes). The vibrational wavefunctions are illustrated in color along with the respective vibrational quantum numbers. d_g and d_e denote the equilibrium bond distance in the ground and excited state, respectively.

Consider a metal cation (M) coordinated by anions (X) in a solid. Viewed in isolation, this $[MX_n]^{m+}$ coordination in the solid has $3(n+1)-6$ fundamental optical vibrations (normal modes), each with its characteristic vibrational energy and phonon occupation number at the given temperature. Exciting the metal ion by a parity-allowed electronic transition typically

causes a change in the equilibrium M–X bond length between the ground state (d_g) and the excited state (d_e) (Figure 8, left). In most cases, the M–X bond is weakened by the electronic excitation so that $d_e > d_g$. As a consequence of the Born-Oppenheimer approximation, the change in bond length *necessitates* the conversion of some of the electronic excitation energy to vibrational energy (wiggly arrows). This leads to the "Stokes shift" of the luminescence relative to its corresponding absorption (*i.e.* $E_L < E_A$) and causes the well-known heating of materials upon excitation. The situation is different for the Ln^{3+} ions. Electronic excitations within the 4*f* electron configuration, *i.e.* transitions between the $^{2S+1}L_J$ multiplets shown in Figure 7, are parity forbidden. In addition, the 4*f* electrons are shielded by the outer 5*s* and 5*p* orbitals, and the M–X chemical bond is only minimally affected by a 4*f* electronic excitation. Consequently, equilibrium bond lengths in the ground and excited states are similar as illustrated in Figure 8 (right). Excitation and relaxation of Ln^{3+} ions can therefore be dominated by electronic transitions with only minimal involvement of vibrational modes ($E_L \approx E_A$, no Stokes shift), thereby eliminating much of the internal heating that is inherent to Stokes-shifted parity-allowed transitions. This key feature makes Ln^{3+} ions particularly attractive for solid-state laser cooling because it allows anti-Stokes fluorescence to dominate in some special cases.

While the crystal-field interaction is relatively weak in lanthanides, it is an essential ingredient for solid-state optical refrigeration. Each $^{2S+1}L_J$ multiplet has a $(2J+1)$-fold degeneracy in the total angular momentum which is lifted into M_J components under the influence of the non-spherical electrostatic field created by the neighboring ions in a solid. The number of resulting $^{2S+1}L_J(M_J)$ crystal-field levels depends on the point symmetry of the crystal field at the location of the lanthanide ion. A complete lifting of the $(2J+1)$-fold degeneracy is

achieved in sufficiently low symmetry (note however that the crystal-field levels of Ln^{3+} ions with an odd number of 4*f*-electrons always maintain at least a 2-fold Kramers degeneracy that can only be lifted in a magnetic field). The magnitude of the overall crystal-field splitting of a $^{2S+1}L_J$ multiplet is typically a few hundred wavenumbers, *i.e.* it is comparable to kT at room temperature ($kT = 209$ cm^{-1} at 300 K).

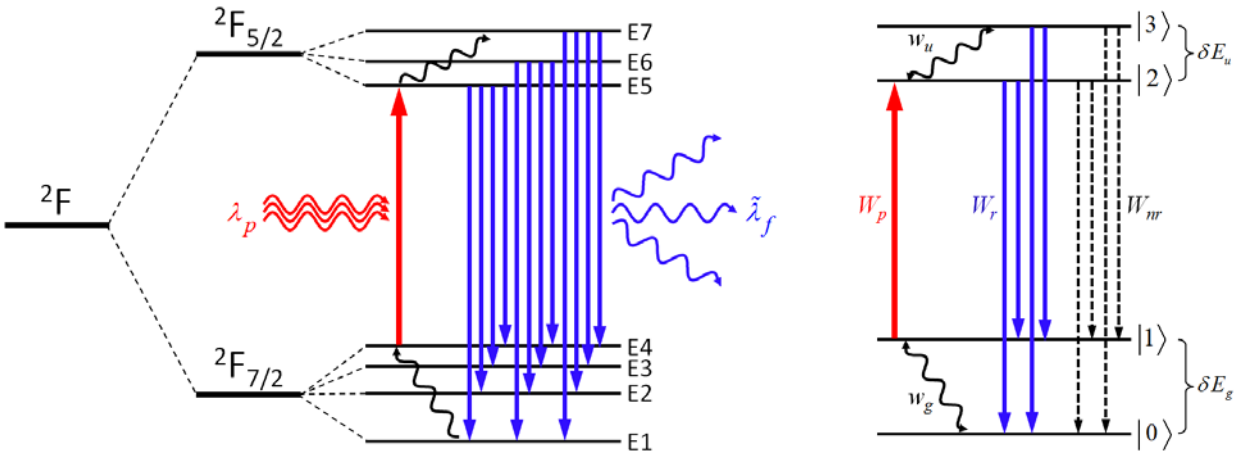

Figure 9: *Left:* Energy-level diagram of Yb^{3+} (not to scale) illustrating the removal of thermal energy from and thus cooling of a solid by anti-Stokes fluorescence (average emission wavelength $\tilde{\lambda}_f$ shorter than the pump laser wavelength λ_p). *Right:* Simplified four-level model of Yb^{3+} used for the derivation of the laser-cooling efficiency (see Section 2.3).

Figure 9 (left) illustrates the energy-level diagram of Yb^{3+}. The [Xe]$4f^{13}$ electron configuration produces only one ^{2}F manifold that splits into a $^2F_{7/2}$ ground state and $^2F_{5/2}$ excited state multiplet under the influence of the spin-orbit interaction. The two multiplets further split into 4 and 3 two-fold (Kramers) degenerate crystal-field levels, respectively, if the point

symmetry of Yb^{3+} is sufficiently low (less than cubic). Note that Figure 9 is not to scale: the $^2F_{5/2}$–$^2F_{5/2}$ splitting is ~10000 cm^{-1} while the $^2F_{7/2}$ crystal-field splitting is about 300–600 cm^{-1}, depending on the material (Hehlen 2010). Further note that the energy-level diagram in Figure 9 implies zero Stokes shift, *e.g.* the E4→E5 absorption occurs at essentially the same energy as the corresponding E5→E4 luminescence. Assuming no Stokes shift allows the electronic energy levels to be represented by horizontal lines rather than the full potential curves as shown in Figure 8 (right).

2.2. Anti-Stokes Fluorescence and Thermal Equilibrium

The lattice strains associated with vibrations in the solid modulate the crystal field. This influences the 4*f* spins via the spin-orbit interaction and thereby induces electron-phonon transitions between the Ln^{3+} crystal-field levels. Such transitions represent an exchange of energy between the vibrational and electronic systems of the solid. A coupling of the lattice vibrations to the spins of an Ln^{3+} ion of this type is referred to as Van Vleck mechanism (Charles P. Poole 2004). The probability P_{pq} for a lattice-induced transition between two crystal-field levels $p \to q$ is related to that for the reverse transition by $P_{pq} = P_{qp} \exp\left[\left(E_p - E_q\right)/kT\right]$, where E_i is the energy of the crystal-field level i (Gill 1975). Here it is assumed that there is no "phonon bottleneck" (Auzel and Pellé 1997), *i.e.* that phonons with energy $E_p - E_q$ can be created or annihilated as needed. In thermal equilibrium, the respective transition rates are equal over the ensemble of Ln^{3+} ions, and the relative population of crystal-field level i at temperature T is given by

$$n_i(T) = g_i \exp\left[-(E_i - E_0)/kT\right] / Z(T) \quad , \tag{1}$$

where $Z(T)$ is the partition function $Z(T) = \sum_{k=0}^{N-1} g_k \exp(-E_k/kT)$ taken over the N crystal-field levels of the system, and g_i is the degeneracy of crystal-field level i. For Yb^{3+} in the ground state, for example, $Z(T)$ has to be taken over all $N = 7$ crystal-field levels. Since the $^2F_{5/2}$ crystal-field levels are at much greater energy than those of the $^2F_{7/2}$ ground state, their respective terms in $Z(T)$ are essentially zero for common temperatures, and taking $Z(T)$ over the 4 crystal-field levels of the $^2F_{7/2}$ ground state provides an adequate description.

The phonon absorption and emission processes that establish the thermal equilibrium in Eq. (1) take place on ns to ps time scales for temperatures >50 K (Kohmoto, Fukuda et al. 2000), *i.e.* much faster than the μs to ms lifetimes typical of many Ln^{3+} excited states. For Yb^{3+}, for example, these disparate time scales are the reason why a $^2F_{7/2} \rightarrow {}^2F_{5/2}$ excitation is first followed by the thermalization of the population among the $^2F_{5/2}$ crystal-field levels, and the subsequent $^2F_{5/2} \rightarrow {}^2F_{7/2}$ radiative decay takes place from this quasi-equilibrium population. This is the fundamental origin of anti-Stokes fluorescence and is illustrated in Figure 9 (left). Tuning a laser to the E4→E5 crystal-field transition at energy $h\nu_p$ (red arrow) excites Yb^{3+} ions exclusively to the $^7F_{5/2}$(E5) level. For temperatures greater than absolute zero, however, exclusive population of E5 in the $^7F_{5/2}$ excited state does not correspond to thermal equilibrium, which therefore is

rapidly established by the net absorption of vibrational energy (wiggly arrow). Subsequently, the ensemble of excited thermalized Yb^{3+} ions can decay radiatively to the $^2F_{7/2}$ ground state via any one of the 12 possible crystal-field transitions (blue arrows). The mean energy of these fluorescence transitions, $h\tilde{\nu}_f$, is given by

$$h\tilde{\nu}_f = \frac{\int \Phi(\nu) h\nu d\nu}{\int \Phi(\nu) d\nu} \tag{2}$$

which corresponds to a mean fluorescence wavelength of

$$\tilde{\lambda}_f = \frac{\int S(\lambda) \lambda d\lambda}{\int S(\lambda) d\lambda} \tag{3}$$

where $\Phi(\nu)$ is the mean photon flux density and $S(\lambda)$ is the power spectral density. Energy conservation requires $\Phi(\nu) h\nu d\nu = S(\lambda) d\lambda$ and thus

$$\tilde{\lambda}_f = \frac{\int S(\lambda)\lambda d\lambda}{\int S(\lambda) d\lambda} = \frac{hc\int \Phi(\nu) d\nu}{h\int \Phi(\nu)\nu d\nu} = \frac{c}{\tilde{\nu}_f}$$

(4)

Since $h\tilde{\nu}_f$ is greater than $h\nu_p$, the thermalization processes lead to anti-Stokes fluorescence that carries vibrational energy (heat) away from the solid in the form of light, cooling the solid in the process. In a final step, thermal equilibrium is re-established in the ground-state multiplet, thereby repopulating the E4 initial state and completing the "laser cooling cycle". Laser-induced cooling can, therefore, occur if $h\tilde{\nu}_f > h\nu_p$, *i.e.* as long as anti-Stokes fluorescence on average predominates over resonant and Stokes fluorescence (Mungan 2005). This is illustrated in Figure 10 for a 5% Yb^{3+}-doped $YLiF_4$ (YLF) crystal. A mean fluorescence wavelength of $\tilde{\lambda}_f \approx 999$ nm is obtained from the luminescence spectrum (blue) at 300 K and Eq. (2). Laser excitation into the "cooling tail" of the absorption spectrum at $\lambda_p > \tilde{\lambda}_f$ (red shaded area) produces a net anti-Stokes luminescence by the ensemble of Yb^{3+} ions and should, in the ideal case, lead to cooling. Figure 10b shows that the measured cooling efficiency (see Section 2.3) indeed crosses from $\eta_c < 0$ (laser-induced heating) to $\eta_c > 0$ (laser-induced cooling) as the pump laser wavelength is tuned from $\lambda_p < \tilde{\lambda}_f$ to $\lambda_p > \tilde{\lambda}_f$ into the "cooling tail". The ratio of the amount of heat extracted per cycle, $Q = h\tilde{\nu}_f - h\nu_p$, to the excitation energy can be viewed as an idealized cooling efficiency, *i.e.* as (Sheik-Bahae and Epstein 2009)

$$\eta_c = \frac{h\tilde{\nu}_f - h\nu_p}{h\nu_p} \tag{5}$$

where positive and negative values of η_c indicate laser-induced cooling and heating, respectively. The next Section will show a more detailed description and find that this idealized cooling efficiency has to be modified by both the external quantum efficiency and the competition with absorption by impurities.

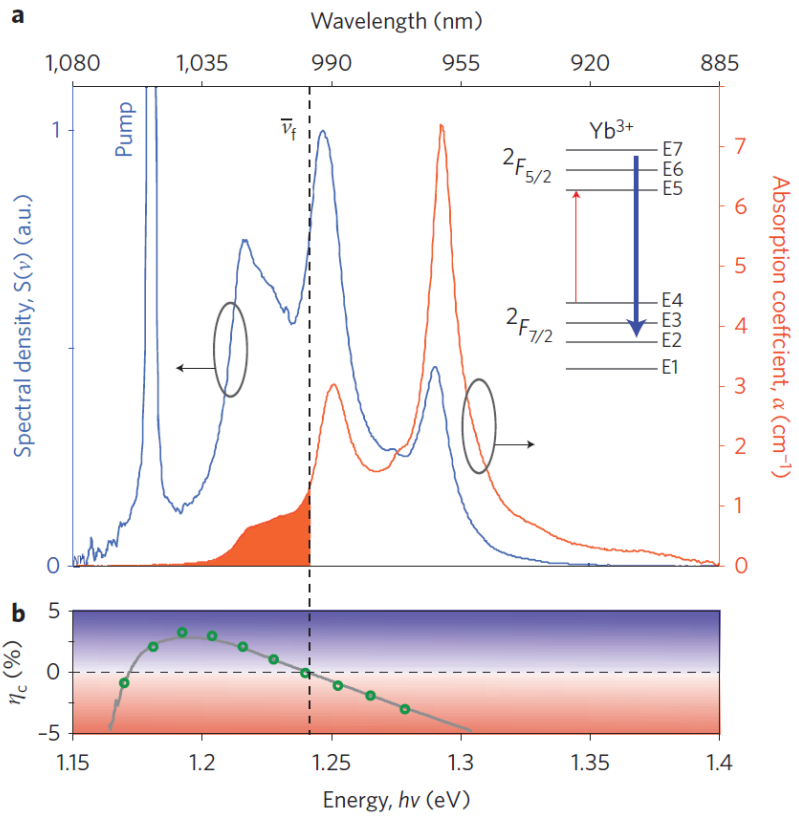

Figure 10: Optical absorption, emission and cooling efficiency spectra of a 5% Yb^{3+}-doped $YLiF_4$ (YLF) crystal (Seletskiy, Melgaard et al. 2010). (a) Absorption (red) and fluorescence emission (blue) spectra, for a laser excitation at 1055 nm polarized along the crystal c-axis. The cooling tail corresponding to the absorption spectrum for photon energies below mean fluorescence energy ($h\tilde{\nu}_f$) is shaded in red. (b) Experimental (open circles) cooling efficiency at 300 K.

2.3. The Four-Level Model and the Laser Cooling Efficiency

The simplified four-level scheme shown in Figure 9 (right) reveals the essential features of solid-state laser cooling with lanthanide ions (Petrushkin and Samartsev 2009). Following the

derivation given in Ref. (Sheik-Bahae and Epstein 2009), we define a system consisting of a ground state with two levels $|0\rangle$ and $|1\rangle$ separated by δE_g, and an excited state with two levels $|2\rangle$ and $|3\rangle$ separated by δE_u. The ensemble of ions is excited by a laser tuned to the $|1\rangle \rightarrow |2\rangle$ transition (red arrow), and the associated pumping rate is given by $W_p = \left(I\sigma_{12}/h\nu_{12}\right) N_1$, where N_1 is the population of level $|1\rangle$, I is the incident laser irradiance, and σ_{12} and ν_{12} are the cross section and frequency of the $|1\rangle \rightarrow |2\rangle$ transition, respectively. The excited levels $|2\rangle$ and $|3\rangle$ can decay to the ground-state levels by radiative relaxation (blue arrows) with rate constant W_r, assumed here to be identical for each of the four radiative transitions. Alternatively, the excited levels can decay by non-radiative relaxation (dashed arrows) with rate constant W_{nr}, likewise assumed identical for each of the four non-radiative transitions. Thermal equilibrium in the ground and excited state is established by spin-lattice interactions, and the respective rate constants w_g and w_u are assumed to be equal ($w = w_g = w_u$) in this model. The population of the four levels is then given by

$$\frac{dN_1}{dt} = -\frac{I\sigma_{12}}{h\nu_{12}}\left(N_1 - \frac{g_1}{g_2}N_2\right) + \frac{R}{2}\left(N_2 + N_3\right) - w_g\left(N_1 - \frac{g_1}{g_2}N_0 e^{-\delta E_g/kT}\right) \tag{6}$$

$$\frac{dN_2}{dt} = \frac{I\sigma_{12}}{h\nu_{12}}\left(N_1 - \frac{g_1}{g_2}N_2\right) - RN_2 + w_u\left(N_3 - \frac{g_3}{g_2}N_2 e^{-\delta E_u/kT}\right) \tag{7}$$

$$\frac{dN_3}{dt} = -RN_3 + w_u\left(N_3 - \frac{g_3}{g_2}N_2 e^{-\delta E_u/kT}\right) \tag{8}$$

$$N_t = N_0 + N_1 + N_2 + N_3 \tag{9}$$

where N_t is the total of Ln^{3+} ions in the ensemble and $R = 2\left(W_r + W_{nr}\right)$ is the total upper state decay rate constant. The latter definition assumes that spin-lattice processes are much faster than the excited-state radiative and non-radiative decay, *i.e.* $w \gg R$. The degeneracy of level i is denoted by g_i, which in the following we assume being equal for all levels. The total power density deposited in the system, P_{net}, corresponds to the difference of the absorbed (P_{abs}) and emitted (P_{rad}) contributions, *i.e.*

$$P_{net} = P_{abs} - P_{rad} = \left[\alpha\left(I\right) + \alpha_b\right]I - W_r\left[N_2\left(E_{20} + E_{21}\right) + N_3\left(E_{30} + E_{31}\right)\right] \tag{10}$$

where $E_{ij} = E_i - E_j$ and the resonant absorption coefficient $\alpha\left(I\right) = \sigma_{12}(N_1 - N_2)$. Equation (10) also introduces the background absorption coefficient α_b. It allows for the possibility that some

of the incident laser light is absorbed by "impurity" species other than the four-level system, and that this absorbed fraction decays non-radiatively, *i.e.* is not reemitted but rather converted to heat. The system cools if $P_{net} < 0$, *i.e.* when the radiated power density exceeds the absorbed one. In steady state ($dN_i/dt = 0$) and assuming the system to be far from saturation ($N_0 + N_1 \gg N_2 + N_3$), the net power density is then obtained as

$$P_{net} = \alpha I \left(1 - \eta_q \frac{h\tilde{\nu}_f}{h\nu_p} \right) + \alpha_b I \tag{11}$$

where $\eta_e = \left(1 + W_{nr}/\eta_{ext} W_r\right)^{-1}$ is the external quantum efficiency with η_{ext} being the extraction efficiency for the fluorescence. In Eq.(11),

$$\alpha = \frac{\sigma_{12} N_t}{1 + \exp\left(\delta E_g / kT\right)} \tag{12}$$

is the absorption coefficient of the $|1\rangle \rightarrow |2\rangle$ (resonant absorption). The derivation also yields the mean fluorescence energy of the four-level system as (Sheik-Bahae and Epstein 2009)

$$h\tilde{\nu}_f = h\nu_p + \frac{\delta E_g}{2} + \frac{\delta E_u}{1+\left(1+R/w_u\right)e^{\delta E_u/kT}}$$

(13)

The cooling efficiency can now be defined as the net deposited power density relative to the total absorbed power density, *i.e.*

$$\eta_c = -\frac{P_{net}}{P_{abs}} = \eta_e \eta_{abs} \frac{h\tilde{\nu}_f}{h\nu_p} - 1$$

(14)

where the absorption efficiency

$$\eta_{abs} = \frac{\alpha}{\left(\alpha + \alpha_b\right)}$$

(15)

has been introduced. It represents the fraction of the *total* absorbed power that has been used to excite the four-level system rather than an impurity species. The definition in Eq. (14) is such that a positive η_c corresponds to laser-induced cooling.

The above derivation highlights several key features of solid-state laser refrigeration. First, Eq. (12) shows that the pump absorption coefficient diminishes exponentially as the temperature is lowered, which is a result of the thermal depletion of the initial state $|1\rangle$. This reduces the net power density that can be extracted from the solid [Eq. (11)] and ultimately sets a lower limit for the temperature that can be reached by laser cooling. Finding materials with a small ground-state crystal-field splitting (δE_g) is advantageous in this respect. Second, the $|1\rangle \rightarrow |2\rangle$ transition competes with absorption by impurities (α_b). As evident from Eq. (15), this can be particularly detrimental if the impurity absorption does not change much with temperature while the resonant absorption α decreases exponentially as the temperature is lowered [Eq. (12)]. The presence of impurities becomes increasingly detrimental as the temperature decreases and an ever larger fraction of the absorbed power is used to excite impurities that cause parasitic heating. Third, Eq. (13) describes how the mean fluorescence energy decreases (red-shifts) at low temperatures which, as seen in Eq. (14), reduces the cooling efficiency. Overall, as the temperature is lowered, the red-shift of the mean fluorescence wavelength combined with the reduction of the resonant absorption reduces the cooling efficiency. Cooling stops at a temperature where $\eta_c = 0$. This minimum temperature can be lowered by reducing the amount of background absorption (*i.e.* reducing the level of impurities), increasing the quantum efficiency, and enhancing the resonant absorption (*e.g.* by choosing crystalline hosts and materials with a small ground-state crystal-field splitting).

2.5. Thermodynamic Considerations

The question whether anti-Stokes fluorescent refrigeration is consistent with the laws of thermodynamics was controversial early on, and it was already considered in the first publication in this field by Pringsheim (Pringsheim 1929). Landau resolved the issue formally in 1946 (Landau 1946). Several authors have since reviewed the thermodynamics of solid-state laser cooling (Edwards, Buchwald et al. 1998, Rayner, Heckenberg et al. 2003, Mungan 2005, Ruan and Kaviany 2006, Ruan, Rand et al. 2007, Nemova and Kashyap 2010). The second law of thermodynamics states that the entropy of an isolated system never decreases, and it sets a maximum for the efficiency of an optical refrigerator. A key insight is that light itself has entropy. The rate at which entropy is carried by a steady, unpolarized beam of light in vacuum across a surface A is given by (Mungan 2005)

$$\dot{S} = \frac{2k}{c^2} \int_A \int_\Omega \int_{\Delta\nu} \left[(1+n) \ln (1+n) - n \ln n \right] \nu^2 \, d\nu \, \cos\theta \, d\Omega \, dA \tag{16}$$

where k is Boltzmann's constant, c is the speed of light, and θ and ϕ are the polar and azimuthal angles, respectively, at which the light is propagating into solid angle element $d\Omega = \sin\theta d\theta d\phi$ relative to the normal to an element dA of the surface. Furthermore, the radiation is distributed among a set of optical modes with mean occupation number n and frequency ν. Note that Eq. (16) is valid for thermal radiation, laser radiation, and the non-

equilibrium photon distribution of fluorescence from an excited state (such as shown in Figure 9). From Eq. (16) it is evident that a monochromatic ($\Delta\nu \to 0$) light source with low divergence ($d\Omega \to 0$) such as a laser carries with it a lower entropy than a broadband ($\Delta\nu \gg 0$) isotropic ($\int \cos\theta \, d\Omega = 4\pi$) light source such as a fluorescent ion. The flux temperature of a light source can then be defined as $T = \dot{E}/\dot{S}$, where $\dot{E}$ and $\dot{S}$ are the energy and entropy flux rates, respectively.

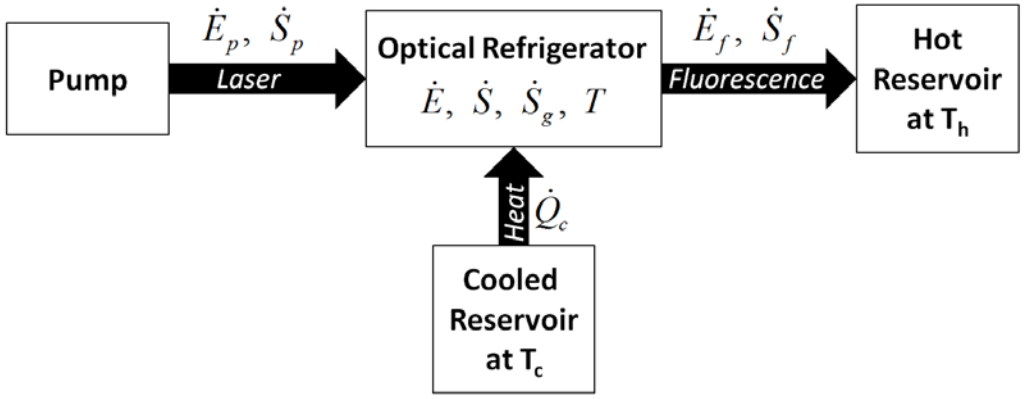

Figure 11: Energy and entropy fluxes for an optical refrigerator.

A complete description of an optical refrigerator has to include the energy and entropy fluxes of the heat load as well as those of the pump and fluorescent radiation. As illustrated in Figure 11 (Edwards, Buchwald et al. 1998), energy and entropy are removed from the pump laser radiation at rates $\dot{E}_p$ and $\dot{S}_p$, respectively. They are added to the fluorescent radiation field at rates $\dot{E}_f$ and $\dot{S}_f$, respectively. The cooled reservoir loses thermal energy at a rate of $\dot{Q}_c$ and thus loses entropy at a rate of $\dot{S}_c = \dot{Q}_c/T_c$. In steady state, conservation of energy requires that

$\dot{E}_p + \dot{Q}_c = \dot{E}_f$, and the second law of thermodynamics requires that the total entropy does not decrease, *i.e.* $\dot{S}_f - \dot{S}_p - \left(\dot{Q}_c / T_c\right) \geq 0$. Using the flux temperatures T_p and T_f for the pump and fluorescent light, respectively, one thus finds that the cooling efficiency for converting light to heat lift is

$$\eta_c = \frac{\dot{Q}_c}{\dot{E}_p} \leq \frac{1 - \left(T_f / T_p\right)}{\left(T_f / T_c\right) - 1} \ . \tag{17}$$

For the conditions of an optical refrigerator one has $T_p \gg T_f > T_c$, which simplifies Eq.(17) to

$$\eta \leq \frac{T_c}{T_f - T_c} \ , \tag{18}$$

an expression which is similar to the Carnot efficiency, except that the temperature of the hot thermal reservoir has been replaced by the fluorescence flux temperature T_f.

For an optical refrigerator, the photon occupation number n in the entropy flux rate [Eq.(16)] has contributions from both the fluorescent photons of the refrigerator, $n_f(\nu)$, and the

ambient thermal photons, $n_a(\nu)$. The latter is given by $n_a(\nu) = 1/\left[\exp(h\nu/kT_a) - 1\right]$, with T_a being the ambient temperature. Therefore, the entropy flux rate due to fluorescence is given by

$$\dot{S}_f = \frac{2k}{c^2}\int_A\int_\Omega\int_{\Delta\nu}\left\{\left[(1+n)\ln(1+n) - n\ln n\right] - \left[(1+n_a)\ln(1+n_a) - n_a\ln n_a\right]\right\}\nu^2\ d\nu\ \cos\theta\, d\Omega\ dA \tag{19}$$

and energy flux rate due to fluorescence is given by

$$\dot{E}_f = \frac{2k}{c^2}\int_A\int_\Omega\int_{\Delta\nu} h\nu_f n_f\ \nu^2\ d\nu\ \cos\theta\, d\Omega\ dA\ , \tag{20}$$

yielding a fluorescent temperature of $T_f = \dot{E}_f / \dot{S}_f$. In Eqs. (19) and (20), fluorescent contributions typically dominate over ambient contributions. Edwards *et al* estimated the thermodynamic properties of an optical refrigerator based on Yb^{3+}-doped ZBLANP fluoride glass that is pumped by a 40 W laser and produces a heat lift of 500 mW (Edwards, Buchwald et al. 1998). After correcting a numerical error, their analysis gives that T_f ~1700 K, which implies that the refrigerator efficiency is limited by thermodynamics to ~5% at 77 K.

3. MATERIAL CONSIDERATIONS

3.1. Energy Levels and Non-Radiative Decay

The detailed analysis of the four-level system in Section 2.3 has shown that the laser-cooling efficiency is inversely proportional to the pump-laser energy $h\nu_p$ [Eq. (14)]. This favors the use of lanthanide ions with a low energy of the first excited state. Most of the work to date has been performed on Yb^{3+}-doped materials. Here, the $^2F_{5/2}$–$^2F_{7/2}$ energy separation of ~9800 cm^{-1} is large compared to kT, limiting the cooling efficiency to ~2.2% at 300 K [Eq.(5)]. The possibility of three times greater cooling efficiencies by going to a cooling ion such as Dy^{3+} (see Figure 7) is tantalizing, but it is met with formidable challenges. This is because an Ln^{3+} excited state can, besides radiative decay, also relax to a lower-energy state via the emission of vibrational energy into the solid. Such a non-radiative (multi-phonon) process is obviously detrimental to laser cooling as it converts electronic excitation energy to heat. It is therefore necessary to find materials in which the competition between the radiative (W_r) and the non-radiative (W_{nr}) decay rates is strongly in favor of radiative decay, *i.e.* $W_r \gg W_{nr}$ such that the internal quantum efficiency $\eta_q = \left(1 + W_{nr}/W_r\right)^{-1}$ approaches unity. Electronic transitions between 4*f* energy levels have oscillator strengths on the order of 10^{-5}–10^{-6} and the radiative relaxation rate of the first excited state is on the order of $W_r = 10^2 - 10^3$ s^{-1} for a wide variety of materials. In contrast, the type and magnitude of the non-radiative relaxation depends on the material. Non-radiative processes primarily include the multi-phonon relaxation of the excited state, but they can also encompass two-ion processes such as cross-relaxation and energy-transfer upconversion that can be active in Ln^{3+} ions with many excited states (e.g. Tm^{3+} and Er^{3+}, see Figure 7). We shall focus on multi-phonon relaxation in the following.

A non-radiative relaxation between an excited electronic state Ψ' and a lower-energy electronic state Ψ separated by ΔE involves both an electronic $\Psi' \rightarrow \Psi$ transition and a vibrational transition that causes the emission of one or multiple vibrational quanta with a combined energy equaling ΔE. The rate of this non-radiative relaxation is proportional to the product of the probabilities of the electronic and vibrational processes, $W_{nr} \propto p_{el} p_{vib}$. At zero Kelvin, p_{vib} is proportional to the overlap integral of the lowest-energy ($n = 0$) vibrational wavefunction of the excited state, $\Psi'(0)$, and the resonant vibrational wavefunction of the ground state, $\Psi(m)$. Here, $m = \Delta E / \hbar\omega$, $\hbar\omega$ is the energy of the accepting vibrational mode, and we have assumed for simplicity that there is only one accepting mode, m is integer, and the Stoke shift is nominally zero. For the hypothetical example shown in Figure 8 (right), the overlap of the vibrational wavefunctions $\Psi'(0)$ and $\Psi(5)$ would be dominant. In the approximation of a diatomic quantum harmonic oscillator with atomic masses M, the vibrational wavefunctions are given by $\Psi_m(y) = (\alpha/\pi)^{1/4} \left(2^m m!\right)^{-1/2} H_m(y) \exp\left(-y^2/2\right)$ with $y = \sqrt{\alpha} x$ and $\alpha = M\omega/\hbar$, where $H_m(y)$ are the Hermite polynomials and x is the internuclear separation. It can be shown that the vibrational overlap integrals $\left|\langle \Psi'_0 | \Psi_m \rangle\right|^2$, also known as the Franck-Condon factors, decrease bi-exponentially with increasing n (and approximately exponentially for $n > 4$). This is the fundamental origin of the energy-gap law (Riseberg and Moos 1968)

$$W_{mp} = \beta e^{-\alpha m} \tag{21}$$

which describes the multi-phonon relaxation rate W_{mp} as a function of the number of emitted vibrational quanta, m, as well as a vibrational (α) and an electronic (β) parameter that are material specific. Modified versions of the energy gap law have been introduced as well, and they take into account both promoting and accepting modes (see (Auzel and Pellé 1997) for a detailed discussion). One common modified energy-gap law yields $W_{mp} = W_0 \exp\left[-\alpha'\left(\Delta E - 2.6\hbar\omega_{\max}\right)\right]$, where the energy gap has been reduced by $2.6\hbar\omega_{\max}$ to take into account the promoting mode, and W_0 and α' are materials specific parameters describing the electronic and vibrational process, respectively (Auzel and Pellé 1997). The energy-gap law has two important implications. First, W_{mp} decreases exponentially with increasing number of phonons created in the process. Second, in a real system with a large number of vibrational modes, the vibration with the highest energy ($\hbar\omega_{\max}$) will have the lowest m and thus be the most likely accepting mode creating the highest multiphonon relaxation rate. The vibration with $\hbar\omega_{\max}$ is typically an optical phonon that corresponds to a local vibration of the anions that coordinate the Ln^{3+} ion, such as the totally symmetric stretching vibration of the [YbF_8] unit in a Yb^{3+}-doped $YLiF_4$ crystal with an energy of ~450 cm^{-1} (Orlovskii, Basiev et al. 2002).

The energy-gap law provides quantitative guidance on the maximum phonon energy a material can have to still enable laser cooling of a transition with energy ΔE (Nemova and Kashyap 2010). Assuming $W_r = 10^3$ s^{-1}, requiring $\eta_q > 0.99$, and using typical values for α and β yields the criterion of $\hbar\omega_{\max} < \Delta E/8$ which is illustrated in Figure 12 (Hehlen 2009). It shows

the $\hbar\omega_{\max} < \Delta E/8$ criterion in relation to the energy of the first excited state of select Ln^{3+} ions (Figure 7), ΔE, and the highest optical phonon energy, $\hbar\omega_{\max}$. W_{nr} should be sufficiently suppressed (relative to W_r) for materials that fall below the $\Delta E/8$ criterion indicated by the solid black line. This is indeed found in practice, as illustrated by the open circles in Figure 12 which indicate Ln^{3+}-doped solids for which laser cooling has been observed. Yb^{3+} is advantageous for solid state optical refrigeration because its large $^2F_{5/2}$–$^2F_{7/2}$ energy gap of ~9800 cm^{-1} (Figure 7) ensures inefficient $^2F_{5/2}$ multi-phonon relaxation and thus high quantum yield for materials with phonon energies up to ~1200 cm^{-1}. This large energy gap makes Yb^{3+} a viable laser cooling ion in all halide (fluorides, chlorides, bromides, iodides) crystals and glasses, some oxide crystals such as Y_2SiO_5, $KGd(WO_4)_2$ and YAG, and possibly even a few non-silica oxide glasses (Hehlen 2009). In contrast, Er^{3+}, Tm^{3+}, Ho^{3+}, and Dy^{3+} have first excited states with much lower energies, *i.e.* ~6100 cm^{-1}, ~5200 cm^{-1}, 4700 cm^{-1}, and ~3150 cm^{-1}, respectively. While the smaller gap and thus lower laser pump energy, in principle, allow for a higher cooling efficiency [see Eq.(14)], finding viable host materials to realize this potential is more challenging. Oxides become marginal for laser cooling with Tm^{3+} for which a halide material such as a fluoride is required. No laser cooling has yet been demonstrated for a Dy^{3+} doped material for which a host material with $\hbar\omega_{\max} < 400$ cm^{-1} is needed. This is only realized in sulfides and the heavy halides (chlorides, bromides, iodides). These materials are generally very hygroscopic and mechanically weak, posing formidable challenges during synthesis and sample preparation.

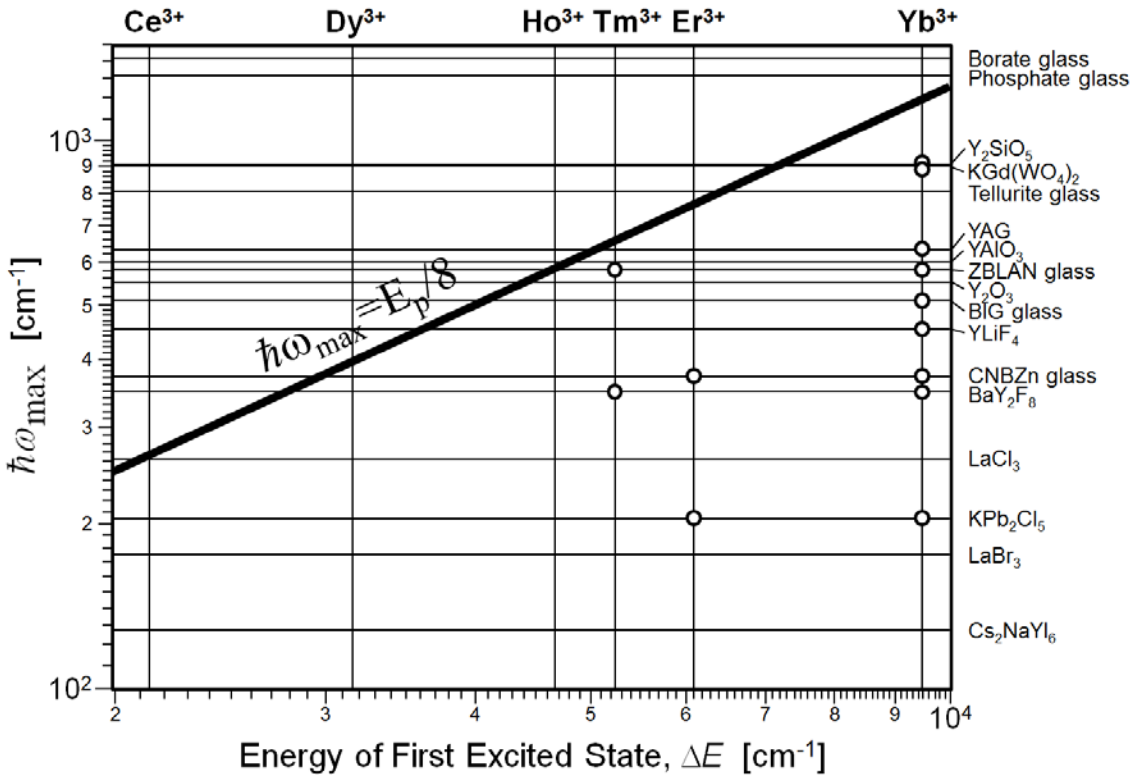

Figure 12: Combinations of Ln^{3+} ions and host materials. Combinations for which $\hbar\omega_{\max} < \Delta E/8$ are expected to be candidates for optical refrigeration. The open circles indicate materials for which optical refrigeration has been observed to date (Hehlen 2009).

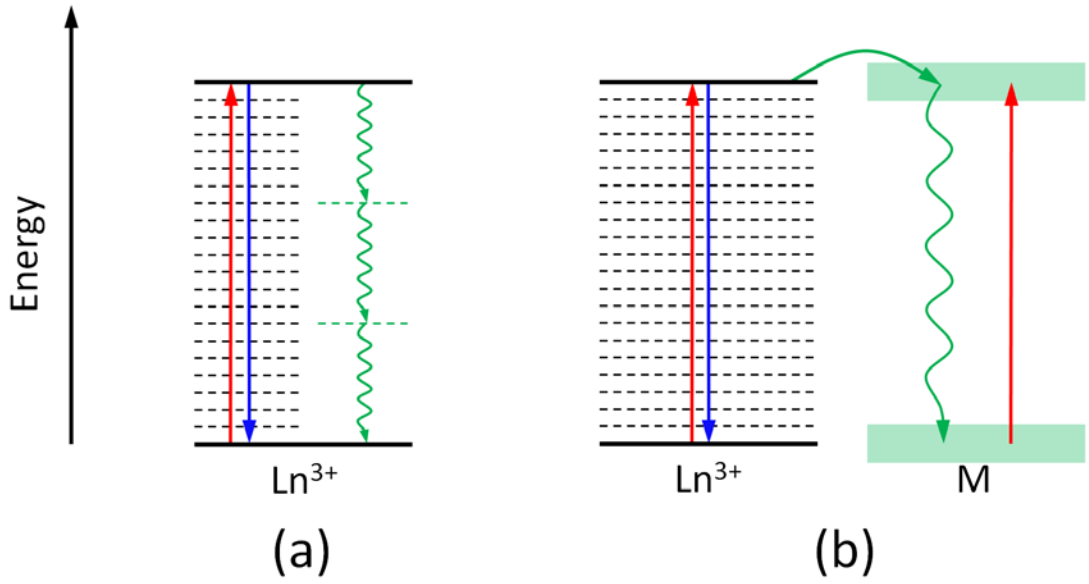

Figure 13: Non-radiative decay mechanisms of the excited state of a laser cooling ion caused by impurities (shown in green). Multiphonon relaxation can be induced by (a) molecular impurities with high-energy vibrational modes (green dashed lines) and (b) energy transfer to an impurity ion having low quantum efficiency. The black dashed horizontal lines indicate the low-energy optical phonon modes of the host material. The red and blue arrows represent the pump and fluorescence wavelength, respectively, of the laser cooling cycle.

3.2. Role of Impurities

Section 3.1 considered multi-phonon relaxation in which the accepting vibrations were modes of the host material itself. As illustrated in Figure 13 however, multi-phonon relaxation can also be introduced by impurities that are present in the material. One possibility is multi-phonon relaxation caused by molecular species that are incorporated inadvertently in the host material. Depending on the preparation conditions, hydroxyl (OH^-), ammonium (NH_4^+), sulfate (SO_4^{2-}),

phosphate (PO_4^{3-}), and carbon dioxide (CO_2) species can be present as impurities. Such molecular species are more easily incorporated into the three-dimensional amorphous network of glasses than into crystals. For example, CO_2 , CO, and O_2 gases can dissolve into or react with ZBLAN glass melts (Parker 1989). Molecular species usually have vibrational modes with much higher energies than the optical phonon modes of the host material. They therefore become likely acceptor modes in multi-phonon relaxation and reduce the quantum efficiency of the Ln^{3+} exited state, as shown in Figure 13a.

Another possibility is the presence of metal ions (M) with absorptions near the laser-cooling wavelength. As shown in Figure 13b, energy can be transferred from the excited Ln^{3+} to a nearby M ion which then decays via multi-phonon relaxation, thereby reducing the quantum efficiency of the Ln^{3+} excited state. The $Ln^{3+} \rightarrow M$ energy transfer can occur non-radiatively due to electric-multipole interactions, and its rate is particularly high if the donor and acceptor levels are in resonance (Dexter 1953). Furthermore, the rate increases with increasing product of the oscillator strengths of the Ln^{3+} emission (donor) and the M absorption (acceptor) transitions. The latter becomes especially large if the transition on the M ion is allowed. Many transition metal ions such as Fe^{2+}, Cu^{2+}, Co^{2+}, Ni^{2+}, Cr^{3+}, V^{3+}, and Ti^{3+} have transitions with high cross sections in the near infrared spectral region (France, Carter et al. 1986) where many of the laser-cooling transitions are located (Figure 7), and they are thus detrimental to laser cooling. Two additional effects further exacerbate the problem. First recall that high Ln^{3+} ion concentrations are desired in order to increase the absorption efficiency [Eq.(15)]. In this regime however, energy migration among the Ln^{3+} ions is efficient, and the M impurities become accessible to a large number of Ln^{3+} ions. The M ions act as efficient traps for excitation energy and further reduce the quantum efficiency. Second, the often large cross section of the M ions causes a background absorption

(α_b) and thus reduces the absorption efficiency [Eq.(15)], *i.e.* a portion of the incident pump laser light is absorbed directly by the M ions followed by conversion to heat. Hehlen *et al* have estimated an upper limit of 10–100 ppb (parts-per-billion) for transition metal impurities in Yb^{3+}-doped ZBLAN glass for efficient laser cooling (Hehlen, Epstein et al. 2007). The upper limit for other Ln^{3+} impurities (such as Er^{3+}, Tm^{3+}, and Ho^{3+} ions in Yb^{3+}-based laser-cooling materials) appears to be much higher than for transition metals. This is because the product of donor and acceptor oscillator strengths is smaller as it involves two forbidden 4*f* transitions. Furthermore, Ln^{3+} excited states have generally higher quantum yields so that Ln^{3+} impurities tend to primarily decay via radiative relaxation without adding excessive heat load. Goldner *et al* studied the effect on Er^{3+} and Tm^{3+} impurities in a ZBLAN glass doped with 2.9 mol% YbF_3 (5×10^{20} Yb^{3+}/cm^3) (Goldner and Mortier 2001). They found that Er^{3+} had a negligible effect up to 10^{17}–10^{18} Er^{3+}/cm^3, *i.e.* a concentration of 6–60 ppm (parts-per-million). The presence of Tm^{3+} was even less problematic, with concentrations up to 10^{19} Tm^{3+}/cm^3 (~600 ppm) having negligible effect on laser cooling.

The aforementioned considerations were recently corroborated by Melgaard *et al* who have performed a detailed analysis of metal impurities in a series of YLF crystals doped with 1%, 5%, 7% and 10% Yb^{3+} (Melgaard 2013, Melgaard, Seletskiy et al. 2013). For this purpose, they managed to dissolve the chemically very stable $YLiF_4$ by boiling finely crushed crystal powder in a 1:1 volume mixture of 15 N nitric acid and 6 N hydrochloric acid (*aqua regia*) for several hours. The reactants were contained in a lidded Teflon container that was previously leached in acid to minimize recontamination from the container. The dissolved YLF:Yb^{3+} was then analyzed by a quadrupole mass spectrometer (ICP-MS) to measure the concentrations of a large number of different trace metals. In addition, they performed optical measurements of α_b

for each of the original YLF:Yb^{3+} crystals. They found that the iron concentration showed a statistically significant correlation with α_b and was the main source of background absorption. The further discovered that α_b decreased with increasing YbF_3 added to $YLiF_4$. Their 10% Yb^{3+} doped YLF crystal had a record-low background absorption coefficient of $\alpha_b = 2.0\times10^{-4}$ cm^{-1} and in turn produced the lowest temperature of 114 ± 1 K of the samples analyzed. This study provided quantitative information on the role of different impurities and serves as valuable guidance for future material purification efforts.

It was observed early on that samples of nominally the same composition and pedigree often differed substantially in their laser-cooling performance. This was considered to be a result of both surface contamination and impurities in the bulk material (Mungan, Buchwald et al. 1997). Reducing the amount of transition-metal impurities was therefore of high priority. Zhou *et al* proposed an electrochemical approach to purifying ZBLAN melts (Zhou, Newman et al. 1992), a method that was further studied by Macfarlane *et al* (MacFarlane, Javorniczky et al. 1999, MacFarlane, Zhou et al. 2004). Their goal was to lower the amount of reduced zirconium species as well as transition metal ions to obtain fluoride glasses suited for the fabrication of ultra-low loss optical fibers. They contained the ZBLAN melt in a glassy carbon crucible at 600 ^oC in nitrogen atmosphere and inserted a three-electrode system into the melt consisting of a 10 mm × 10 mm Pt plate as working electrode, a Pt wire as reference electrode, and the crucible itself as the counter electrode. The electrochemical window of the glass extended from +400 mV, a potential at which fluorine is generated at the anode, to -1300 mV, a potential at which Zr^{4+} or Al^{3+} are reduced at the cathode. They showed that within this window, transition metal ions could be removed from the melt by depositing them at the cathode at -220, -400, -400, and -650 mV for Cu, Ni, Co, and Fe, respectively (Zhou, Newman et al. 1992, Zhou, Newman et al. 1993,

Zhou, Newman et al. 1993). The electrochemical treatment also lowered the amount of reduced Zr species. Fajardo *et al* explored this approach for preparing high-purity fluoride glasses for laser-cooling (Fajardo, Sigel Jr et al. 1997). During the preparation of ZBLANP:Yb^{3+}, they exposed the melt to a voltage for a periods of 1, 6, 12, and 24 hours at 600 ^{o}C. Their main focus was the removal of iron impurities, and the voltage was therefore slowly increased to above the cathodic deposition potential for Fe. Using photothermal deflection spectroscopy to probe internal cooling, they found that glasses made from melts that were electrochemically treated for <6 hours (or not at all) exhibited no laser cooling while glasses that were treated for >6 hours did. The magnitude of the improvement however was less than expected, and their result indicated that some level of impurities remained. Murtagh *et al* used resonant laser ablation combined with mass spectrometry to obtain a semi-quantitative analysis of trace transition metals in fluoride glasses fabricated with and without electrochemical purification (Murtagh, Sigel Jr et al. 1999). They found that exposing a ZBLANP:Yb^{3+} melt to a voltage for 18 hours at 600 ^{o}C reduced Fe, Cr, and Cu impurities by factors of 4.2, 5.5, 18.0 with respect to the untreated glass. Removal of Cu was more efficient than of Fe due to the smaller cathodic plate-out potential of Cu (-220 mV) compared to Fe (-650 mV). This sample showed internal cooling by 0.33 K as measured by photothermal deflection spectroscopy. Another glass (BIG:Yb^{3+}) showed a much smaller improvement upon electrochemical purification, likely because the electrochemical window of BIG glass was not known and the treatment potential may have been chosen incorrectly.

Patterson *et al* pursued a different purification method (Patterson, Stark et al. 2011). Instead of purification at the melt stage, they developed a procedure for purifying each of the starting materials of Yb^{3+}-doped ZBLANI (ZrF_4–BaF_2–LaF_3–AlF_3–NaF– InF_3) glass prior to

glass melting. The chemical inertness and relatively high melting temperatures of metal fluorides makes them unsuited for many standard purification techniques such as recrystallization, zone refining, sublimation, or distillation. Therefore, Patterson *et al* started from high purity commercial precursors that were not fluorides, *i.e.* $ZrCl_2O{\cdot}8H_2O$, $BaCO_3$, La_2O_3, $AlCl_3{\cdot}6H_2O$, Na_2CO_3, La_2O_3, In metal, and Yb_2O_3. These precursors were dissolved in ultra-high purity water or acids, filtered through 0.2 μm pore size filters, and then subjected to a three-step solvent extraction process. It first involved the addition of ammonium-pyrrolidinedithio-carbamate (APDC) to the aqueous metal ion solution followed by addition of methyl-isobutylketone (MIBK), an organic solvent that is immiscible with water, thus forming a two-phase system. APDC had a strong affinity for transition-metal ions, and the respective APDC-metal coordination complexes were extracted to the MIBK phase because they were more soluble in the organic than in the aqueous phase. Hydrofluoric (HF) acid was added in a final step to precipitate the high purity metal fluoride that was subsequently dried in hot HF gas before being used in ZBLANI:Yb^{3+} glass fabrication. They tracked the evolution of trace metals in the Zr solution as it was purified by solvent extraction, and they found that the total transition-metal concentration (Cu, Fe, Co, Ni, V, Cr, Mn, Zn) was reduced from 72540 ppb to 115 ppb after the third solvent extraction step, a 650-fold purification. Of these, Fe was the dominant impurity and was reduced 882-fold from 51600 ppb to 58.5 ppb. A sample of ZBLANI:Yb^{3+} fabricated by this process showed internal laser cooling to a temperature of 238 K (Patterson, Seletskiy et al. 2010), a result that was on par with the best cooling results achieved with ZBLAN-based materials. However, the many components of ZBLANI glass make such a purification method extremely laborious and also prone to recontamination during the numerous processing steps.

Chelate-assisted solvent extraction is therefore more attractive for the purification of crystalline systems that typically have a small number of precursors.

The above melt and solvent purification methods were developed for fluoride glasses, and they are expected to be adaptable to crystalline systems. We also note that the process of growing a crystal is in itself a purification method; the growth of a highly ordered crystal lattice tends to include or exclude trace impurities based on both their ionic radius and their charge. This area of research has not received much attention yet, and studies analyzing impurity concentrations in starting materials and laser-cooling crystals grown from those are expected to yield valuable insights.

3.3. Homogeneous and Inhomogeneous Broadening

The quasi-zero Stokes shift associated with electronic transitions within the 4*f* shell produces spectral profiles in absorption and emission that are relatively narrow compared to allowed Stokes-shifted transitions (see Figure 8). In a Ln^{3+}-doped solid, the spectral width of electronic transitions is determined by both homogeneous and inhomogeneous effects. Homogeneous broadening equally affects all Ln^{3+} ions in the solid and includes the broadening induced by (1) the modulation of the crystal-field via the thermal motions of the coordinating atoms and (2) the decay (lifetime) of the transition final state. The magnitude of both contributions is temperature dependent, and the homogeneous width of the Lorentzian spectral profile increases with increasing temperature with a T^k dependence. $k \approx 2$ above the Debye temperature, but lower values of $k = 1 \ldots 2$ are often observed at $T < 50$ K (Lei, Anderson et al. 1998). In contrast,

inhomogeneous broadening is a result of different local coordination geometries of the Ln^{3+} ions. The distribution of different local crystal fields causes a distribution of transition energies for the ensemble of Ln^{3+} ions in the solid, independent of temperature. Inhomogeneous broadening is generally well described by a Gaussian distribution of crystal fields and thus transition energies. It is absent in a perfect crystal in which all Ln^{3+} ions are subjected to an identical crystal field and thus produce the same transition energies (assuming that there is only one site for the Ln^{3+} ion in crystal lattice). In contrast, the structural disorder in glassy materials offers a range of different coordination environments for Ln^{3+} ions and can correspondingly lead to substantial inhomogeneous broadening. In this case, the Lorentzian homogeneous lineshape profile $g_L(\nu)$ with width $\Delta\nu_L$ is convoluted with the inhomogeneous Gaussian distribution of transition energies $g_G(\nu)$ with width $\Delta\nu_G$. The resulting spectral shape is described by the Voigt profile $g_V(\nu,T)=\int_{-\infty}^{\infty} g_G(\nu')\,g_L(\nu-\nu',T)\,d\nu'$ (Schreier 1992, Di Bartolo 2010), which includes the dependence of the homogeneous linewidth on temperature.

Lei *et al* have performed a detailed study of the magnitude of homogeneous and inhomogeneous broadening as a function of temperature in a 1% Yb^{3+}-doped ZBLANP glass (Lei, Anderson et al. 1998). They deconvoluted the Voigt profiles measured for the $^2F_{7/2}\rightarrow{}^2F_{5/2}$ absorption and $^2F_{5/2}\rightarrow{}^2F_{7/2}$ emission and determined an inhomogeneous linedwidth of 990 ± 40 GHz, a value that was found to be essentially independent of temperature (see Figure 14). The homogeneous linewidth increased with a nearly T^2 dependence in the 10–300 K temperature range, as expected. It is important to note that inhomogeneous broadening dominated homogeneous broadening for all temperatures in this range.

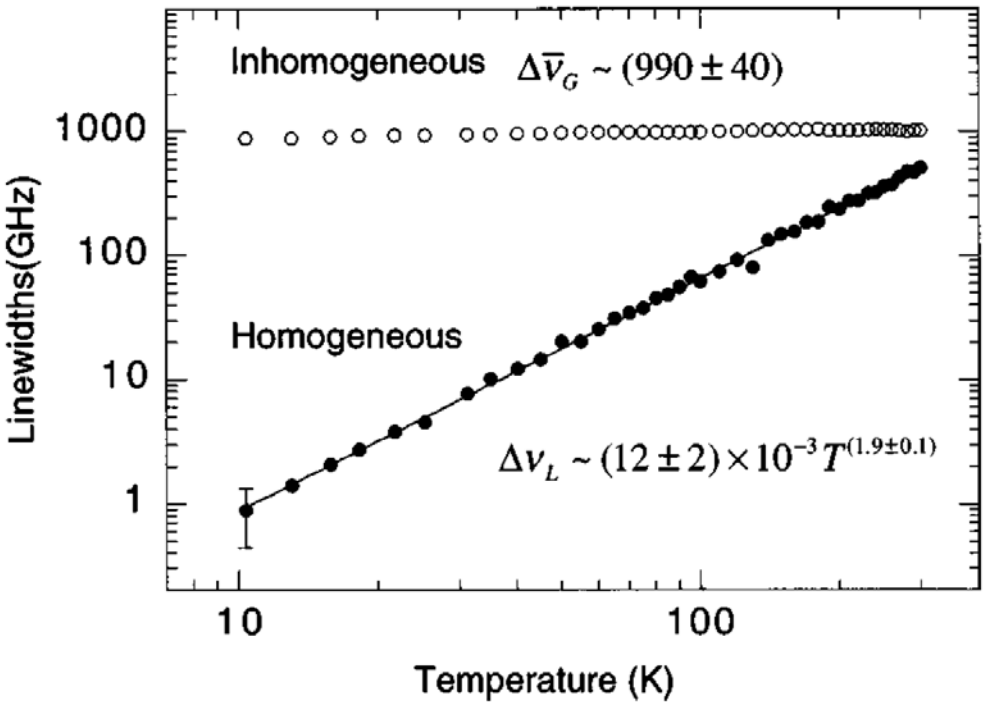

Figure 14: Homogeneous and inhomogeneous linewidths of the $^2F_{5/2}(E5) \rightarrow {}^2F_{7/2}(E1)$ transition of Yb^{3+} (see Figure 9, left) in ZBLANP fluoride glass (Lei, Anderson et al. 1998). Reproduced with permission from the American Physical Society, Copyright (2014).

The absorption coefficient of a crystal-field transition is given by $\alpha(\nu,T) = \sigma(\nu,T)N(E_i,T)$. The cross section is given by $\sigma(\nu,T) = (1/8\pi)(g_2/g_1)\lambda^2 A_{21} \cdot g_V(\nu,T)$, where A_{21} is the Einstein coefficient for spontaneous emission, g_1 and g_2 are the degeneracy factors of the ground and excited state, respectively, λ is the transition wavelength, and $g_V(\nu,T)$ is the spectral lineshape function. $N(E_i,T)$ is the thermal population density of the initial state at energy E_i at T, and it is proportional to $\exp(-E_i/kT)$. Therefore, $\alpha(\nu,T)$ is proportional to $g_V(\nu,T)\exp(-E_i/kT)$. In a glassy

material such as ZBLAN where inhomogeneous broadening dominates, therefore $g_V(\nu,T) \approx$ constant, and the peak absorption coefficient decreases exponentially with temperature. For a crystal, in contrast, inhomogeneous broadening is negligible, and the homogeneous lineshape is given by the area-normalized Lorentzian profile

$$g_V(\nu,T) = g_L(\nu,T) = \frac{2}{W\pi} \; \frac{1}{1+\frac{4(\nu-\nu_0)^2}{W^2}} \tag{22}$$

where ν_0 is the mean transition frequency, and W is the full width at half maximum. Assuming that the homogeneous linewidth scales as $W \propto T^2$, one finds that the peak value of the lineshape ($\nu = \nu_0$) is proportional to T^{-2}, thus the peak absorption coefficient is proportional to $T^{-2}\exp(-E/kT)$. That is, as temperature decreases, the decrease in thermal population is partially offset by the reduction in homogeneous linewidth and the corresponding increase in peak cross section. As a result, an electronic transition maintains a higher *peak* absorption coefficient, α, with decreasing temperature in a crystal than in a glass. Using the linewidths shown in Figure 14, one predicts that at 150 K, the peak value of α is 6.4× greater in a crystal than in ZBLAN glass. This is indeed found for the E4→E5 transition in ZBLAN:Yb^{3+}, as was shown earlier in Figure 6. The α advantage of crystals over glasses is predicted to grow to ≈23 fold at 80 K, and it directly translates into an increased absorption efficiency [Eq.(15)] and thus

cooling power [Eq.(10)]. This is one reason why crystals have generally shown better laser-cooling performance than glasses. Conversely, the higher peak absorption coefficient of crystals enables them to tolerate a higher background absorption for the same absorption efficiency, thus relaxing the purity requirements to reach a given laser-cooling performance.

4. EXPERIMENTAL TECHNIQUES

4.1. Reciprocity of Absorption and Luminescence

Equation (12) has highlighted the need for measuring the absorption spectrum as a function of temperature, in particular the absorption coefficient at the pump wavelength, $\alpha(T)$. Laser excitation is usually performed in the long-wavelength tail of the absorption spectrum (see Figure 10) to maximize the cooling efficiency [see Eq. (14)]. However, the absorption coefficients are typically small in this regime because of the low thermal population of the initial state, and they decrease rapidly with decreasing temperatures. This poses experimental challenges that make it difficult to determine $\alpha(T)$ directly from absorption spectroscopy. Absorption spectra are therefore often calculated from luminescence via reciprocity. McCumber has shown in 1964 (McCumber 1964) that the absorption and luminescence spectra of a given transition $i \leftrightarrow j$ are related because the Einstein coefficients of absorption, spontaneous emission, and stimulated emission are governed by the same matrix elements ($\sigma_{ij} = \sigma_{ji}$) and because of the principle of detailed balance (Siegman 1986). Quimby *et al* have explored the

applicability of McCumber's theory and shown that it is only strictly valid if the linewidth of all crystal-field transitions is $\ll kT$ (Quimby 2002). Following their derivation and notation, we consider luminescence transitions between the crystal-field transitions of an excited state (i) and of the ground state (j). Assuming thermal equilibrium among the crystal-field levels, the emission cross section is given by an average over initial states and a sum over final states, *i.e.*

$$\sigma_e(h\nu) = \sum_i \sum_j \frac{\sigma_{ij}(h\nu) e^{-\Delta_i/kT}}{Z_2} \tag{23}$$

where the partition function $Z_2 \equiv \sum_i \exp(-\Delta_i/kT)$ and Δ_i is the energy of the initial state with respect to the lowest crystal-field level of the excited state. In analogy, the absorption cross section is given by

$$\sigma_a(h\nu) = \sum_j \sum_i \frac{\sigma_{ji}(h\nu) e^{-\Delta_j/kT}}{Z_1} \tag{24}$$

where the partition function $Z_1 \equiv \sum_j \exp(-\Delta_j/kT)$ and Δ_j is the energy of the initial state with respect to the lowest crystal-field level of the ground state. Note that $\Delta_i + E_0 = \Delta_j + E_{ij}$, where

E_0 is the energy difference between the lowest crystal-field levels of the excited and ground state multiplets and E_{ij} is the transition energy. This yields the exact relation

$$Z_2\sigma_e(h\nu) = \sum_i \sum_j \sigma_{ij}(h\nu)\, e^{-\Delta_j/kT} e^{-(E_{ij}-h\nu)/kT} e^{-(E_0-h\nu)/kT} \tag{25}$$

Assuming that the linewidth δE_{ij} is much less than kT yields $\left|E_{ij}-h\nu\right|/kT \ll 1$. Using the relation $\sigma_{ij}(h\nu) = \sigma_{ji}(h\nu)$ and introducing an effective energy, ε, according to $e^{\varepsilon/kT} \equiv (Z_1/Z_2)e^{E_0/kT}$ simplifies Eq. (25) to the usual McCumber equation

$$\sigma_e(h\nu) = \sigma_a(h\nu)e^{(\varepsilon-h\nu)/kT} \tag{26}$$

The assumption $\delta E_{ij} \ll kT$ is quite good for homogeneously broadened 4*f* crystal-field transitions in the 0–300 K temperature range. At 300 K, homogeneous linewidths are in the 20–80 cm^{-1} range, which is small compared to $kT \approx 210$ cm^{-1}. Equation (26) can therefore be used to relate emission and absorption spectra of crystalline systems for $T \le 300$ K, which encompasses many situations in solid-state laser cooling studies.

The presence of substantial inhomogeneous broadening in glasses adds complication. Quimby *et al* have studied this case in detail (Quimby 2002). Starting from the homogeneous case discussed above, they introduced inhomogeneous broadening by defining a "site" variable, Q, that followed a Gaussian distribution $f(Q) = \left(1/\sqrt{\pi}\right)\exp\left(-Q^2\right)$. They assumed an $f(Q)$ distribution of energies for each crystal-field level and a linear dependence of the cross section on Q. They found that there is no simple relationship between absorption and emission profiles in the presence of inhomogeneous broadening. As seen in Section 3.3, the presence of both homogeneous and inhomogeneous broadening leads to Voigt profiles that arise from the convolution of the respective Lorentzian and Gaussian lineshapes. Quimby *et al* showed that the McCumber equation for the inhomogeneous case

$$\sigma_e^{\text{inh}}(h\nu) = \sigma_a^{\text{inh}}(h\nu)e^{(\varepsilon - h\nu)/kT} \tag{27}$$

is still valid as long as the width of the Voigt profile, δE_V, is less than kT. This implies that both the homogeneous and the inhomogeneous width must be $\ll kT$. Subsequent studies by Martin *et al* of Nd^{3+}-doped fluorozirconate glass and Nd^{3+}-doped silicate glass found that the McCumber theory deviated significantly from observations for $kT < 1.8\ \Delta\nu_{\text{inh}}$ (Martin and Quimby 2006, Martin and Quimby 2007). Referring back to Figure 14, the homogeneous and inhomogeneous linewidths in ZBLANP:Yb^{3+} at 300 K were ~ 20 and ~ 33 cm^{-1}, respectively,

which are small compared to $kT \approx 210$ cm^{-1} and justify the use of McCumber's equation. The lower limit of validity is expected at ~ 85 K below which $kT < 1.8\ \Delta\nu_{inh}$.

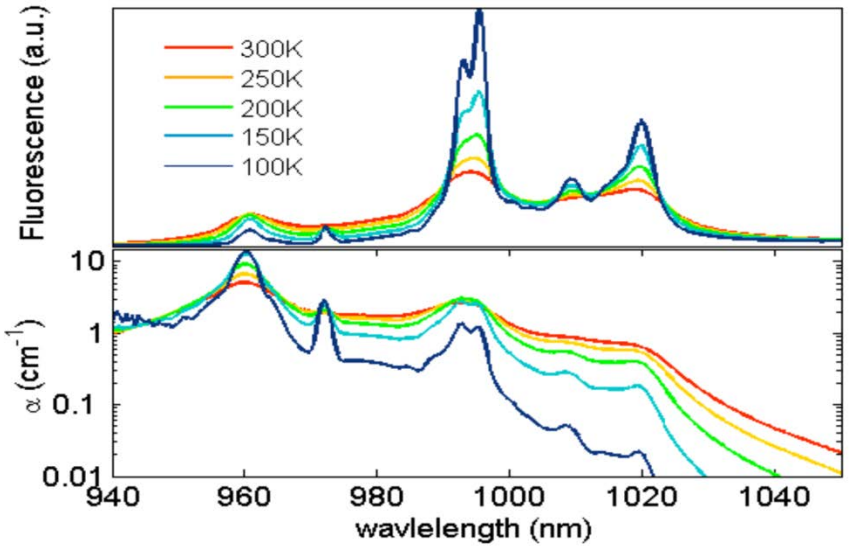

Figure 15: Determination of the absorption spectrum of a YLF:Yb^{3+} crystal via reciprocity from luminescence spectra (Melgaard, Seletskiy et al. 2010). Note the rapid decrease in the absorption coefficient at the E4→E5 pump transition around 1020 nm with decreasing temperature.

McCumber and Martin have shown that the error in absorption cross sections derived from emission spectra within the validity range of McCumbers equation is on the order of 3–5%. Despite such errors, reciprocity is a particularly valuable tool for the characterization of laser cooling materials. Direct absorption measurements become impractical for absorption coefficients <0.03 cm^{-1}, a regime in which background subtraction errors dominate the measured absorption signal (Epstein, Brown et al. 2001). An example of a reciprocity analysis for Yb^{3+}-

doped YLF is shown in Figure 15 (Melgaard, Seletskiy et al. 2010). The absorption coefficient of the pumped E4→E5 crystal-field transition around 1020 nm in the long-wavelength of the spectrum rapidly drops into the $10^{-2} - 10^{-3}$ cm^{-1} range with decreasing temperature. Reciprocity is therefore preferred over direct absorption measurements to quantify the small pump absorption coefficients at low temperatures.

4.2. Thermometry Techniques

The measurement of the sample temperature is clearly one of the key experiments in solid-state optical refrigerator research, and a great amount of work has been dedicated to developing a variety of techniques. Typical experiments include the measurement of the local temperature at the laser focal area inside a sample, the measurement of the bulk sample temperature, and the measurement of the temperature of a payload attached to the laser-cooling material. Infrared cameras, thermocouples, laser deflection, Mach-Zehnder interferometers, and luminescence thermometry have all been employed in a variety of configurations for this purpose. Each method has a set of advantages and disadvantages as well as an inherent temperature range in which sufficient sensitivity is achieved. The main distinction is between contact and non-contact techniques, with the latter having prevailed in recent times. A review published in 2003 by Rayner *et al* discussed the earlier thermometry techniques including photo-thermal deflection spectroscopy, fluorescence thermometry, and micro-thermocouples (Rayner, Heckenberg et al. 2003). These are described below along with more recent advances in optical thermometry.

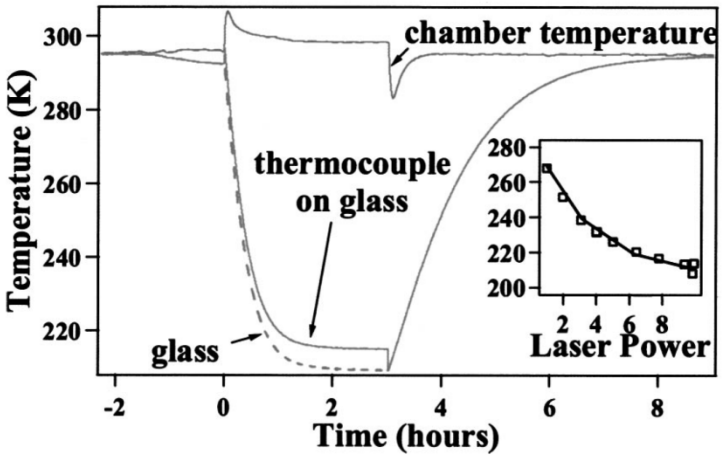

Figure 16: Measurement of optical refrigeration in ZBLANP:Yb^{3+} glass using thermocouples (TC) (Thiede, Distel et al. 2005). The lower solid curve corresponds to the TC readings from cooling element, and the upper solid curve corresponds to the TC readings attached to the sample chamber. The pump laser ($\lambda = 1026$ nm, $P_0 = 9.6$ W) is turned on at $t = 0$ hrs and blocked at $t = 3.1$ hrs. The inset shows the lowest temperatures achieved for different pump powers ($\lambda = 1026$ nm).

Thermocouples

The most obvious and deceptively simple method is to attach a thermocouple or diode to the laser-cooling medium and measure the temperature via the electrical response of the sensor. As early as 1968, Kushida *et al* used a thermocouple attached to the Nd^{3+}-doped YAG crystal in their first observation of reduced heating in a solid upon optical pumping (Kushida and Geusic 1968). Edwards *et al* used both *T*- and *K*-type thermocouples glued to ZBLAN:Yb^{3+} glass (Edwards, Anderson et al. 1999). They recognized that conduction of heat through the thermocouple wires as well as absorption of sample fluorescence by and associated heating of

the thermocouple distorted the measurements. Some improvement was achieved by reducing the diameter of the thermocouple wires from 1 to 0.5 mil (12.7 μm). Thiede *et al* used a similar setup in their record-cooling result with ZBLANP:Yb^{3+} to 208 K (Thiede, Distel et al. 2005). They epoxied a 0.5 mil diameter *K*-type thermocouple to the backside of the cooling element, accompanied by thermocouples on the sample chamber and the chamber base. As shown in Figure 16, the chamber and cooling-element temperature rose quickly when the laser was turned on (at $t = 0$ hr), and both showed a drop when the laser was turned off (at $t = 3.1$ hr). This effect was attributed to fluorescent heating of the chamber and the cooling-element thermocouple when the pump laser was on. Rayner *et al* have pointed out correctly that such fine-gauge thermocouple are mechanically quite fragile and difficult to mount to the cooling element (Rayner, Heckenberg et al. 2003). They used an *E*-type (Ni:Cr–Ni:Cu) unsheathed fine-gauge thermocouple with a sensitivity of 0.05 mV K^{-1} in the -20–70 ^{o}C temperature range (Rayner, Hirsch et al. 2001). They first pumped the 250-μm diameter ZBLAN:Yb^{3+} fiber (cooling medium) for 3 min to induce steady-state optical cooling, then they blocked the laser, brought the thermocouple in contact with the sample, and measured its signal as it equilibrated with the sample temperature over the course of about 2 minutes. Condon *et al* used a fine-wire (1 mil diameter) *T*-type (copper/constantan) thermocouple in contact with their KPb_2Cl_5:Er^{3+} sample and its complementary junction in contact with an isothermal block (Condon, Bowman et al. 2009, Condon, Bowman et al. 2010). A second identical thermocouple was placed near the sample as a reference. As in the above experiment by Rayner *et al*, they avoided the undesired heating of the thermocouple by sample fluorescence and stray pump light by first exciting the sample for ~6 minutes, then turning off the laser, and recording the thermocouple signal at 5 Hz for 200 s. Depending on the final temperature of the crystal, the thermocouple would either cool

or heat in an exponential fashion as it re-equilibrated back towards ambient temperature. This procedure was repeated for different pump wavelengths, and they were able to quantify the transition from laser-induced cooling to laser-induced heating as the pump wavelength was tuned from 1567.6 to 1527.0 nm. Murtagh *et al* used a calibrated silicon diode, rather than a thermocouple, in their laser-cooling evaluation of various Yb^{3+}-doped fluorozirconate glasses (ZBLANP and BIGaZYbTZr), however, they did not provide detailed information on the diode type and arrangement (Murtagh, Sigel Jr et al. 1999).

Such contact measurements of temperature are appealing because they provide a direct measure of the bulk cooling element temperature. Furthermore, the extraction of heat from an attached sensor is in itself a demonstration of cooling a thermal load. However, the use of thermocouples becomes difficult because of fluorescent heating and heat conduction through the wires. These drawbacks can be avoided with some of the non-contact thermometry methods reviewed in the following.

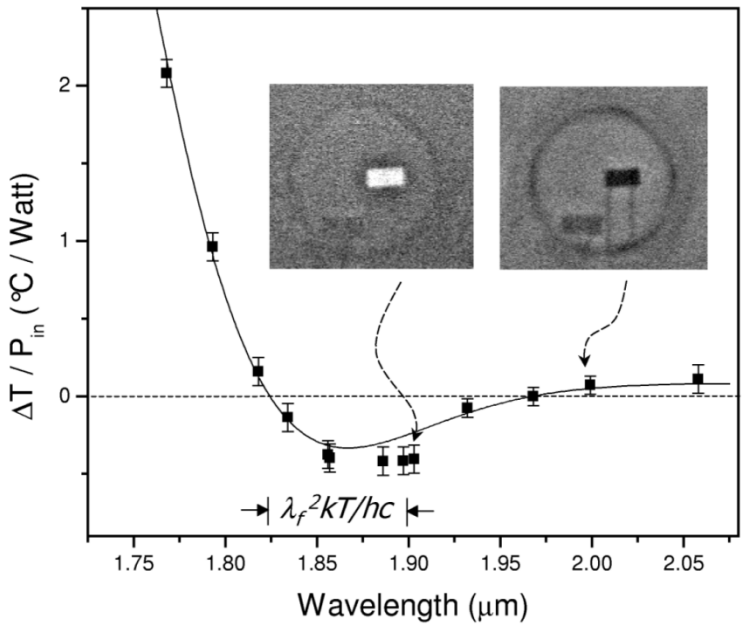

Figure 17: Temperature measurement of a Tm^{3+}-doped ZBLANP sample using a pyroelectric infrared camera (inset) (Hoyt, Sheik-Bahae et al. 2000). The pumped sample (middle right in chamber) is compared to an un-pumped reference sample (bottom left in chamber) to determine the net temperature change. The sample changes from cooling to heating as the pump laser wavelength is tuned from 1.90 to 2.00 μm (main graph).

Thermal Cameras

The first report of optical refrigeration in ZBLANP:Yb^{3+} used a liquid-nitrogen cooled InSb infrared camera for the non-contact measurement of temperature (Epstein, Buchwald et al. 1995). InSb has spectral sensitivity in the 3–5 μm spectral range while being insensitive to the pump laser light and Yb^{3+} fluorescence around 1 μm. However, ZBLANP glass like all fluorides has a low emissivity in the 3–5 μm spectral range. Therefore, a 1-mm^2 gold foil was attached to the ZBLANP:Yb^{3+} sample and painted black on the outside in order to enhance the emissivity.

The assumption was that the outer black surface of the foil would be a good measure of the sample temperature while the inner shiny surface would reflect >90% of the fluorescence light and therefore not experience substantial fluorescent heating. This method was susceptible to drifts of the ambient temperature, and a reference sample was therefore placed next to the pumped sample in the field of view of the camera. The authors were able to resolve temperature differences of 0.02 K between the two samples. Hoyt *et al* used a pyroelectric camera to measure the temperature of a Tm^{3+}-doped ZBLANP sample (Hoyt, Sheik-Bahae et al. 2000, Sheik-Bahae, Hoyt et al. 2000, Sheik-Bahae, Hoyt et al. 2001). The thermal images in Figure 17 (inset) clearly show the sample (middle right in chamber) changing from cooling to heating as the pump-laser wavelength is tuned from 1.90 μm (maximum cooling) to 2.00 μm (heating due to background absorption). The un-pumped reference sample is seen faintly at the bottom left in the chamber, and it allowed the determination of the net temperature change induced by optical refrigeration. In this study, the sample was imaged directly, *i.e.* without the application of a black foil. Similar infrared camera based temperature measurements were reported by Epstein *et al* for Yb^{3+}-doped YAG and Y_2SiO_5 (Epstein, Brown et al. 2001), Patterson *et al* for $BaY_2F_8:Tm^{3+}$ (Patterson, Hasselbeck et al. 2004, Patterson, Bigotta et al. 2008), Bigotta *et al* $BaY_2F_8:Tm^{3+}$ (Bigotta, Parisi et al. 2006, Bigotta, Parisi et al. 2006), Guiheen *et al* for Yb^{3+} and Tm^{3+} doped ABCYS glasses (Guiheen, Haines et al. 2006), Bigotta *et al* for $BaY_2F_8:Yb^{3+}$ (Bigotta, Di Lieto et al. 2007), and Seletskiy *et al* for ZBLAN:Yb^{3+} (Seletskiy, Hasselbeck et al. 2010). Hoyt *et al* found that thermal pyroelectric or microbolometer based thermal cameras have an absolute resolution of ~0.2 K in the $\Delta T = \pm 10$ K range from room temperature (Hoyt, Hasselbeck et al. 2003), which limits their use to the study of cooling performance around room temperature. However, thermal cameras are relatively easy to use and therefore attractive for sample screening purposes.

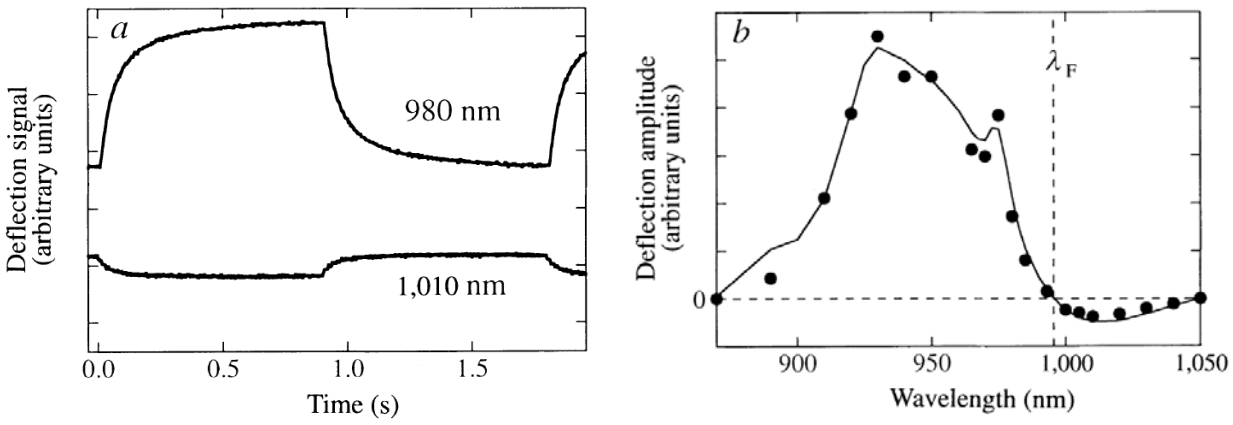

Figure 18: Photo-thermal deflection waveforms of ZBLANP:Yb^{3+} glass. (a) Deflection waveforms for two pump wavelengths showing the 180° phase difference between pumping at 980 nm (heating) and at 1010 nm (cooling); (b) Deflection amplitude as a function of wavelength showing sign reversal as wavelength is tuned from the heating ($\lambda_p < \tilde{\lambda}_f$) to the cooling ($\lambda_p > \tilde{\lambda}_f$) regime. *Reprinted by permission from Macmillan Publishers Ltd: Nature, R. I. Epstein et al, Vol. 377, pp. 500–503, Copyright 1995.*

Photo-Thermal Deflection Spectroscopy (PTDS)

PTDS is another non-contact thermometry technique that has found widespread use in the field. It measures the local temperature near the pumped volume within a sample. It was first described in detail by Boccara *et al* who used this technique for measuring ultra-low absorption coefficients (10^{-5} cm^{-1}) in highly transparent solids (Boccara, Jackson et al. 1980). The technique is based on the thermo-optic coefficient, *i.e.* the change of refractive index with temperature, which is typically negative. When a laser beam is incident on an absorbing medium, a local radial temperature gradient is established which in turn induces a local radial refractive-index

gradient via the thermo-optic effect. This index gradient causes a probe laser beam propagating parallel or anti-parallel to the pump laser to deflect. If the pump laser heats the sample, a divergent lens is formed and the probe beam is deflected away from the pump beam. Conversely, if the pump laser cools the sample, a convergent lens is formed and the probe beam is deflected toward the pump laser (Rayner, Heckenberg et al. 2003). This 180° phase reversal can be used to detect the presence of laser-induced heating and cooling. The thermo-optic effect can be assumed linear for small temperature changes, and the deflection magnitude is therefore proportional to the heating or cooling power induced by the pump laser (Rayner, Heckenberg et al. 2003). This makes PTDS a useful technique for analyzing small temperature changes and for screening laser-cooling samples.

Epstein *et al* used PTDS in their first demonstration of solid-state laser cooling of ZBLANP:Yb^{3+} glass (Epstein, Buchwald et al. 1995). They pumped the sample with a titanium-sapphire laser that was mechanically chopped with a period of 1.8 s. A helium-neon laser probe beam propagating in the opposite direction was co-aligned with and slightly displaced from the pump beam. The ZBLANP sample was transparent at the 632.8 nm wavelength of the probe beam, which thus did not introduce any temperature change itself. The angular deflections of the probe beam, caused by thermally-induced refractive-index gradients, were then measured using a position-sensitive detector. As shown in Figure 18a, the PTDS waveform reversed sign as the pump wavelength was changed from 980 nm to 1010 nm, *i.e.* from laser-induced heating to laser-induced cooling. The results of the full investigation are shown in Figure 18b and clearly demonstrate the 180° phase difference between pumping at wavelengths less than (heating) or greater than (cooling) the mean fluorescence wavelength. Fajardo, Murtagh, and coworkers used PTDS for testing ZBLANP:Yb^{3+} samples fabricated under different electrochemical purification

conditions (see Section 3.2) (Fajardo, Sigel Jr et al. 1997, Murtagh, Sigel Jr et al. 1999). A similar setup was used by Mungan *et al* who displaced the probe beam laterally from the pump beam by 50 μm in order to sensitively probe the pump-induced thermal gradient (Mungan, Buchwald et al. 1997). The lateral displacement of the probe beam had to be chosen carefully. Rapid artificial transients due to the finite time required for the chopper blade to cross the 2-mm pump beam were observed if the probe beam was closer than 50 μm to the pump beam. Bowman *et al* measured photo-thermal deflections in Yb^{3+}-doped YAG, YLF, $KGd(WO_4)_2$, and ZBLANP samples by placing a large-area dual-cathode silicon diode several meters away from the sample, and they were able to resolve angular probe beam deflections as small as 0.01 μrad, taking care to minimize vibrations and air turbulence (Bowman and Mungan 2000). They also used temperature control and optical isolation of the helium-neon laser to minimize pointing fluctuations. PTDS techniques were also used by Rayner *et al* for characterizing a 250-μm diameter ZBLAN:Yb^{3+} fiber (Rayner, Friese et al. 2001) and a ZBLAN:Yb^{3+} bulk sample (Rayner, Friese et al. 2001), Fernandez *et al* for Yb^{3+}-doped CNBZn and BIG glasses (Fernández, Mendioroz et al. 2000, Fernández, Mendioroz et al. 2001, Fernández, Mendioroz et al. 2001, Fernandez, Mendioroz et al. 2002, Fernández, García-Adeva et al. 2012), Mendioroz, Fernandez, and co-workers for KPb_2Cl_5:Yb^{3+} (Fernandez, Mendioroz et al. 2002, Mendioroz, Fernández et al. 2002, Fernández, García-Adeva et al. 2012), García-Adeva *et al* for KPb_2Cl_5:Er^{3+} (Fernandez, Garcia-Adeva et al. 2006, Garcia-Adeva, Balda et al. 2007, Garcia-Adeva 2008, Garcia-Adeva, Balda et al. 2009, Fernández, García-Adeva et al. 2012), García-Adeva *et al* for KPb_2Br_5:Er^{3+} (Garcia-Adeva 2008, Garcia-Adeva, Balda et al. 2009), and Fernandez *et al* for Er^{3+}-doped CNBZn glass (Fernandez, Garcia-Adeva et al. 2006, Fernández, García-Adeva et al. 2012).

Following the derivation presented by Fernandez *et al* (Fernández, Mendioroz et al. 2001) and using the notation of Section 2, assume a quasi two-level system such as that shown for Yb^{3+} in Figure 9 pumped at $h\nu_p$ with amplitude modulation frequency ω_m and emitting at the mean luminescence energy $h\tilde{\nu}_f$. The heat the sample exchanges per unit time and unit volume is then given by

$$H = N_2\left[W_{nr}h\nu_p + W_r h\left(\nu_p - \tilde{\nu}_f\right)\right] \tag{28}$$

where N_2 is the population density in the excited state, and W_r and W_{nr} are the radiative and non-radiative relaxation rates of the excited state, respectively. Here, N_2 is given by $dN_2/dt = N_1\left(\sigma_a I/h\nu_p\right) - \left(N_2/\tau\right)$, where $\tau = 1/\left(W_r + W_{nr}\right)$ is the excited-state lifetime and σ_a is the absorption cross section. Assuming a low pump laser amplitude modulation frequency ($\tau\omega_m \ll 1$), Eq.(28) simplifies to

$$H = N_1\sigma_a I_0\left[1 - \eta_q\frac{\tilde{\nu}_f}{\nu_p}\right] \tag{29}$$

where $\eta_q = W_r / (W_r + W_{nr})$ is the internal quantum efficiency of the excited state. Salazar *et al* have shown that in the collinear geometry of a PTDS experiment, the angular deviation of the probe beam is proportional to the amount of heat the sample exchanges (Salazar, Sánchez-Lavega et al. 1993). With this assumption, the photothermal deflection signal (PDS) can be related to the spectroscopic parameters of the active ion according to

$$\frac{\text{PDS}}{\alpha(\lambda_p, T) I_o} = C\left[1 - \eta_q \frac{\lambda_p}{\tilde{\lambda}_f}\right] + \frac{\alpha_b}{\alpha(\lambda_p, T)} \tag{30}$$

where C is a constant, I_0 is the incident pump intensity, and $\alpha(\lambda_p, T)$ is the resonant absorption coefficient. Here we have included the heating caused by background absorption (α_b) (Mungan and Gosnell 1999). From Eq. (30) one therefore expects a nearly linear dependence of the normalized photothermal deflection as a function of pump wavelength. This linear relationship has been found experimentally for a number of materials such as Yb^{3+}-doped ZBLAN, KGW, YLF, and YAG (Bowman and Mungan 2000). The quantum efficiency can then be deduced from the slope and intercept of a linear fit to the experimental PDS data (Epstein, Buchwald et al. 1995, Bowman and Mungan 2000, Epstein, Brown et al. 2001, Fernández, Mendioroz et al. 2001).

PTDS has several significant drawbacks. First, it depends on careful alignment of the pump and probe laser beams and is therefore only used for single-pass pump geometries. This

limits its use to the screening of laser-cooling materials, and PTDS is not a useful thermometry method for multi-pass power cooling experiments. Second, the refractive index depends not only on temperature through the thermo-optic effect (thermal lensing) but also on the density of excited activator ions (population lensing) (Antipov, Bredikhin et al. 2006, Passilly, Haouas et al. 2006, Messias, Catunda et al. 2007, Anashkina and Antipov 2010, Seletskiy, Melgaard et al. 2011). While the thermo-optic effect usually dominates and is an indication of temperature, population lensing distorts the thermal signal and can become important. This is another reason why the probe beam has to be laterally displaced from the pump beam, as described above. The lateral displacement reduces the effect of activator excitation, which is local, while maintaining sufficient sensitivity for thermo-optic effects since heat diffuses in a radial direction with respect to the pump beam. This makes the optimum alignment of pump and probe lasers even more challenging and can even lead to erroneous results (Seletskiy, Melgaard et al. 2011).

Silva *et al* have presented an alternate photo-thermal experiment in which pump and probe beams are collinear and the sample temperature is determined from probe-beam phase shifts rather than probe-beam deflection (Silva, Andrade et al. 2013, Silva, Malacarne et al. 2013). Their experimental arrangement used a continuous-wave Gaussian (TEM_{00} with radius w_e) pump beam and a weak collinear (*i.e.* zero lateral displacement) He-Ne laser probe beam (TEM_{00} with radius w_P), and they tested Yb^{3+}-doped fluorozirconate (ZBLAN) and aluminsoilicate (LACAS) glass. They measured the intensity of the central portion of the probe beam in the far field (pinhole/photodiode assembly) as a function of time, which is expected to follow

$$I(t) = I(0)\left|\int_0^\infty \exp\left[-(1+iV)g - i\Phi(g,t)\right]dg\right|^2 . \tag{31}$$

Here, $I(0)$ is the signal at $t = 0$, $g = \left(r/w_p\right)^2$, and $V = Z_1/Z_c$, where r is the radial coordinate, Z_c is the confocal distance of the probe beam, and Z_1 is the distance from the probe beam waist to the sample. Besides these geometric factors, the intensity $I(t)$ is governed by the total phase shift, $\Phi = \Phi_{th} + \Phi_{PL}$, the probe beam experiences as it propagates through the pumped volume and acquires contributions from both thermal (th) and population effects (PL). Both Φ_{th} and Φ_{PL} depend on a number of material parameters such as the thermal diffusivity, thermal conductivity, excited-state lifetime, activator ion density, refractive index, and absorption and emission cross sections. Fits of Eq. (31) to measured transients yielded material parameters that were in good agreement with published results. The average temperature change of the pumped volume could then be found from the transients because the probe beam phase shift is directly proportional to the temperature change. Furthermore, the amplitude of the thermal effect was expected to be proportional to the net power density [Eq.(11)] and thus allowed measurement of the cooling efficiency. The temperature and cooling efficiency results are shown in Figure 19 and were in good agreement with previously published results obtained by photothermal deflection. This time-resolved collinear method eliminates the difficulties in finding an optimum lateral displacement of the probe beam relative to the pump beam; its quantitative use however necessitates exact knowledge of several optical and material parameters.

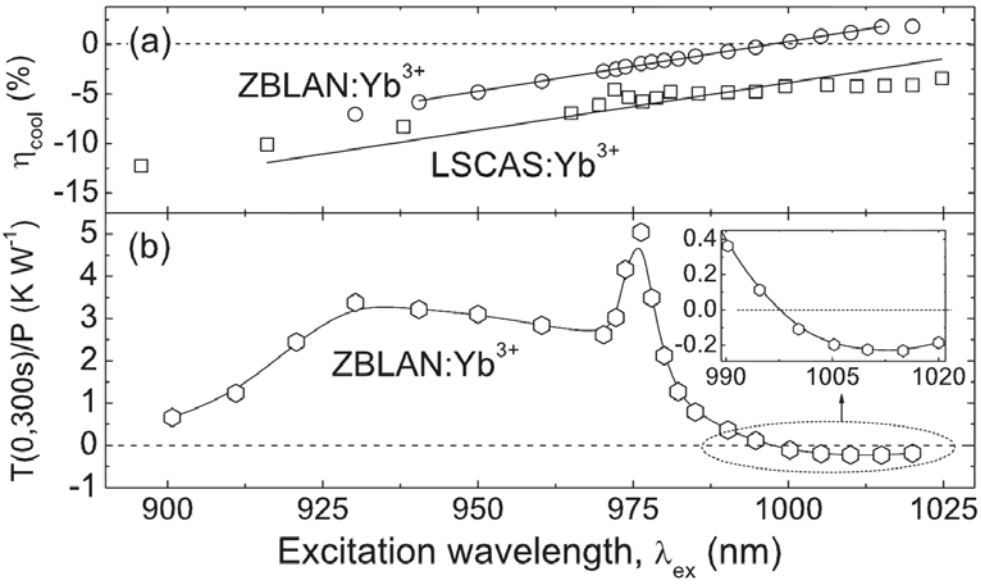

Figure 19: (a) Cooling efficiency and (b) normalized temperature change determined from collinear photothermal transients recorded for Yb^{3+}-doped ZBLAN and LSCAS glass pumped at different wavelengths (Silva, Andrade et al. 2013). *Reproduced with permission from J.R. Silva, L.H.C. Andrade, S.M. Lima, M.P. Hehlen, Y. Guyot, Laser-induced lensing effects in solid-state optical refrigerators, Appl. Phys. Lett.* ***102*** *(2013) 141910. Copyright 2013, AIP Publishing LLC.*

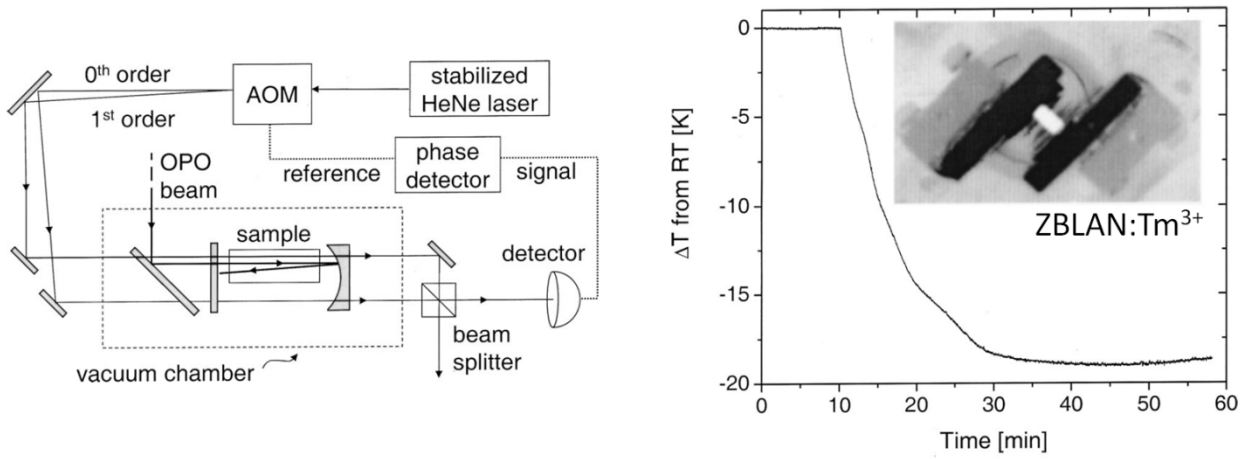

Figure 20: *Left:* Experimental setup for non-contact thermometry using a calibrated Mach-Zehnder (MZ) heterodyne interferometer (AOM = acousto-optic modulator, OPO = optical parametric oscillator) (Hoyt, Hasselbeck et al. 2003). *Right:* Temperature change from room temperature (RT) of a 1 wt% Tm^{3+}-doped ZBLAN glass (pumped at 1.9 μm with ~3.5 W starting at $t = 10$ min) deduced from MZ measurements. The inset shows an infrared image of the cold sample (white rectangle in center) and the hot mirror mounts (black rectangles).

Mach-Zehnder Interferometry

Mach-Zehnder (MZ) interferometry is another technique that has been used for non-contact thermometry. The technique is based on the fact that the optical path length in the sample changes linearly over a wide temperature range (Jewell, Askins et al. 1991, Lima, Sampaio et al. 2000). Figure 20 (left) shows the MZ interferometer used by Hoyt *et al* to measure the laser-induced temperature change in Tm^{3+}-doped ZBLAN glass (Hoyt, Hasselbeck et al. 2003). One advantage of this technique over PTDS is that it can be applied to both single and multi-pass pump geometries and yields a measure of the bulk sample temperature. The difference in optical

path length between the two interferometer arms is given by $\mathcal{L} = nL - L$, where L is the sample length and n is the sample refractive index. As a function of temperature one then obtains (Hoyt, Hasselbeck et al. 2003)

$$\frac{d\mathcal{L}}{dT} = L\left[\frac{dn}{dT} + \beta(n-1)\right] \tag{32}$$

where $\beta = (1/L)(dL/dT)$ is the coefficient of thermal expansion, for which values of $-5.8\times10^{-6} \pm 0.4$ K^{-1} (Lima, Sampaio et al. 2000) and -5.9×10^{-6} K^{-1} (Jewell, Askins et al. 1991) have been reported. They placed the ZBLAN:Tm^{3+} in a cryostat and calibrated Eq. (32) by determining the quantity in brackets. The interferometer measurements were found to agree to within 1 K when compared to thermal camera images. The resolution of this technique was found to be ± 3 K and was limited by background phase drifts that occurred over time scales of 1 hour. Figure 20 (right) shows the temperature change deduced from MZ measurements for a Tm^{3+}-doped ZBLAN glass sample pumped at 1.9 μm with ~3.5 W from an optical parametric oscillator (OPO). Cooling by 19 K starting at room temperature was observed after pumping for ~30 min. Thermometry with a MZ interferometer was also used by Gainov *et al* who measured the temperature in the core of a strongly pumped Yb^{3+}-doped fiber under lasing conditions (Gainov, Shaidullin et al. 2010).

Luminescence Thermometry

Luminescence thermometry has become the most common non-contact technique in recent years. As shown in Section 2.2, the crystal-field levels of the excited state rapidly thermalize after an excitation and, as a result, the luminescence spectrum varies as a function of temperature. Furthermore, thermal equilibrium is rapidly established regardless of the crystal-field transition that has been used for the excitation, causing the luminescence spectral profile to become independent of the pump wavelength (DeLoach, Payne et al. 1993). Absolute, differential, and ratios of luminescence intensities have been used as thermometers. Mungan *et al* were the first to use a basic implementation of this technique for the measurement of laser-induced temperature changes in 1 wt% Yb^{3+}-doped ZBLANP fiber (Mungan, Buchwald et al. 1997). They first performed a calibration by placing the sample in a He filled chamber, measuring the chamber temperature with a thermocouple, weakly exciting the sample at the mean fluorescence wavelength such as to induce neither cooling nor heating, and measuring the luminescence spectrum. This was repeated for different temperatures in the 280–303 K range, and the difference spectra between the high (303 K) and lower temperature luminescence spectra were calculated. They found that the integral of the difference spectra was proportional to ΔT within this narrow temperature range. This differential luminescence thermometry (DLT) method allowed them to resolve temperature changes down to at least 1 K and measure a 16 K local temperature drop in the sample when pumped at 1015 nm with 770 mW. The same technique was used by Luo to measure a 21 K temperature drop in a ZBLAN:Yb^{3+} fiber (Luo, Eisaman et al. 1998). Gosnell used a similar approach but could not rely on a linear dependence of the magnitude of the difference spectra on temperature because of the larger 65 K temperature drop observed in his experiment (Gosnell 1999). Rather, he recorded reference spectra in 1-K

intervals from 140 K to room temperature and subsequently deduced the temperature by a least-squares comparison of the sample spectrum and the reference spectra. Similar experiments using differences of the full luminescence spectra have been reported recently in Refs. (Seletskiy, Melgaard et al. 2009, Seletskiy, Melgaard et al. 2010, Melgaard, Seletskiy et al. 2013, Melgaard, Seletskiy et al. 2013). The technique was also used to perform thermometry of a semiconductor payload that was attached to a laser cooling crystal. Seletskiy *et al* conducted an experiment in which a GaAs/InGaP double-heterostructure attached to a YLF:Yb^{3+} crystal was cooled to 165 K in order to demonstrate the ability to cool a device by means of solid-state optical refrigeration (Seletskiy, Melgaard et al. 2010). Probe light from a GaAs laser diode (25 mW at 650 nm) was launched through a Y-split optical fiber to excite the GaAs/InGaP payload, and its fluorescence was collected through the other fiber arm for detection by a spectrometer. The shift of the GaAs bandgap with temperature is well known and causes the GaAs luminescence spectrum to blue shift from ~850 nm at 265 K to ~839 nm at 165 nm. This large change enabled thermometry to within ±2 K at low temperatures, the limiting factor being the wavelength resolution of the spectrometer.

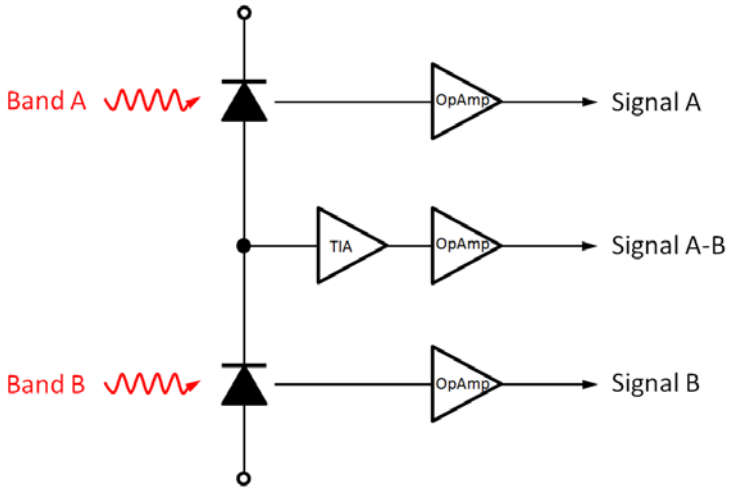

Figure 21: Functional block diagram of a detector using a pair of balanced photodiodes, a transimpedance amplifier (TIA), and operational amplifiers (OpAmp). This circuit is implemented in commercial balanced detectors such as PDB450C from ThorLabs.

A variation of the full-spectrum techniques takes the difference in the luminescence intensity of only two spectral bands, an approach that was used by Patterson *et al* (Patterson, Seletskiy et al. 2010, Patterson, Sheik-Bahae et al. 2010, Patterson, Stark et al. 2011). They collected the luminescence from ZBLAN:Yb^{3+} with a multimode optical fiber and divided the sample light into two beams using a non-polarizing beam splitter. The first beam was passed through an interference filter having high transmittance in the $935 < \lambda < 965$ nm spectral range (Band A) while the second beam was passed through a filter with a $995 < \lambda < 1010$ nm transmission range (Band B). The two beams were then detected by a pair of photodiodes having well-matched responsivities and being arranged according to the functional diagram shown in Figure 21. The balanced detector provided signals that were proportional to the optical powers in each band A and B. In addition, an ultra-low noise high-speed transimpedance amplifier (TIA)

provided a signal whose magnitude was proportional to the difference A–B of the two luminescence intensities. The difference signal A–B was then used as a sensitive non-contact thermometer. The advantages of using a balanced detector include rejection of common-mode noise (*e.g.* noise in the luminescence signal due to fluctuation in the pump laser intensity) and corresponding improvement of the signal-to-noise ratio, possibility of high electrical gain of the detected signal, and fast response time (>100 kHz bandwidth sampling rates). Seletskiy *et al* used a similar balanced detection approach but improved on the light collection efficiency by coupling the light into multimode fiber that was circular (600 μm diameter) on the input side and elongated (200 μm × 5000 μm) on the output side, which served as the input to a monochromator (Seletskiy, Hasselbeck et al. 2008, Seletskiy, Melgaard et al. 2011, Seletskiy, Melgaard et al. 2013). A bi-cell balanced detector was placed at the monochromator exit to detect the intensity of two spectral bands as described above. Compared to Patterson's color filter approach, the use of a monochromator provided additional experimental flexibility for thermometry of Yb^{3+} as well as semiconductor (e.g. GaAs) payloads that fluoresce around 800–900 nm (Melgaard, Seletskiy et al. 2010).

Rayner *et al* used the strong temperature dependence of the luminescence from ZBLAN:Yb^{3+} at 950 nm directly as a thermometer rather than using reference or difference spectra (Rayner, Hirsch et al. 2001, Rayner, Heckenberg et al. 2003). They performed a calibration by mounting the ZBLAN:Yb^{3+} fiber in good thermal contact with a Peltier device, exciting it with ~200 mW of laser light at 1015 nm, and recording the luminescence intensity at 950 nm as a function of temperature as measured with a thermistor. Their calibration found an essentially linear intensity decrease of ~20% upon lowering the sample temperature from 298 to 268 K, corresponding to a sensitivity of 0.67% K^{-1}. Heeg *et al* used the ratio of the ZBLAN:Yb^{3+}

luminescence intensities at 950 and 973 nm as a thermometer (Heeg, Stone et al. 2004). The former is on the short-wavelength tail of the 973-nm luminescence peak of Yb^{3+}, and the ratio is therefore sensitive to the decrease in homogeneous linewidth with decreasing temperature. They measured the ratio at 20-K intervals between 100 and 300 K with the sample in a liquid-nitrogen cryostat. An essentially linear dependence on temperature with a sensitivity of ~0.45% K^{-1} and a root-mean-square temperature variance of ~0.5 K were found. This allowed them to sensitively measure a 6 K temperature drop from room temperature by pumping the sample at 1027 nm with an absorbed power of 1.25 W. Sui *et al* utilized the ratio of $^2H_{11/2} \rightarrow {}^4I_{15/2}$ (at 524 nm) and $^4S_{3/2} \rightarrow {}^4I_{15/2}$ (at 547 nm) luminescence from Er^{3+} as a thermometer, transitions that have been used extensively for thermometry before (Sui, Li et al. 2013). The authors explored the possibility of using the closely-spaced $^4S_{3/2}$ and $^2H_{11/2}$ multiplets for solid-state laser cooling in Er^{3+}-doped telluride and germanate glasses. The ~800 cm^{-1} $^4S_{3/2}$–$^2H_{11/2}$ multiplet spacing makes this a useful thermometer for higher temperatures, and they achieved a sensitivity of 0.65–0.85% K^{-1} around 550–600 K in different glasses. The sensitivity, conversely, is much lower at temperatures well below 300 K where $kT \ll 800$ cm^{-1}, likely limiting the usefulness of this technique to room-temperature material screening studies.

4.3. Measurement of Minimum Achievable Temperature

We have shown in Section 2.3 [Eq.(14)] that the cooling efficiency, η_c, depends on the external quantum efficiency, η_e, and the background absorption coefficient, α_b. Furthermore, η_c depends on temperature via the temperature dependence of both the mean fluorescence wavelength, $\tilde{\lambda}_f$, and the pump absorption coefficient, α. Thus, for a given material pumped at

λ_p there will be a temperature – referred to as the minimum achievable temperature (MAT) (Seletskiy, Hasselbeck et al. 2008) – for which $\eta_c = 0$. The sample will show laser-induced cooling for $T > \text{MAT}$ while it will show laser-induced heating for $T < \text{MAT}$. Separate measurements of η_e, α_b, $\alpha(\lambda, T)$, and $\tilde{\lambda}_f(T)$ can serve as input for the calculation of the cooling efficiency as a function of both T and λ_p. An example of such a calculation is shown in Figure 22(c) for a 5 mol% Yb^{3+}-doped YLF crystal where red and blue indicate areas of laser-induced heating and cooling, respectively, and the white dividing line indicates the MAT (Seletskiy, Hasselbeck et al. 2008, Seletskiy, Melgaard et al. 2013). While there is a MAT for a given pump wavelength, there is also one global MAT that indicates the lowest possible temperature the material can be cooled to. In this case, the global MAT corresponds to exciting the E4→E5 crystal field transition around 1020 nm (see Figure 9 and insert in Figure 22c). Seletskiy *et al* performed luminescence thermometry experiments in order to experimentally verify the calculated MAT. They mounted the YLF:Yb^{3+} crystal on a coldfinger in a liquid-nitrogen cryostat that allowed them to hold the sample at different temperatures T_0 (see Figure 22c). As described in Section 2.2., they attached a GaAs/GaInP double-heterstructure to the side of the laser-cooling crystal, excited it with a weak GaAs laser diode, and observed the differential luminescence using a balanced photodiode. They achieved ~250 μK temperature resolution on a sub-millisecond timescale with this technique, allowing them to follow the rapid local temperature change as the pump laser was turned on. As shown in Figure 22b, the signs of the signals obtained from cooling and heating conditions are reversed. They fixed the pump wavelength and then measured the differential luminescence signal at various sample temperatures T_0 in order to find the MAT at which cross-over from cooling to heating occurred.

The results are shown as black circles in Figure 22c, and they provided excellent confirmation of the theoretical predictions from Eq.(14).

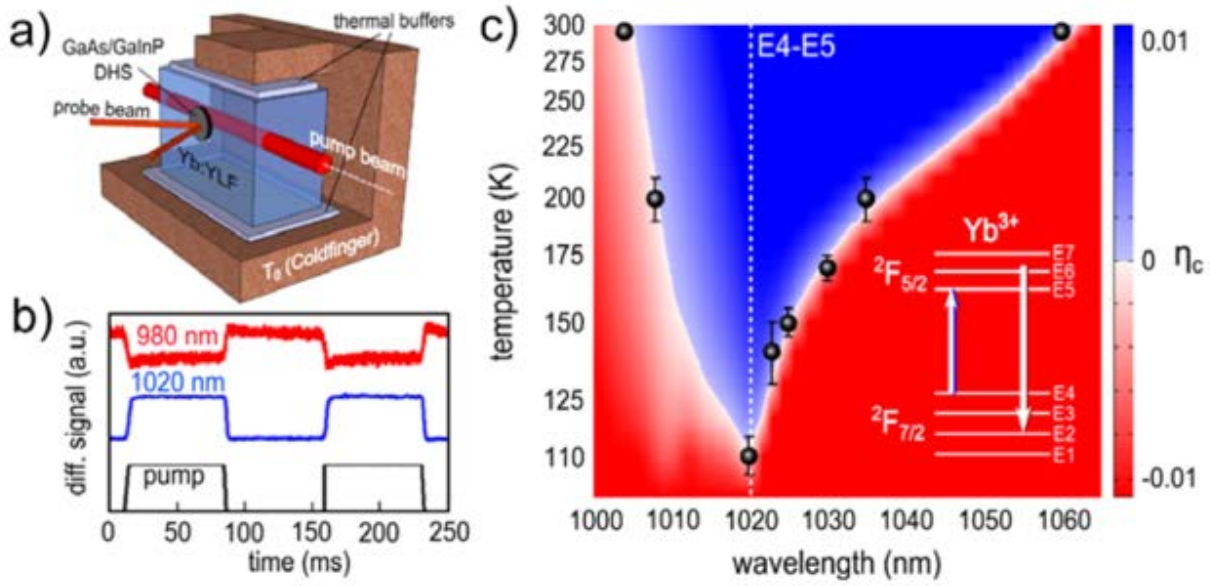

Figure 22: Measurement of the minimum achievable temperature (MAT) in a Yb^{3+}-doped YLF crystal (Seletskiy, Melgaard et al. 2011). (a) Experimental arrangement showing the YLF:Yb crystal mounted on a cold-finger (temperature T_0) and being pumped by a tunable Ti:sapphire laser. Also shown is a small GaAs/GaInP double-heterostructure (DHS) attached to the side of the crystal and being used for luminescence thermometry. (b) Examples of luminescence thermometry traces (at 300 K) for heating ($\lambda_p = 980$ nm) and cooling ($\lambda_p = 1020$ nm) as the pump laser is cycled on and off. (c) Calculated cooling efficiency (η_c) as a function of temperature and pump wavelength with red and blue indicating areas of laser-induced heating and cooling, respectively, and the white dividing line indicating the MAT. The measured MAT values are shown as black circles.

Table 1: Yb^{3+} doped materials for which a net laser-induced bulk cooling effect has been reported.

Host	Yb	ΔT (K)	Final T (K)	P_{pump} (W)	λ_{Pump} (nm)	Notes	Reference
$YLiF_4$ (YLF)	10%	178.5	93	54	1020	Brewster cut, $\vec{E} \parallel \vec{c}$, $\alpha_b = 2.0\times10^{-4}$ cm^{-1}, $\eta_e = 0.996$, non-resonant cavity, external mirrors	(Melgaard, Seletskiy et al. 2014)
$YLiF_4$ (YLF)	10%	185	114	50	1020	Brewster cut, $L = 12$ mm, $\vec{E} \parallel \vec{c}$, $\alpha_b = 2.0\times10^{-4}$ cm^{-1}, $\eta_e = 0.996$, non-resonant cavity, external mirrors	(Melgaard, Seletskiy et al. 2013)
$YLiF_4$ (YLF)	5%	162	123	40	1020	Brewster cut, $L = 12$ mm, $\vec{E} \parallel \vec{c}$, $\alpha_b = 4.6\times10^{-4}$ cm^{-1}, $\eta_e = 0.995$, non-resonant cavity, external mirrors	(Melgaard, Seletskiy et al. 2013)
$YLiF_4$ (YLF)	5%	176	124	45	1020	Brewster cut, $3\times3\times12$ mm^3, $\vec{E} \parallel \vec{c}$, non-resonant cavity, external mirrors, 50 mW heat lift	(Melgaard, Seletskiy et al. 2013)

$YLiF_4$ (YLF)	7%	155	130	12	1020	Brewster cut, $2\times2\times2$ mm^3, $\vec{E} \parallel \vec{c}$, intra-cavity VECSEL, 150mW heat lift	(Ghasemkhani, Albrecht et al. 2014)
$YLiF_4$ (YLF)	5%	145	155	9	1023	Brewster cut, $3\times3\times11$ mm^3, $\vec{E} \parallel \vec{c}$, non-resonant cavity, external mirrors, 90mW heat lift	(Seletskiy, Melgaard et al. 2010)
$YLiF_4$ (YLF)	5%	143	164	15.5	1022	Brewster cut, $L = 11$ mm, $\vec{E} \parallel \vec{c}$, resonant cavity, 110mW heat lift	(Seletskiy, Melgaard et al. 2009)
$YLiF_4$ (YLF)	5%	135	165	9	1023	Brewster cut, $\vec{E} \parallel \vec{c}$, non-resonant cavity, external mirrors, attached GaAs/GaInP load (2 μm thick, 800 μm diameter)	(Seletskiy, Melgaard et al. 2010)
ZBLANP glass	2wt%		208	10	1026	8 mm diameter, $L = 8$ mm, non-resonant cavity, dielectric mirrors on sample, 29 mW heat lift	(Thiede, Distel et al. 2005)
$YLiF_4$ (YLF)	5%	69		45	1030	Piezo-electrically controlled Fabry-Perot cavity	(Seletskiy, Hasselbeck et al. 2008)
ZBLANP glass	1wt%	65		2.2	1015	Multimode fiber, 175 μm diameter core, $L = 7$ mm, double pass	(Gosnell 1999)

ZBLAN glass		48		1.6	1030	Fiber perform, 12 mm diameter, mm, non-resonant cavity, dielectric mirrors on sample	(Edwards, Anderson et al. 1999)
ZBLANP glass	1wt%	21		1.36	1015	Multimode fiber, 175 μm diameter core, $L = 10$ mm, single pass	(Luo, Eisaman et al. 1998)
ZBLANP glass	1wt%	16		0.77	1015	Multimode fiber, 250 μm diameter core, $L = 10$ mm, single pass	(Mungan, Buchwald et al. 1997)
ZBLAN glass	1wt%	13		0.85	1015	Multimode fiber, 250 μm diameter, 175 μm diameter core, $L = 40$ mm, single pass	(Rayner, Friese et al. 2001)
$Y_3Al_5O_{12}$ (YAG)	2.3	8.9		1.8	1030	Non-resonant cavity, external mirrors	(Epstein, Brown et al. 2001)
$YLiF_4$ (YLF)	5	6.3		3	1025	$4 \times 4 \times 12$ mm^3, single pass	(Bigotta, Di Lieto et al. 2007)
ZBLAN glass	2	6		6	1027	$2 \times 2 \times 3$ mm^3, intra-cavity with KYW:Yb laser	(Heeg, Stone et al. 2004)
BaY_2F_8 (BYF)	2.5	4		3	1025	$3 \times 4 \times 10$ mm^3, single pass	(Bigotta, Parisi et al. 2006, Bigotta, Parisi et al. 2006, Bigotta, Di Lieto et al. 2007)

ZBLAN glass	1wt%	3.7		1	1013	250 μm diameter, 175 μm diameter core, single pass	(Rayner, Hirsch et al. 2001)
$Y_3Al_5O_{12}$ (YAG)	1wt%	1.9		2.2	1030	Double pass	(Sheik-Bahae, Hoyt et al. 2001)
Y_2SiO_5 (YSO)	5%	1		0.75	1050	Single pass	(Epstein, Brown et al. 2001)
ZBLANP glass	1wt%	0.3			1015	$2.5\times2.5\times6.9$ mm^3, single pass	(Epstein, Buchwald et al. 1995)
ABCYS glass	2 wt%	0.13			1030		(Guiheen, Haines et al. 2006)

Table 2: Tm^{3+} doped materials for which a net laser-induced bulk cooling effect has been reported.

Host	Tm	ΔT (K)	P_{pump} (W)	λ_{Pump} (nm)	Notes	Reference
ZBLANP glass	1wt%	19	3.5	1900	$4\times4\times8$ mm^3, non-resonant cavity, external mirrors	(Hoyt, Hasselbeck et al. 2003)
ZBLANP glass	1wt%	8		1850	Internal reflections (Monolithic Optical Maze)	(Sheik-Bahae, Hoyt et al. 2001)
BaY_2F_8 (BYF)	1.2%	3.2	4.4	1855	15 mm diameter, $L = 55$ mm, single pass	(Patterson, Bigotta et al. 2008)
ZBLANP glass	2wt%	2	2.72	1900	$3\times3\times10$ mm^3, single pass	(Hoyt, Hasselbeck et al. 2003)
BaY_2F_8 (BYF)	2wt%	1.5	6	1902	$7\times4.5\times4.5$ mm^3, single pass	(Patterson, Hasselbeck et al. 2004)

ZBLANP glass	1wt%	1.25	3	1857	$5\times5\times9$ mm^3	(Sheik-Bahae, Hoyt et al. 2000)
ZBLANP glass	1wt%	1.2	3	1900	$5\times5\times9$ mm^3, single pass	(Hoyt, Sheik-Bahae et al. 2000)

Table 3: Er^{3+} doped materials for which a net laser-induced bulk cooling effect has been reported.

Host	Er	ΔT (K)	P_{pump} (W)	λ_{Pump} (nm)	Notes	Reference
KPb_2Cl_5 (KPC)	0.5%	0.7	1.9	870	$4.5\times6.5\times2.7$ mm^3	(Fernandez, Garcia-Adeva et al. 2006, Fernández, García-Adeva et al. 2012)
CNBZn glass	0.5%	0.5	1.9	860	$10.7\times10.7\times2.2$ mm^3	(Fernandez, Garcia-Adeva et al. 2006, Fernández, García-Adeva et al. 2012)
KPb_2Cl_5 (KPC)	3.6×10^{19} cm^{-3}	0.0136	0.0053	1567.6	3 mm diameter, $L=13.6$ mm	(Condon, Bowman et al. 2009)

5. LANTHANIDE-DOPED LASER COOLING MATERIALS

5.1. Yb^{3+}-Doped Materials

Glasses and crystals doped with Yb^{3+} represent the majority of laser-cooling materials studied to date. Table 1 summarizes the systems in which net laser-induced bulk cooling has been observed experimentally. The dominance of Yb^{3+} is because of both fundamental and practical reasons. First, the simple energy-level structure of Yb^{3+} is advantageous since it most closely resembles the ideal case of a four-level laser cooling cycle (see Figure 9). The absence of any other excited state eliminates competing processes such as excited-state absorption and upconversion that are possible with ions such as Tm^{3+} (see Section 5.2) and Er^{3+} (see Section 5.3) and that can introduce non-radiative processes and associated internal heating. Second, the $^2F_{7/2} \leftrightarrow {}^2F_{5/2}$ transitions of Yb^{3+} have significantly larger cross-sections than many 4*f* transitions of other lanthanides because of relatively strong electron-phonon coupling (Bigotta, Parisi et al. 2006), an effect that is more pronounced at the beginning and end of the lanthanide series (Yen, Scott et al. 1964, Buchanan, Wickersheim et al. 1967, Malta 1995, Lupei, Lupei et al. 1999). This facilitates absorption of the pump laser light and relaxes the purity requirements [see Eq.(15)]. Third, the energy gap between the $^2F_{5/2}$ excited-state and the $^2F_{7/2}$ ground-state multiplet is ~10000 cm^{-1}, an energy that is large compared to the highest-energy optical phonons of many oxide and halide glasses and crystals (see Section 3.3). As a result, $^2F_{5/2}$ multiphonon relaxation rates are small compared to $^2F_{5/2}$ radiative relaxation, *i.e.* the Yb^{3+} luminescence can have the high quantum efficiency that is desired for maximizing the laser-cooling efficiency [see Eq.(14)]. Fourth, high-power pump lasers in the ~1 μm pump wavelength range of Yb^{3+} are available from commercial vendors. This facilitates initial laboratory-based studies and is also attractive for the development

of deployable devices. High-power compact diode lasers with high efficiency and excellent reliability can, in principle, be manufactured at a desired Yb^{3+} pump wavelength. In contrast, lasers operating around 1.9 μm (Tm^{3+}) or 3.1 μm (Dy^{3+}) are less mature.

5.1.1. Glasses

ZBLAN

Optical fibers made from fluoride glasses were a major focus of research and development in the 1980s and early 1990s (Tran, Sigel et al. 1984). Fluoride glasses have an intrinsically low propagation loss in the near infrared spectral region (1.5–4 μm) where the sum of multiphonon absorption (increases towards longer wavelengths) and Rayleigh scattering (increases towards shorter wavelengths) is at a minimum (Gan 1995). The theoretical propagation loss of 0.001–0.01 dB/km held the promise of enabling long-haul fiber-optic telecommunication links with minimal need for expensive optical amplifiers and opto-electronic repeaters. Various fluoride glass compositions were developed commercially in very high purity and fabricated into fiber preforms from which optical fibers were then drawn. Despite intensive efforts, the goal of ultra-low propagation loss was not reached in part because of issues with mechanical strength, scattering by noble metal and oxide inclusions, glass stability and crystallization, and chemical durability that are inherent to fluoride glasses (Takahashi 1992). The competing technology of using mechanically rugged and chemically stable silica-based fibers with higher propagation loss (~0.2 dB/km) in conjunction with erbium-doped fiber amplifiers penetrated the telecom market in the late 1990s, and research on fluoride glasses diminished considerably as a result. Besides scattering and multiphonon absorption losses intrinsic to fluoride glass, absorption by trace metal

impurities was another factor contributing to the overall propagation loss of a fluoride fiber. Common transition metals such as Fe^{3+}, Fe^{2+}, Cu^{2+}, Ni^{2+}, Co^{2+}, V^{2+}, Ti^{3+}, and Cr^{3+} have optical absorptions in the visible and near infrared spectral range (France, Carter et al. 1986) that had to be minimized in order to approach the intrinsic propagation loss. By the mid 1990s, therefore, tremendous progress had been made in the fabrication of high-purity fluoride glasses, and glass preforms with trace-metal concentrations in the 1–200 ppb range were available (Takahashi 1992).

This advanced fluoride glass technology enabled the first observation of net solid-state laser cooling by Epstein in 1995 as described in Section 1.3 (Epstein, Buchwald et al. 1995). They used a preform of the fluoride glass ZBLANP doped with Yb^{3+}. The acronym stands for the constituents ZrF_4–BaF_2–LaF_3–AlF_3–NaF–PbF_2, a glass composition that is part of the family of heavy-metal fluoride (HMF) glasses. Such glasses were first discovered around 1974 by Lucas, Poulain, and co-workers who used ZrF_4 as the primary glass former, BaF_2 as the main network modifier, and other fluorides such as ThF_4, LaF_3, and alkali fluorides as glass stabilizers (Tran, Sigel et al. 1984). An important property of a glass is its stability against crystallization (devitrification), which typically increases with increasing difference $T_x - T_g$ between the glass transition (T_g) and the crystallization (T_x) temperature. Fluoride glasses are generally more prone to devitrification than oxide glasses, making their fabrication significantly more challenging. Fluorozirconate glasses with at least four constituents have $T_x - T_g$ in the range of 100–150 K and are among the most stable fluoride glasses, with ZBLAN consisting of 53%ZrF_4–20%BaF_2–4%LaF_3–3%AlF_3–20%NaF (mol%) being a common composition. Besides limited glass stability, the synthesis of fluoride glasses poses several additional challenges. Fluoride melts have low viscosity and readily react with oxygen and water present in the ambient

atmosphere or crucible materials. Moreover, Zr^{4+} has a tendency to undergo reduction to Zr^{3+} or even lower oxidation states in the melt, causing the formation of black residue and associated absorption and scattering loss in the final glass. A typical fabrication begins with the thorough fluorination of the starting materials in order to reduce oxide contaminations. This is most effectively achieved by treatment of the metal oxides or nominal metal fluorides in hydrogen fluoride (HF) gas at elevated temperatures. All subsequent steps have to be carried out under inert atmosphere in glove boxes. The mix of starting fluorides is then melted under either inert (Ar, N_2, or He) or reactive (CCl_4, SF_6, HF, CF_4, or BF_4) atmosphere. The latter is often used to effect oxidation of zirconium to the desired Zr^{4+} oxidation state without having to introduce an oxygen-based oxidizer. Melting is performed in non-reactive crucible materials such as glassy carbon, platinum or gold (Tran, Sigel et al. 1984), and it is followed by casting of the melt into pre-heated molds for solidification, controlled cooling, and finally annealing of the glass.

A typical glass composition used for many of the early laser-cooling studies was $53\%ZrF_4–18\%BaF_2–3\%LaF_3–3\%AlF_3–20\%NaF–2\%PbF_2–1\%YbF_3$ (ZBLANP:Yb^{3+}) (Murtagh, Sigel Jr et al. 1999). They were custom fabricated by commercial vendors from ultra-high purity starting materials in a process that typically involved melting at 950 ^oC in glassy carbon crucibles for 1 hour in inert atmosphere, reactive atmosphere processing (SF_6 gas) at 775 ^oC for 1 hour to lower the amounts of residual oxygen impurities and reduced zirconium species, and finally casting. The samples were produced as cylindrical preforms consisting of an Yb^{3+}-doped core comprising ~70% of the total diameter and an undoped ZBLAN cladding having a refractive index that was ~1% lower than the 1.52 index of the core (often by addition of HfF_4 to the composition), creating a structure with numerical aperture of 0.2 (Mungan, Buchwald et al. 1997). Some studies used the preforms as is (Edwards, Anderson et al. 1999, Thiede, Distel et al.

2005). They polished the endfaces to high optical quality and applied a dielectric coating to create a non-resonant cavity. The pump light was launched into the cavity through a small (<1 mm diameter) pinhole in one of the mirrors at an off-normal angle to achieve multi-pass excitation of the Yb^{3+}-doped core. Edwards *et al* achieved 48 K of cooling from room temperature with such a geometry by pumping a ZBLAN:Yb^{3+} sample with 1.6 W at 1030 nm (Edwards, Anderson et al. 1999). The largest net laser-cooling in this geometry was achieved by Thiede et al who cooled a 2% Yb^{3+}-doped ZBLANP glass to 208 K from room temperature using ~10 W of pump light from a diode-pumped YAG:Yb laser operating at 1026 nm (Thiede, Distel et al. 2005). This result is the lowest temperature achieved to date using an Yb^{3+}-doped glass host. Other studies drew the preform into a multimode fiber to improve the confinement of the pump light to the Yb^{3+}-doped core (Mungan, Buchwald et al. 1997, Luo, Eisaman et al. 1998, Gosnell 1999, Rayner, Friese et al. 2001, Rayner, Hirsch et al. 2001). They launched pump light into the fiber core (typically 175 μm diameter) in a single-pass geometry or, by addition of a retro-reflector at the output, a double-pass geometry. The largest net cooling of a ZBLAN multimode fiber was achieved by Gosnell using a 1wt% Yb^{3+}-doped sample in a double-pass geometry producing cooling by 65 K from room temperature when pumped with 2.2 W at 1015 nm (Gosnell 1999). Besides using higher power than previous experiments, Gosnell *et al* also implemented a multimode silica fiber to achieve transverse mode scrambling of the pump laser prior to launch into the ZBLAN:Yb^{3+} fiber. This reduced optical saturation and thus increased the absorbed power and cooling power compared to pumping with a single-mode beam.

Other Glasses

As discussed above, the standard composition of ZBLAN glass contains 4 mol% of LnF_3. Increasing the LnF_3 content to above ~6 mol% causes the glass to become increasingly unstable. This is a drawback for laser cooling because higher Yb^{3+} concentrations are generally desired as they afford a greater resonant absorption coefficient α and may enable a greater net cooling power density [see Eq.(11)]. This is one of the reasons why some glass compositions other than ZBLAN have been considered. The family of fluoride glasses of general composition BaF_2–InF_3–GaF_3–ZnF_2–LuF_3–GdF_3 (BIG) are stable for higher lanthanide fluoride concentrations than ZBLAN. For example, the composition 30%BaF_2–18%InF_3–12%GaF_3–20%ZnF_2–10%YbF_3–6%ThF_4–4%ZrF_4 (mol%) (BIGaZYbTZr) contains 10 mol% Yb^{3+} and has been considered for laser cooling (Murtagh, Sigel Jr et al. 1999). Another family of glasses are fluorochlorides such as the composition CdF_2–$ClCl_2$–NaF–BaF_2–$BaCl_2$–ZnF_2 (CNBZn). The admixture of heavier chloride ions to a fluoride glass lowers the average phonon energy and will tend to reduce multiphonon relaxation rates. This may be of particular value for laser-cooling experiments with Ln^{3+} ions having a low energy of the first excited state such as Tm^{3+}, Ho^{3+}, or Dy^{3+} (see Figure 7). Fernandez *et al* have studied optical refrigeration in BIG (Fernández, Mendioroz et al. 2000, Fernández, Mendioroz et al. 2001) and CNBZn (Fernández, Mendioroz et al. 2000, Fernández, Mendioroz et al. 2001, Fernández, Mendioroz et al. 2001, Fernández, García-Adeva et al. 2012) glasses doped with 1 mol% Yb^{3+}. Photothermal deflection measurement showed that CNBZn:Yb^{3+} had an estimated cooling efficiency of 2.0% at 300 K when pumped at 1010 nm, while the cooling efficiency of the BIG:Yb^{3+} glass was estimated to be only ~0.6%.

5.1.2. Crystals

Oxide Crystals

The need for non-hygroscopic materials with high hardness and thermal conductivity has made oxide crystals attractive soon after the first experimental demonstration of laser cooling in Yb^{3+}-doped fluoride glasses that do not possess these properties. Furthermore, it was recognized early that the higher peak absorption cross sections in crystals compared to glasses would be advantageous for laser cooling to low temperatures (Bowman and Mungan 2000). Bowman and Mungan were the first to demonstrate laser cooling in a crystal (Bowman and Mungan 2000). They used the photothermal deflection technique to look for signs of cooling in Yb^{3+}-doped $KGd(WO_4)_2$ (KGW), $YLiF_4$ (YLF), and $Y_3Al_5O_{12}$ (YAG) crystals. While no net bulk cooling was achieved, they observed local internal cooling in 3.5 at% Yb^{3+}-doped $KGd(WO_4)_2$ when the pump laser was tuned to wavelengths >1009 nm, *i.e.* to wavelengths longer than the mean emission wavelength of 993 nm.

The first crystal host to show net laser-induced bulk cooling was Yb^{3+}-doped YAG (Epstein, Brown et al. 2001). The authors pumped a 1 wt% Yb-doped YAG crystal with 2.2 W of laser power at 1030 nm in a double-pass geometry and observed a temperature drop of 1.9 K from room temperature. YAG is particularly attractive because its thermal conductivity is 14× greater than that of ZBLAN glass (13 W/m·K *vs* 0.9 W/m·K), and it is mechanically rugged and chemically durable. The main drawback its higher refractive index (1.93) compared to ZBLAN (1.5), which enhances undesired trapping and reabsorption of the fluorescence within the crystal and thus reduces the external quantum efficiency. YAG also has a higher phonon energy (~630 cm^{-1}) which, however, should still allow for near-unity quantum yield of the Yb^{3+} excited state. Epstein *et al* performed detailed spectroscopic studies on a commercial YAG:Yb^{3+} crystal. They

found an internal quantum efficiency of 98.8% and a background absorption coefficient of 2.2×10^{-4} cm^{-1}. The crystal showed internal cooling down to 252 K in a photothermal deflection setup. The crystal was then placed onto the edges of glass cover slides in a vacuum chamber (10^{-6} Torr) to minimize conductive and convective heat loads. The crystal temperature was measured with a thermal camera through a NaCl window as the crystal was excited at 1030 nm with 750 mW from a Ti:sapphire laser of which only ~10% was absorbed. They observed a temperature drop of 0.36 K from room temperature. In a subsequent experiment, a non-resonant external cavity was created around the YAG:2.3%Yb^{3+} crystal, and a temperature drop of 8.9 K was measured in this multi-pass pump geometry. Epstein *et al* also showed 1 K of bulk cooling in a Y_2SiO_5:Yb^{3+} crystal pumped at 1050 nm (Epstein, Brown et al. 2001).

KPb_2Cl_5 (KPC)

KPC has a very low maximum phonon energy of ~203 cm^{-1} (Nostrand, Page et al. 2001) and may therefore enable high quantum yields even in laser cooling ions that have a small energy gap (Er^{3+}, Tm^{3+}, Ho^{3+}, Dy^{3+}). Most strikingly, KPC is one of only two chloride hosts known to be only slightly hygroscopic (see Section 5.3). Mendioroz *et al* studied laser cooling of a KPC crystal doped with ~5×10^{19} Yb^{3+} cm^{-3} (Mendioroz, Fernández et al. 2002). KPC is monoclinic and crystallizes in the space group $P2_1/c$ with a unit cell volume of 876.3 $Å^3$ (Z=4) (Merkulov, Isaenko et al. 2005), suggesting that their doping level corresponded to ~0.55 mol% Yb^{3+} with respect to Pb^{2+}. The KPC:Yb^{3+} single crystal was grown in a two-zone Bridgman furnace under a chloride atmosphere at a growth rate of 1 mm/h. A $4.6 \times 4 \times 3.3$ mm^3 sample was cut from the boule and polished. They measured a mean fluorescence wavelength of $\tilde{\lambda}_f = 986$ nm at

300 K and observed internal laser cooling for pump wavelengths >986.5 nm using a photothermal deflection technique. A cooling efficiency of 0.2% at room temperature was deduced from the measurement, a value that was low because of the relatively low Yb^{3+} concentration.

BaY_2F_8 (BYF)

The group of Tonelli and Di Lieto at the University in Pisa, Italy, have performed extensive studies on Yb^{3+}-doped fluoride crystals. Before their work, solid-state laser cooling focused primarily on Yb^{3+}-doped fluoride glasses such as ZBLAN. Work on Yb^{3+}-doped crystals had been minimal with small net bulk cooling observed in YAG (Sheik-Bahae, Hoyt et al. 2001) and $Y_2Si_2O_5$ (Epstein, Brown et al. 2001) and internal laser cooling detected in KPb_2Cl_5 (Mendioroz, Fernández et al. 2002) and $KGd(WO_4)_2$ (Epstein, Brown et al. 2001) by using the photothermal deflection technique. In 2006, Bigotta *et al* reported laser cooling in a Yb^{3+}-doped BaY_2F_8 (BYF) single crystal (Bigotta, Parisi et al. 2006). BYF has a monoclinic crystal structure (C2/m) with two BYF formula units per unit cell (Izotova and Aleksandrov 1970). This crystal has a number of attractive properties. The low phonon energy of ~350 cm^{-1} (Toncelli, Tonelli et al. 1999) is expected to completely suppress multiphonon relaxation of the $^2F_{5/2}$ excited state, enabling a high internal quantum efficiency. The crystal has high transparency in the infrared up to 12 μm, making it less susceptible to radiative heat loading than materials with narrower transparency ranges (such as fluoride glasses and oxide crystals). The thermal conductivity of BYF is ~7× greater than that of ZBLAN glass (Bigotta, Parisi et al. 2006), facilitating the extraction of heat in an optical refrigerator. Finally, in contrast to fluoride glasses such as ZBLAN, fluoride

crystals such as BYF are not moisture sensitive, facilitating the preparation of high-quality samples and guaranteeing long-term durability.

Bigotta *et al* grew a BYF crystal doped with 2.5 mol% Yb^{3+} (with respect to the Y^{3+} site) using a Czochralski crystal growth furnace and performed an extensive study of the spectroscopic and laser-cooling properties of this sample (Bigotta, Parisi et al. 2006, Bigotta, Di Lieto et al. 2007). The starting material was BaY_2F_8 to which BaF_2 and YbF_3 powders were added to achieve the desired doping level. The powders were treated in hot HF gas by AC Materials (Tarpon Springs, FL, USA) in order to reduce oxygen impurities such as water and OH^-, and they had an estimated purity of 99.999%. The starting materials were baked out in vacuum (10^{-5} Pa), and the subsequent crystal growth was carried out in an atmosphere of high-purity argon and CF_4. The latter had to be added to prevent the reduction of Yb^{3+} to Yb^{2+}. The Czochralski crystal growth was performed with resistive heating at 995 ^oC, a pulling rate of 0.5 mm/h, and the crystal rotating at 5 rpm. The system had an automatic optical diameter control and yielded a sample of high optical quality and free of cracks or mico-bubbles. The crystal was oriented by the X-ray Laue technique, and a ~$3 \times 4 \times 10$ mm^3 sample was cut and polished such that the *a*- and *b*-axes were oriented parallel to the shorter sides of the sample. Careful absorption and emission spectroscopy at 10 K allowed the identification purely electronic transitions, yielding the crystal-field level energies of 0, 215, 447, and 546 cm^{-1} for the $^2F_{7/2}$ ground-state multiplet and 10306, 10425, and 10770 cm^{-1} for the $^2F_{5/2}$ excited-state multiplet. Importantly, Bigotta *et al* pointed out that the absorption spectrum offered peaks that were spectrally narrower and therefore had higher peak cross section (*e.g.*, the E3→E5 transition around 1015 nm, see Figure 23, left) than corresponding transitions in ZBLAN glass. This is a result of the much reduced inhomogeneous broadening in the crystal compared to the glass and allows more

efficient excitation of Yb^{3+}. A $^2F_{5/2}$ lifetime of 2.0 ms and a mean fluorescence wavelength $\tilde{\lambda}_f = 995$ nm were measured at 300 K. They used a pair of diode lasers mounted with their junctions oriented perpendicularly, operating at 1024 nm (~2 nm bandwidth), and providing ~3 W of pump power. The crystal was mounted in a $10 \times 10 \times 10$ cm^3 steel vacuum chamber (<0.1 Pa) by suspending it on two crossed microscope cover slips in order to minimize the convective and conductive heat loads from the environment. The crystal temperature was measured by a thermal camera (calibrated against a thermocouple) that imaged the crystal through a BaF_2 window. The crystal showed a temperature drop of 4 K (starting from 293 K) in ~30 min when pumped in a single-pass configuration. From these measurements, a cooling power of 2.4 mW and a cooling efficiency of ~3% were estimated. The laser diodes had limited tunability and prevented excitation of the sample at the predicted optimum wavelength of 1015 nm.

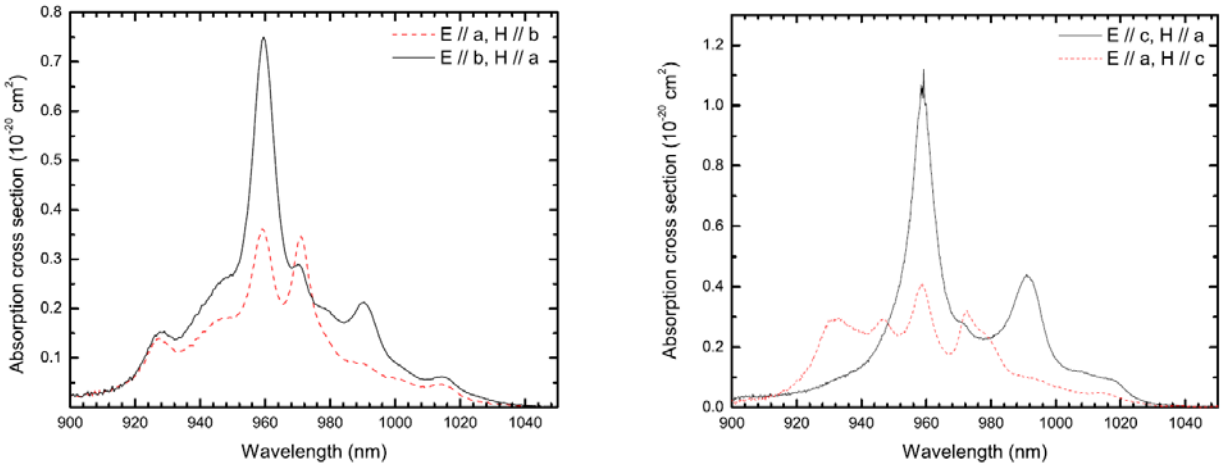

Figure 23: Polarized absorption spectra of BaY_2F_8:2.5%Yb^{3+} (left) and $YLiF_4$:5%Yb^{3+} (right) at room temperature (Bigotta, Di Lieto et al. 2007). *Reproduced with permission from S. Bigotta, A. Di Lieto, D. Parisi, A. Toncelli, M. Tonelli, Single fluoride crystals as materials for laser cooling applications, in Laser Cooling of Solids, Proc. SPIE Vol. 6461, 2007.*

$YLiF_4$ (YLF)

Bigotta *et al* presented a first laser-cooling study of Yb^{3+}-doped $YLiF_4$ (YLF) in 2007 (Bigotta, Di Lieto et al. 2007). YLF is one of the most common laser materials. It has a scheelite structure and crystallizes in the $I4_1/a$ space group (Bensalah, Guyot et al. 2004). The thermal conductivity is 6.3 W/m·K (Bigotta, Di Lieto et al. 2007), similar to that of BYF. The highest phonon energy in YLF is ~450 cm^{-1} (Orlovskii, Basiev et al. 2002) which is higher than that BYF (~350 cm^{-1}) but still sufficiently low to suppress multiphonon relaxation of the $^2F_{5/2}$ excited state. Bensalah *et al* performed a detail study of YLF:Yb^{3+} and reported the crystal-field level energies of 0, 218, 248, and 485 cm^{-1} for the $^2F_{7/2}$ ground-state multiplet and 10293, 10416, and 10554 cm^{-1} for the $^2F_{5/2}$ excited-state multiplet. Note that the total crystal-field splitting of the ground state in

YLF:Yb^{3+} is smaller ($\delta E_g = 485\,\mathrm{cm}^{-1}$) than in BYF:$Yb^{3+}$ ($\delta E_g = 546\,\mathrm{cm}^{-1}$) which may, in principle, allow YLF:Yb^{3+} to reach lower temperatures (see Section 2.3).

Bigotta *et al* used a Czochralski furnace to grow a 5 mol% Yb^{3+}-doped YLF crystal at a pulling rate of 1 mm/hr at 845 ^{o}C (Bigotta, Di Lieto et al. 2007). The starting materials and growth conditions were otherwise identical to the BYF crystal growth described above. The crystal was oriented by the X-ray Laue technique, and a ~$4 \times 4 \times 12$ mm^3 sample was cut and polished such that the *a*- and *c*-axes were oriented parallel to the shorter sides of the sample. The sample had a mean fluorescence wavelength of $\tilde{\lambda}_f = 1002$ nm at 300 K. As shown in Figure 23, the Yb^{3+} absorption cross section was found to be greater in YLF than in BYF, which compensated for its longer mean fluorescence wavelength. They pumped the crystal in single-pass configuration with 2.6 W at 1026 nm in the vacuum-chamber geometry described above and observed a temperature drop of 6.3 K with an estimated cooling efficiency of ~2%.

Since 2008, the focus has been on using Czochralski-grown YLF crystals doped with varying amounts (1–10 %) of Yb^{3+} for the development of optical refrigerators that can reach temperatures in the cryogenic regime. Research and further progress on Yb^{3+}-doped glasses had essentially ceased since Thiede *et al* cooled ZBLANP:Yb^{3+} glass to 208 K in 2005 (Thiede, Distel et al. 2005). Significant effort was now devoted to developing the optical, thermal, and mechanical aspects of the pump cavities the crystals were placed in. Seletskiy *et al* in collaboration with Bigotta and Tonelli built on recent success with YLF:Yb^{3+} and introduced a cavity-enhanced resonant absorption scheme (Seletskiy, Hasselbeck et al. 2008). They placed a YLF:5%Yb^{3+} crystal inside an actively-stabilized Fabry-Perot cavity that allowed them to achieve ~89% absorption of the incident pump light (see Section 6.1). The ~45 W output of a

YAG:Yb disk laser operating at 1030 nm was used to pump the crystal, inducing a temperature drop of 69 K from room temperature. Additional measurements showed that this particular crystal had a minimum achievable temperature (MAT) of 170 ± 10 K, *i.e.* its cooling potential was not fully realized in this experiment.

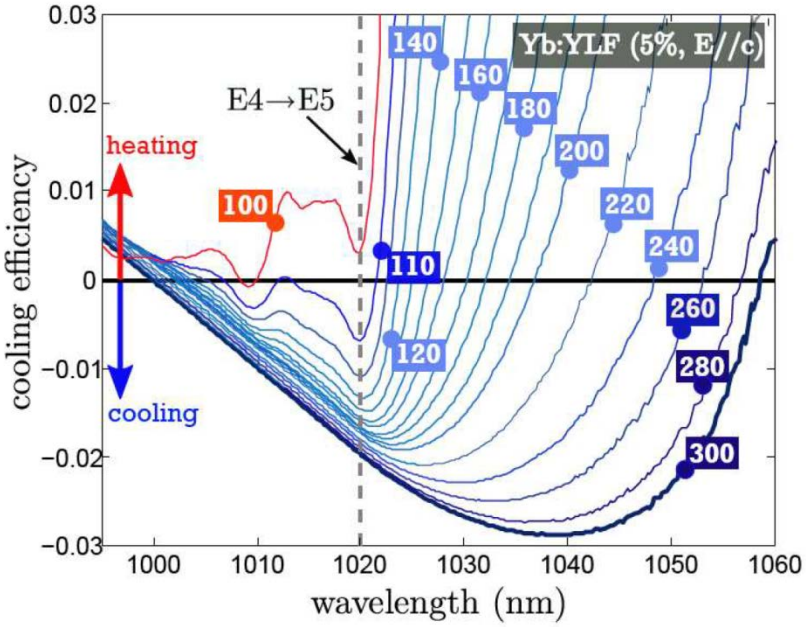

Figure 24: Measurement of cooling efficiency as a function of wavelength at different temperatures (in Kelvin, boxed values) in a 5% Yb^{3+}-doped YLF crystal excited with laser light polarized parallel to the crystal *c*-axis (Seletskiy, Melgaard et al. 2009). Given the level of background absorption in this crystal, a minimum achievable temperature (MAT) of ~105 K is predicted for pumping the E4→E5 transition at 1020 nm.

Shortly thereafter, the same team demonstrated a temperature drop of 143 K with a YLF:Yb^{3+} crystal placed in a similar actively-stabilized cavity (Seletskiy, Melgaard et al. 2009). The sample was a Czochralski-grown YLF crystal doped with 5% Yb^{3+}, Brewster-cut to a length of 1.1 cm, and oriented such that its crystal *c*-axis was parallel to the polarization of the laser. A 15.5 W pump laser operating at 1022 nm near the E4→E5 absorption at 1020 nm was used (see Figure 23, right), producing a heat lift of ~110 mW at the lowest crystal temperature. A careful spectroscopic analysis of this crystal allowed them to use Eq.(14) with $\alpha_b = 4\times10^{-4}$ cm^{-1} and measured fluorescence spectra to calculate the wavelength dependence of the cooling efficiency at different temperatures (Figure 24). This data showed that a minimum temperature of ~105 K could be possible with this sample for resonant excitation of E4→E5 at 1020 nm and indicated that cryogenic temperatures would be within reach. This result of net cooling by 143 K to ~164 K with a 110 mW heat lift not only set a new laser-cooling record but also surpassed the lowest temperatures of ~180 K that can practically be reached with thermo-electric refrigerators (Mills, Mord et al. 2002). Some subsequent improvements allowed this crystal to cool to 155 ± 1 K with a heat lift of 90 mW (Seletskiy, Melgaard et al. 2010).

5% Yb^{3+}-doped YLF crystals were also used in experiments that cooled a GaAs/InGaP semiconductor load attached to the cooling crystal to 165 K (Seletskiy, Melgaard et al. 2010). This crystal composition was also used for recent experiments that demonstrated laser cooling to 124 K (Melgaard, Seletskiy et al. 2013). The latest record cooling results were achieved with 10% Yb^{3+}-doped crystals, which enabled cooling to 114 K (Melgaard, Seletskiy et al. 2013) and 93 K (Melgaard, Seletskiy et al. 2014).

5.2. Tm^{3+}-Doped Materials

The first excited state of Tm^{3+} ($^3F_4$) is at approximately half the energy of the first excited state of Yb^{3+} ($^2F_{5/2}$) (see Figure 7). Therefore, the cooling efficiency of Tm^{3+}-doped materials can potentially be about twice as high than for Yb^{3+}-doped materials [see Eq.(14)], making Tm^{3+} attractive for optical refrigeration. Multiphonon relaxation of the $^3F_4$ excited state to the $^3H_6$ ground state multiplet is insignificant in fluorides (maximum phonon energy 350–600 cm^{-1}, see Figure 12) given the ~5000 cm^{-1} energy gap, enabling the required high quantum efficiency of the emitting state. Note that there is inconsistency in the literature regarding the notation of the first exited state of Tm^{3+}. Some studies refer to it as $^3H_4$, which originates from the somewhat confusing albeit correct labeling of the ^3H and ^3F manifold levels in the original paper by Dieke (Dieke and Crosswhite 1963). The correct notation of the first excited state of Tm^{3+} is $^3F_4$ as shown in Figure 7 (Hehlen, Brik et al. 2013).

Tm^{3+}-doped ZBLANP glass was the first non Yb^{3+}-based solid to be cooled (Hoyt, Sheik-Bahae et al. 2000, Hoyt 2003). Hoyt *et al* demonstrated that the cooling efficiency scales inversely with the energy gap as expected from Eq. (5). Several studies of net bulk laser cooling in Tm^{3+}-doped materials have been reported in the 2000–2008 time period, and the respective results are summarized in Table 2. Compared to Yb^{3+}, however, Tm^{3+} has received considerably less attention. There are no fundamental obstacles for laser cooling to cryogenic temperatures with Tm^{3+}, and the reasons for the limited number of efforts seem to have more practical origins. For example, all laser-cooling studies with Tm^{3+} reported to date (Table 2) used rather complex Nd:YAG laser pumped OPOs. Turn-key thulium-fiber lasers with >100 Watt output power have only recently become available at the ~1900 nm pump wavelength of the $^3H_6 \rightarrow {}^3F_4$ transition. Such lasers are much less commonly found in laboratories than the widespread commercial

tunable Ti:sapphire or semiconductor diode lasers, which may have biased research towards Yb^{3+} materials. Furthermore, the recent advances in the thermal and optical design of laser cooling cavities achieved with YLF:Yb^{3+} (see Section 6) have not yet been applied to Tm^{3+}-doped crystals for which they promise to allow for equally dramatic improvements of laser cooling performance. A revival of laser-cooling research on Tm^{3+}-doped materials may therefore be called for and result in high-efficiency cryogenic optical refrigerators in the not too distant future.

5.2.1. Glasses

The only glass in which net cooling with Tm^{3+} has been reported is ZBLANP:Tm^{3+}. Sheik-Bahae *et al* first observed laser cooling by 1.25 K in ZBLANP:Tm^{3+} in 2000 (Sheik-Bahae, Hoyt et al. 2000). Follow on studies by Hoyt *et al* reported laser cooling in a ZBLANP glass sample doped with 1 wt% Tm^{3+} cut from a high-purity fiber perform (Hoyt, Sheik-Bahae et al. 2000, Sheik-Bahae, Hoyt et al. 2001). The sample was pumped by a Nd:YAG pumped OPO having an average output power of 6.2 W and tunability across the 1750–2050 nm wavelength range. The sample was placed on thin glass supports in a vacuum chamber and showed 1.2 K of cooling from room temperature when pumped at 1900 nm in single-pass configuration with 40 mW of absorbed power. The result is presented in Figure 17 where the normalized temperature change is shown for different pump wavelengths. The sample showed bulk cooling as the laser wavelength exceeded the mean fluorescence wavelength of 1820 nm, showed maximum cooling around 1900 nm, and heated at pump wavelengths >1965 nm due to background absorption by impurities. These first studies were followed by cooling of a ZBLANP:1wt%Tm^{3+} sample in multi-pass pump geometry (Hoyt, Hasselbeck et al. 2003). A temperature drop of 19 K from

room temperature was achieved (see Figure 20, right), a result that still represents the current laser cooling record with Tm^{3+}. The authors also conducted measurements of the cooling efficiency and were able to experimentally confirm the expected factor of ~2 greater cooling efficiency in ZBLANP:Tm^{3+} compared Yb^{3+}-doped systems.

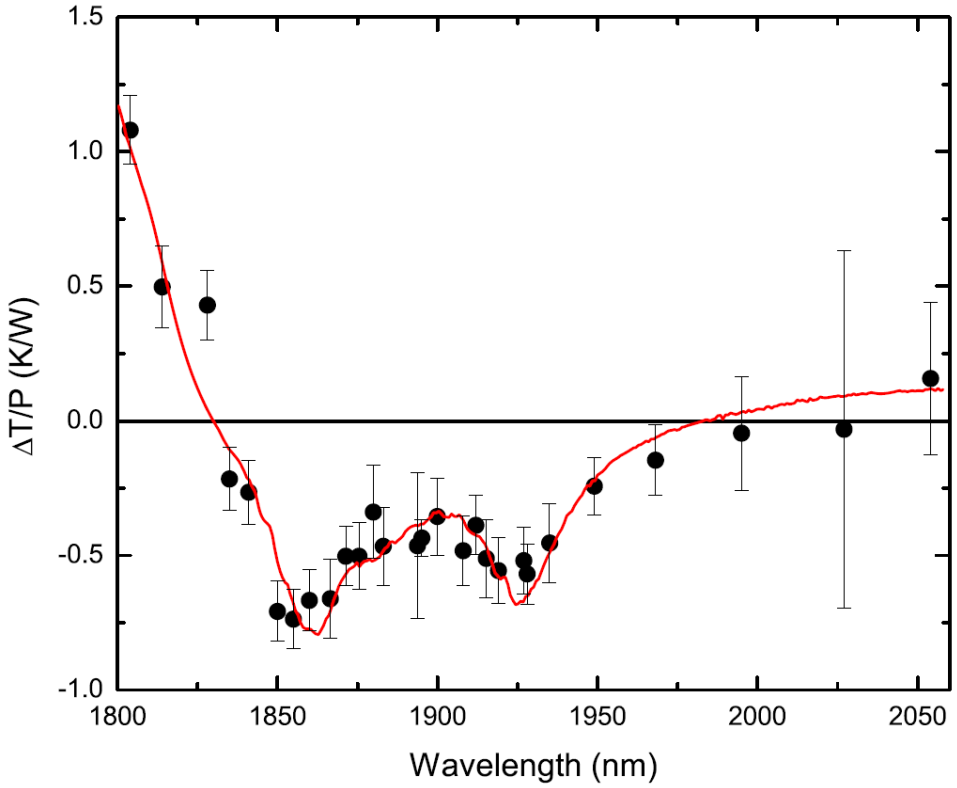

Figure 25: Normalized temperature change in 1.2% Tm^{3+}-doped BaY_2F_8 for $E \parallel b$ pump polarization (Patterson, Bigotta et al. 2008). . Data below the horizontal line indicate net cooling.

5.2.2. Crystals

The only Tm^{3+}-doped crystal system studied so far has been $BaY_2F_8:Tm^{3+}$. In 2004, Patterson *et al* reported laser cooling of a Tm^{3+}-doped crystal for the first time (Patterson, Hasselbeck et al. 2004). They used a $BaY_2F_8:Tm^{3+}$ crystal grown by the Czochralski method and pumped it in single-pass geometry using a high-power OPO with 4–6 W output power in the 1700–2100 nm tuning range to achieve cooling by ~1.5 K when pumping at 1902 nm. A second study by Patterson *et al* used a high-purity BaY_2F_8 crystal doped with 1.2% Tm^{3+} pumped in single-pass geometry (Patterson, Bigotta et al. 2008). They measured a mean fluorescence wavelength of 1793 nm at room temperature and pointed out the advantageous higher peak absorption cross sections afforded by the crystalline host compared to the amorphous ZBLAN samples studied earlier. The measurement of normalized temperature drop for different pump wavelengths is shown in Figure 25 and indicates maximum cooling at 1855 nm, where a net temperature drop of 3.2 K was obtained with 4.4 W of pump power. The red curve shown in Figure 25 is a fit to the experimental data and yielded a quantum efficiency of $\eta = 0.98$ and a background absorption coefficient of 2×10^{-4} cm^{-1}. The cooling efficiency was highest with 3.4% at a pump wavelength of 1934 nm.

5.3. Er^{3+}-Doped Materials

Several laser-cooling studies of Er^{3+}-doped materials have been reported, and the respective results are summarized in Table 3. Unlike Yb^{3+}, the $[Xe]4f^{11}$ electron configuration of Er^{3+} produces a large number of $^{2S+1}L_J$ electronic states (see Figure 7). While any excited state can – in principle – be chosen for performing a laser cooling cycle such as shown in Figure 9,

interference from other excited states has to be considered. Absorption from the excited state to even higher excited states (excited state absorption, ESA) or multiphonon relaxation to a lower state may be possible. Two-ion processes such as energy transfer upconversion (ETU), cross relaxation (CR), or energy migration to defects may become active at higher Er^{3+} ion densities. While the other excited states may have a high quantum efficiency in low-energy phonon hosts, such side processes are in most cases accompanied by some degree of exothermic non-radiative relaxation (heating) and are generally expected to be detrimental to laser cooling. This possible drawback, however, is offset by the possibility of implementing a cooling cycle with lower pump energy and thus potentially higher efficiency compared to Yb^{3+}. As seen in Figure 7, the first excited state of Er^{3+}, $^4I_{13/2}$, is at an energy of ~6400 cm^{-1}, *i.e.* only about two-thirds of the energy of the Yb^{3+} $^2F_{5/2}$ excited state. Everything else being equal, this may allow for a ~50% higher cooling efficiency compared to Yb^{3+}.

KPb_2Cl_5 (KPC)

KPb_2Cl_5 (Nostrand, Page et al. 2001) and $Cs_3Tl_2Cl_9$ (Kamber, Egger et al. 1998) are the only heavy-halide hosts known to be only slightly hygroscopic. While $Cs_3Tl_2Cl_9$ is attractive because it offers a crystallographic site for a M^{3+} ion and is therefore suited for doping with high concentrations of Ln^{3+} ions, the high toxicity of this thallium compound poses challenges for sample preparation and handling. KPb_2Cl_5 is friendlier in this respect, but its Pb^{2+} site requires charge compensation when doping with Ln^{3+} ions. Jenkins *et al* presented a spectroscopic study of Er^{3+}-doped KPC and concluded that Er^{3+} replaced Pb^{2+} accompanied by the formation of K^+ vacancies (Jenkins, Bowman et al. 2003)). The need for charge compensation and thus disruption of the crystal lattice limits the maximum doping level to ~3% (Condon, O'Connor et al. 2006).

KPC is attractive for its very low maximum phonon energy of ~203 cm^{-1} (Nostrand, Page et al. 2001) that effectively suppresses multiphonon relaxation for most Er^{3+} excited states and thus enables high quantum efficiencies.

KPC crystals however have poor mechanical properties and are rather difficult to grow (Voda, Al-Saleh et al. 2004). Fernandez *et al* grew a 0.5 mol% Er^{3+}-doped KPC single crystal in a sealed silica ampoule by the Bridgman technique (Fernandez, Garcia-Adeva et al. 2006). The KCl and $PbCl_2$ starting materials were first dried under vacuum at 220 ^oC in quartz vessels. The samples were then cooled, an atmosphere of high-purity argon and CCl_4 was introduced, and the temperature was raised from room temperature to 50 K above the melting point of the respective compound. Quantitative removal of oxygen and water traces was indicated when the meniscus of the melt in the vessel changed from concave to convex, *i.e.* the melt became non-wetting (Voda, Al-Saleh et al. 2004). This was followed by zone-refining with 5–10 passes in a horizontal furnace. The resulting starting materials were then mixed stoichiometrically because KPC melts congruently at 434 ^oC (Gabriel and Pelton 1985). The mixture was again dried under vacuum, treated with Ar/CCl_4, and finally sealed under chlorine atmosphere. The subsequent crystal growth was performed in a two-zone vertical and transparent Bridgman furnace at a growth rate of 1–2 mm/h and under tight temperature control to within 0.1 K at the location of crystallization. The resulting crystals boules were 12–16 mm in diameter and 20–40 mm long, from which a $4.5 \times 6.5 \times 2.7$ mm^3 sized sample was cut. Photothermal deflection measurements were performed with the sample in a vacuum chamber (~10^{-2} mbar) and pumped by a 1.5 W tunable laser operating in the 835–875 nm range to excite the $^4I_{15/2} \rightarrow {}^4I_{9/2}$ transition, *i.e.* the third excited state of Er^{3+} (see Figure 7). Internal local laser cooling was observed when the pump wavelength exceeded ~852.5 nm. A subsequent bulk cooling experiment utilized a thermal

camera and found a temperature drop of ~0.7 K over the course of 1500 s when pumping at 870 nm with 1.9 W.

This work was followed in 2009 by Condon *et al* who pumped the $^4I_{15/2} \rightarrow {}^4I_{13/2}$ transition at 1568 nm to excite Er^{3+} to its first rather than its third excited state (Condon, Bowman et al. 2009). They grew a KPC crystal with a concentration of 3.6×10^{19} Er^{3+}/cm^3 (i.e. ~0.39 mol% with respect to Pb^{2+}). They used a modified Bridgman technique with zone-refined KPC starting materials and an extended cool-down routine (Condon, O'Connor et al. 2006). A crystallographically oriented rod 3 mm in diameter and 13.6 mm long was cut from the boule, polished, and placed on the edges of glass cover slips inside a vacuum chamber. A fine-wire (0.001") thermocouple was put in contact with the surface in the middle of the crystal to allow for a direct temperature measurement. A mean fluorescence wavelength of $\tilde{\lambda}_f = 1539.8$ nm was measured at room temperature. Several low-power laser diodes were then used to provide pumping at different wavelengths. Bulk heating was observed for pumping at 1527.0 and 1533.3 nm ($\lambda < \tilde{\lambda}_f$), almost no temperature change was found for pumping at 1557.7 nm, and bulk cooling by 0.0072 and 0.0136 K was found for pumping at 1564.2 and 1567.6 nm, respectively. Note that the wavelength for cross-over from heating to cooling occurred at a significantly longer wavelength (1557.7 nm) than $\tilde{\lambda}_f$ even though the quantum efficiency of the $^4I_{13/2}$ excited state was expected to be ~100%. The authors attributed this to an additional heat load that was created by excited states other than $^4I_{13/2}$ participating in the excitation and relaxation processes.

CNBZn glass

CNBZn designates a fluorochloride glass having the composition CdF_2–$CdCl_2$–NaF–BaF_2–$BaCl_2$–ZnF_2. Fernandez *et al* procured a 0.5 mol% ErF_3-doped CNBZn sample from the Laboratoire de Verres et Ceramiques of the University of Rennes (Fernandez, Garcia-Adeva et al. 2006). A 10.7 × 10.7 × 2.2 mm^3 sized sample was prepared and characterized following their procedures described above for KPC:Er^{3+}. The photothermal deflection experiments showed local internal laser cooling for pump wavelengths >843 nm. A subsequent bulk cooling experiment found a temperature drop of ~0.5 K over the course of 1200 s when pumping at 860 nm with 1.9 W.

5.4. Other Lanthanides

Yb^{3+}, Tm^{3+}, and Er^{3+} are the only lanthanide ions that have shown net laser-induced bulk cooling to date. As shown in Figure 7, Ho^{3+} and Dy^{3+} have even lower energy first excited states and may therefore enable even higher cooling efficiencies. The energy of the first excited state of Ho^{3+} ($^5I_7$) is similar to that of Tm^{3+} ($^3F_4$) and is therefore expected to have minimal multiphonon relaxation in fluoride hosts. The Ho^{3+} $^5I_8 \leftrightarrow {}^5I_7$ transition is at slightly longer wavelength than the Tm^{3+} $^3H_6 \leftrightarrow {}^3F_4$ transition, making it somewhat better suited for pumping with modern Tm-doped fiber lasers that can have 10–50 W (air cooled) or 50–200 W (water cooled) output power in the 1900-2050 nm wavelength range (*e.g.* IPG Photonics). Another advantage may be the higher absorption cross section of Ho^{3+} compared to Tm^{3+} in the long-wavelength (cooling) tail of the respective absorption spectra (Scholle, Lamrini et al. 2010). As shown in Figure 26, the features

of the $^5I_8 \rightarrow {}^5I_7$ absorption in YLF:Ho^{3+} in the 2000–2080 nm range have peak absorption cross sections of up to 5×10^{-21} cm^2 (π-polarization), which is almost 10× greater than the absorption cross sections YLF:Tm^{3+} in the 1820–1970 nm range (Walsh, Barnes et al. 1998) and may allow for a higher cooling efficiency in Ho^{3+}. A comparative study of Tm^{3+} and Ho^{3+} in various fluoride crystalline materials would provide the detailed spectroscopic information needed to assess the tradeoffs relevant for laser cooling.

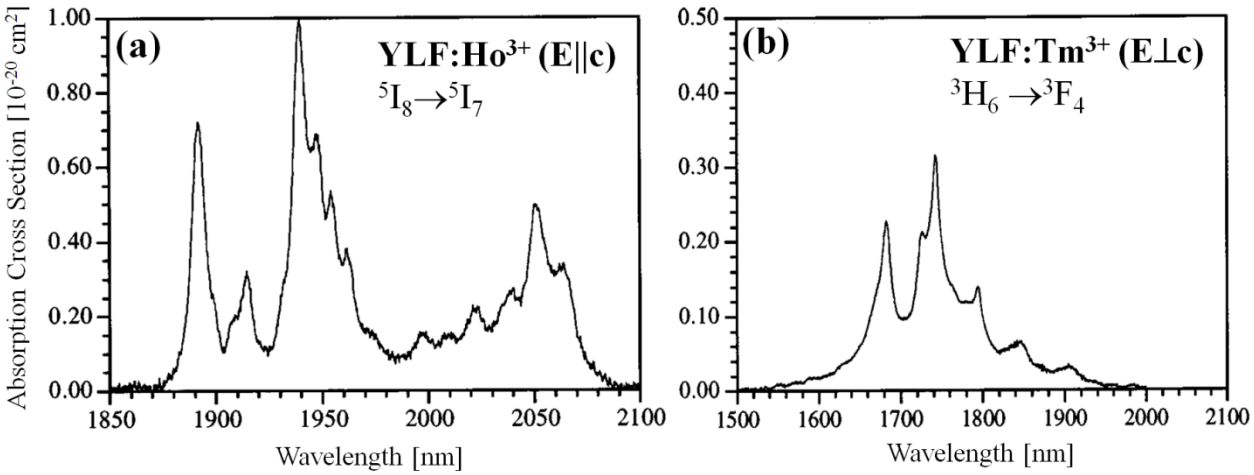

Figure 26: Polarized absorption cross sections of (a) Ho^{3+} and (b) Tm^{3+} doped YLF at room temperature (Walsh, Barnes et al. 1998). *Reproduced with permission from B.M. Walsh, N.P. Barnes, B. Di Bartolo, Branching ratios, cross sections, and radiative lifetimes of rare earth ions in solids: Application to Tm^{3+} and Ho^{3+} ions in $LiYF_4$, J. Appl. Phys.* ***83*** *(1998) 2272. Copyright 1998, AIP Publishing LLC.*

Another interesting candidate for solid-state laser refrigeration is the $^6H_{15/2} \leftrightarrow {}^6H_{13/2}$ transition of Dy^{3+}, which may offer a 3× greater cooling efficiency than Yb^{3+} (see Figure 7). The low energy of the $^6H_{13/2}$ excited state of ~3500 cm^{-1} however makes multiphonon relaxation competitive with radiative relaxation in most oxide and fluoride materials. The high quantum efficiencies needed for efficient laser cooling can likely only be achieved by doping Dy^{3+} into a chloride or bromide host material. KPb_2Cl_5 may be a candidate host as its highest-energy optical phonon energy is only ~203 cm^{-1} (Nostrand, Page et al. 2001), and it is substantially less hygroscopic than other heavy halide materials (see Section 5.3).

6. TOWARDS LASER COOLING DEVICES

6.1. Optical Cavities

Practical solid-state optical refrigerators aim at cooling a payload such as an optical or radiation sensor. The specifics of an application will require a tradeoff between the refrigerator temperature and the heat lift within the constraints of the laser-cooling material and available pump laser power. A real-world macroscopic payload is likely to represent a significant heat source and will require hundreds of mW or more of heat lift. As shown in Section 2.3, the total power density deposited in the laser-cooling element is given by $P_{net} = -\eta_c P_{abs}$ [see Eq.(14)], with $P_{net} < 0$ denoting cooling. The refrigerator therefore has to be designed to maximize the absorption efficiency [see Eq.(15)], *i.e.* maximize αL, where α and L are the resonant

absorption coefficient and the path length, respectively. The rapid decrease of α with decreasing temperature (see Figure 15) therefore necessitates a pump geometry that allows for long path lengths of the pump light in the cooling material. Useful path lengths will typically exceed the physical size of the cooling material by a large factor and thus require some sort of cavity in order to create a geometry in which the pump laser makes more than one round trip through the cooling element. A variety of non-resonant and resonant cavities have been suggested and implemented over the years.

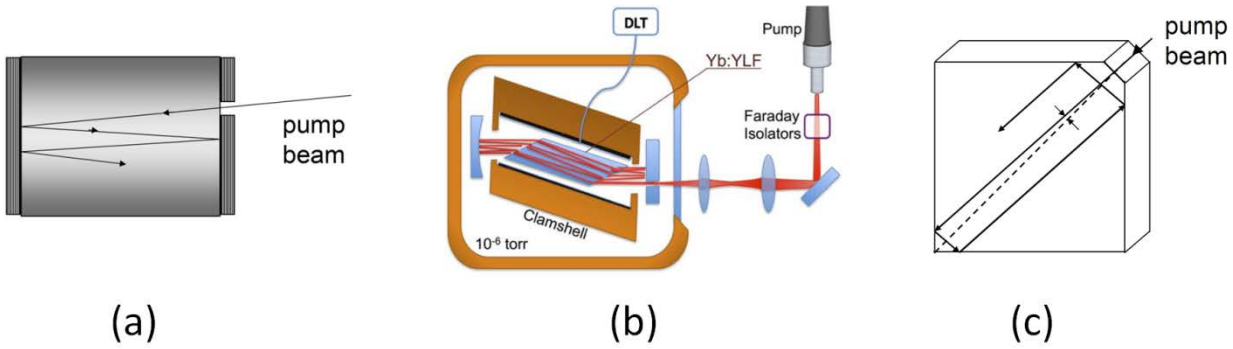

Figure 27: Non-resonant pump cavities used in solid-state optical refrigeration (Hoyt 2003, Melgaard, Seletskiy et al. 2013). (a) Monolithic cavity with dielectric mirrors deposited directly onto the cooling element and a small hole in the mirror to admit the pump light; (b) non-resonant cavity with an external curved back mirror and an external planar mirror with a hole to admit the pump light; (c) monolithic optical maze using multiple total internal reflections to trap the pump light that is injected through a small facet.

Non-resonant pump cavities

In non-resonant cavities, the pump light traverses the cooling element multiple times at an angle slightly off-normal to the mirrors (Hoyt 2003). Edwards *et al* were the first to directly deposit high-reflectivity dielectric mirrors onto opposing faces of a cylindrical ZBLAN:Yb^{3+} sample to form a monolithic non-resonant cavity for the pump light (Edwards, Buchwald et al. 1998, Edwards, Anderson et al. 1999). They created a 150-μm diameter hole in one of the mirrors to admit the pump laser beam which was then trapped between the two mirrors. This geometry is shown in Figure 27a. Thiede *et al* used the same geometry with a <1-mm hole in their record-cooling result of ZBLANP:Yb^{3+} to 208 K (Thiede, Distel et al. 2005). Depositing the mirrors directly onto the cooling element is attractive because it allows for a potentially large number of passes. However, Epstein *et al* found that YAG:Yb^{3+} crystals did not cool when dielectric mirrors were deposited directly onto the crystal to form a monolithic cavity, whereas the same samples cooled in a single-pass pump geometry (Epstein, Brown et al. 2001). A similar observation was made by Hoyt *et al* for ZBLANP:Tm^{3+} (Hoyt, Hasselbeck et al. 2003). They attributed this effect to absorption by and thus heating of the mirrors by the pump light. This is particularly detrimental because the mirrors are in contact with the cooling element and directly degrade the cooling performance. Mirror heating effectively represents another contribution to background absorption. Furthermore, trapping of the fluorescence in the crystal is increased because the mirrors are also reflective at the nearby fluorescence wavelengths. These drawbacks have steered subsequent efforts towards non-resonant cavities with external mirrors placed some distance away from the cooling element (see Figure 27b). Such a geometry eliminates the conduction of heat generated in the mirror to the cooling element and significantly reduces the solid angle for fluorescence trapping. A non-resonant cavity with external mirrors having

~99.9% reflectance was first reported by Hoyt *et al* in their work on laser cooling of ZBLANP:Tm^{3+} (Hoyt, Hasselbeck et al. 2003). Their cavity was formed by a planar dielectric mirror with a ~0.4 mm-diameter hole to admit the pump beam and a second dielectric mirror with a 1 m radius of curvature. A similar geometry was used in recent record-cooling experiments by Seletskiy and Melgaard *et al* using YLF:Yb^{3+} (Seletskiy, Melgaard et al. 2010, Seletskiy, Melgaard et al. 2010, Melgaard, Seletskiy et al. 2013). They prepared the facets of the YLF:Yb^{3+} crystal to form Brewster's angle with the laser propagation direction in order to minimize reflection losses. A lens pair was used to mode-match the laser to the non-resonant cavity which consisted of a flat mirror with a 1-mm diameter hole and a concave back mirror ($R = 25$ cm) separated by ~3.5 cm. Care was taken to avoid saturation of the resonant absorption by optimizing the lens pair separation and focusing spot size at the flat mirror. They achieved five to eight roundtrip passes of the pump laser through the crystal for an effective pump path length of 10–20 cm through the crystal. With a resonant absorption coefficient of ~0.03 cm^{-1} (at 1020 nm, $E \| \vec{c}$) for YLF:Yb^{3+} at cryogenic temperatures (see Figure 6), this corresponds to absorption of 50–75% of the incident pump power. This was confirmed by Melgaard *et al* who estimated ~18 W of absorbed power for an incident pump power of 45 W with five roundtrip passes through a 1.2-cm long YLF:Yb^{3+} crystal (Melgaard, Seletskiy et al. 2013).

Sheik-Bahae *et al* and Hoyt proposed the use of a Monolithic Optical Maze (MOM) for trapping pump light by multiple total internal reflections (Sheik-Bahae, Hoyt et al. 2001, Hoyt 2003). As shown in Figure 27c, the laser cooling element can be shaped into a cuboid with a small triangular facet on one corner or a small rectangular facet on one edge of the slab. The pump beam is then coupled through this facet into the slab at a shallow angle with respect to the cuboid diagonal and undergoes multiple total internal reflections to create an extended path

length for the pump beam. The authors were able to demonstrate 7.5 K of cooling from room temperature in ZBLANP:Tm^{3+} pumped with 2.8 W at 1880 nm in such a MOM geometry. This constituted a 6-fold increase of the pump absorption compared to a single-pass geometry using a 10-mm long sample of identical composition.

Resonant pump cavities

Hoyt, Hasselbeck, and Sheik-Bahae pointed out in 2003 that – in principle – complete absorption of the incident pump light by the cooling element can be achieved in a resonant cavity where the pump light interferometically couples to cavity modes. As shown in Figure 28, the resonant cavity consists of an input coupling mirror with reflectivity R_I and a back mirror with high reflectivity R_B. The absorption of the pump light by the cooling element in the cavity is given by (Seletskiy, Hasselbeck et al. 2010)

$$A = 1 - \left(\frac{\sqrt{R_I} - e^{-\alpha L}}{1 - e^{-\alpha L}\sqrt{R_I}} \right)^2 \tag{33}$$

where L is the length and α is the absorption coefficient of the crystal. Maximum absorption occurs if $R_I = R_B \exp(-2\alpha L)$. Note that the absorption can reach $A = 1$ if $R_B = 1$. In practice, R_I and R_B are fixed, and the cavity length is actively tuned via piezo-control of the input-coupling

mirror. Further note that the cavity length has to be adjusted as α changes with changing temperature. Using such a setup, Seletskiy *et al* achieved an absorption of 0.89 ± 0.02 with 5% Yb^{3+}-doped YLF (Seletskiy, Hasselbeck et al. 2008, Seletskiy, Melgaard et al. 2009) and 0.89 ± 0.03 with 2% Yb^{3+}-doped ZBLAN (Seletskiy, Hasselbeck et al. 2010). This absorption is on par with the best non-resonant light-trapping schemes (Thiede, Distel et al. 2005). A resonant cavity geometry is attractive for a number of reasons including the elimination of losses associated with the pinhole in non-resonant cavities, insensitivity to mirror heating, absence of pump light leakage, and scalability by matching the cavity mode volume to the size of the cooling element (Seletskiy, Hasselbeck et al. 2010). The primary drawback of this approach is the complexity associated with the active piezo-electric stabilization of the cavity.

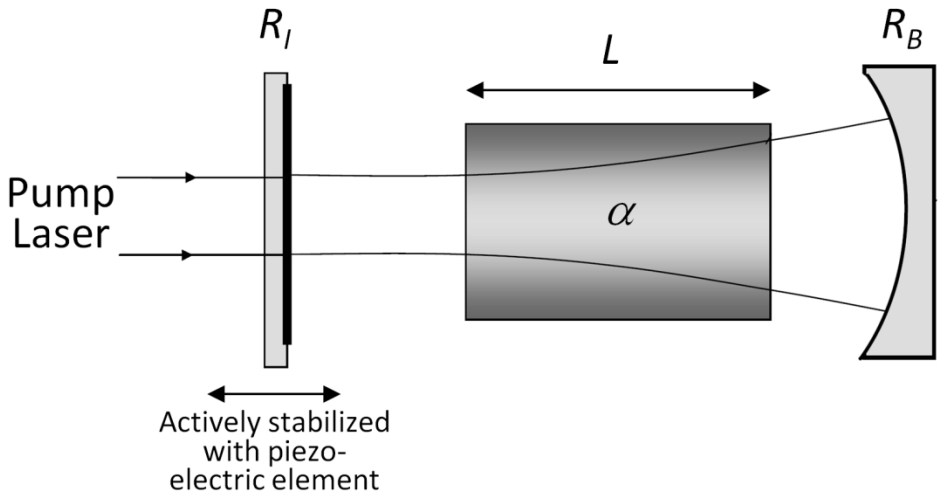

Figure 28: Resonant cavity consisting of a partially reflective planar mirror and a highly reflective concave back mirror. As the sample cools, the resonance condition changes and the cavity length must be actively stabilized (Hoyt 2003).

Another variation of pumping the cooling element in a resonant cavity is to place the sample inside a laser cavity. This approach was used in the 1968 experiment by Kushida *et al* who placed the YAG:Nd^{3+} cooling element inside the YAG:Nd^{3+} laser cavity and observed less-than-expected heating (Kushida and Geusic 1968). In 2004, Heeg *et al* achieved bulk cooling of a 2% Yb^{3+}-doped ZBLAN glass using intracavity pumping (Heeg, Stone et al. 2004). The pump laser consisted of a 10% Yb^{3+}-doped $KY(WO_4)_2$ crystal pumped longitudinally by two counterpropagating 4 W stripe diode lasers operating at 981.2 nm, and it was tunable from ~1020 to 1040 nm by means of a Brewster prism (maximum power of 1.2 W at 1032 nm). The Brewster-cut ZBLAN:Yb^{3+} sample was mounted inside a vacuum cell which was then inserted into the laser cavity. They achieved a 6 K temperature drop from room temperature. A more recent intra-cavity pumping approach uses a vertical external cavity surface emitting laser (VECSEL) (Ghasemkhani, Albrecht et al. 2014). Ghasemkhani *et al* designed a VECSEL cavity that consisted of a distributed Bragg reflector (DBR) made from 24 pairs of GaAs/AlAs layers, followed by a GaAs barrier, 12 InGaAs quantum wells that formed the active region, and a capping layer. This structure was deposited onto a diamond heat spreader and attached to a heat sink. A curved output coupler formed the other side of the cavity. The active structure was optically pumped by a 75 W diode laser operating at 808 nm, and the VECSEL produced ~20 W of output power at 1020 nm with tunability from 1003 to 1030 nm by means of a birefringent filter. A 7% Yb^{3+}-doped YLF crystal was placed inside the cavity and showed cooling by 155 K (to 130 K from room temperature) with a heat lift of 150 mW for an absorbed power of 12 W. Such a cavity design is particularly amenable to scaling to high pump powers.

6.2. Thermal Management

The performance of a solid-state optical refrigerator is determined by the competition between the cooling power, P_{cool}, and the heat load on the cooling element, P_{load}. The change in temperature of the cooling element is given by (Edwards, Anderson et al. 1999, Melgaard 2013)

$$C(T)\frac{dT}{dt} = -P_{cool} + P_{load} \tag{34}$$

where $C(T) = c_v(T)\rho V_s$ is the heat capacity, which depends on the specific heat, $c_v(T)$, the density, ρ, and the sample volume, V_s. In thermal equilibrium ($dT/dt = 0$) one has $P_{cool} = P_{load}$. The heat load power has contributions from convective, conductive, and radiative heat transfer from the environment to the cooling element, $P_{load} = P_{conv} + P_{cond} + P_{rad}$. Including these in Eq.(34) yields (Melgaard 2013)

$$C(T)\frac{dT}{dt} = \eta_c P_{abs} + A_s\kappa_h(T_c - T_s) + \frac{N\kappa_L(T)A_L}{d_L}(T_c - T_s) + \frac{\varepsilon_s A_s\sigma}{1+\chi}\left(T_c^4 - T_s^4\right). \tag{35}$$

In Eq.(35), the subscripts s and c denote the sample and the surrounding chamber, respectively. The first term on the right hand side is the cooling power derived earlier [Eq.(14)]; the second term is the convective heat load, P_{conv}, given by the sample area, A_s, and the convective heat transfer coefficient, κ_h; the third term is the conductive heat load, P_{cond}, given by the number of contact points, N, with area A_L, length d_L, and thermal conductivity κ_L; and the fourth term is the radiative (black body) heat load, P_{rad}, given by the areas A and thermal emissivities ε, where $\chi = (1-\varepsilon_c)(\varepsilon_s A_s / \varepsilon_c A_c)$ and σ is the Stefan-Boltzmann constant having a value of 5.67×10^{-8} W/m^2/K^4.

The convective heat load can be minimized by placing the cooling element inside a chamber under vacuum. The convective heat transfer coefficient at a pressure p below standard pressure can be approximated by $\kappa_h = \kappa_h^0 \left[pd/(pd + CT) \right]$, where κ_h^0 is the coefficient at standard pressure, T is the sample temperature, d is the distance between the sample and the chamber, and $C = 7.6\times10^{-5}$ N/m·K is a constant (Electric 1982). Lowering the pressure to 10^{-5} Torr with the sample at 300 K therefore reduces the convective heat transfer coefficient by a factor of ~17200×. Assuming a sample surface area of $A_s = 100$ mm^2 and a convective heat transfer coefficient for air at 300 K of 5–25 W/m^2·K thus gives a convective heat load of $\sim 2\times10^{-7}$ W/K (Melgaard 2013). The conductive heat load is reduced by mounting the sample in a way that minimizes the contact area with the warm chamber. Glass slides as well as glass fibers have been used for this purpose. Melgaard has used six 500-μm diameter glass fibers ($\kappa \approx 1.0$ W/m·K) to support a YLF:Yb^{3+} crystal 1 mm from the surrounding chamber walls and estimated an upper limit for the conductive heat load of $\sim 1.2\times10^{-5}$ W/K (Melgaard 2013). This

conductive contribution is a factor of ~60 greater than the convective contribution (at 10^{-5} Torr) and therefore requires careful attention in the device design. The radiative heat load from the surrounding chamber is by far the greatest contribution. By assuming small temperature changes, the heat load can be approximated as $P_{rad} = 4\varepsilon_s \sigma A T_c^3 \Delta T / (1+\chi)$. Seletskiy *et al* have studied the warming dynamics of a sample after turning off the pump laser at low temperatures (Seletskiy, Melgaard et al. 2010). The sample had a surface area of 150 mm^2 and was held in a chamber having inside walls with a low thermal emissivity coating. The found $\chi = 2.1$ and $\varepsilon_s \approx 0.8$ from which Melgaard estimated a radiative heat load of $\sim 2.4\times10^{-4}$ W/K with the chamber at 300 K (Melgaard 2013). This illustrates that the radiative load dominates the convective and conductive contributions by factors of 1.2×10^3 and 2.0×10^1, respectively. The key parameter χ is maximized by creating a chamber that fits tightly around the laser cooling element ($A_s/A_c \to 1$) and coating the chamber with low thermal emissivity material ($\varepsilon_c \ll \varepsilon_s$) such as Maxorb™, which is a treated nickel surface having a high solar-spectrum absorptivity of 0.97 and a low infrared emissivity of $\varepsilon_c = 0.08$ (Judkoff and Sokol 1981, Mason and Brendel 1982). The radiative heat load can also be reduced by lowering the temperature of the chamber. For example, P_{rad} is reduced by a factor of 4 if the chamber is cooled from 300 K to ~190 K, a temperature that could be reached by using a thermo-electric cooler. This was experimentally verified by Melgaard, who cooled the sample chamber to 208 K and achieved laser cooling of a YLF:5%Yb^{3+} sample to the minimum achievable temperature (MAT) of 118.7 K (Melgaard 2013).

The discussion so far has focused on the laser cooling elements itself. However, practical applications require the cooling of an actual payload. Recall that the quantum efficiency of laser-

cooling materials is close to unity, and nearly all of the absorbed laser power is re-emitted as fluorescence. Therefore, simply attaching the payload directly to the laser-cooling material is not feasible because it would be exposed to (and absorb) the large fluorescence photon flux and consequently heat up. A "thermal link" therefore has to be found that prevents most of the fluorescence from reaching the payload while offering good thermal conductivity between the laser-cooling material and the payload. Parker *et al* have presented a detailed theoretical and experimental study of four thermal link designs that included a cascaded mirror design, a kinked waveguide, a hemispherical design, and a tapered waveguide, with the latter showing the best overall performance (Parker, Mar et al. 2009). Melgaard *et al* have performed an experimental analysis of a kinked waveguide thermal link as shown in Figure 29 (Melgaard, Seletskiy et al. 2014). They fabricated the kinked waveguide from sapphire which has an excellent thermal conductivity of 46 W m^{-1} K^{-1} at 273 K and ~1000 W m^{-1} K^{-1} at 75 K (Dobrovinskaya, Lytvynov et al. 2009). The sapphire was attached to YLF crystal only by means of van-der-Waals interactions, *i.e.* atomic-scale adhesion by the intimate contact of two planar surfaces. This method eliminated any chemical adhesives that could have been the source of parasitic heating. As shown in Figure 29b, there was no measureable temperature gradient between the YLF crystal (cooling element) and the payload side of the thermal link. The optical rejection of this design was measured to 92.9%. A dielectric or metal coating at the payload side of the link could further reduce the amount of fluorescence and residual pump light reaching the payload. Also note that the thermal link, like the laser-cooling element, has to be cooled to the operating temperature and is thus subject to thermal loads from the environment. It is therefore necessary to integrate it into the tightly-fitting vacuum chamber structure along with the laser cooling element.

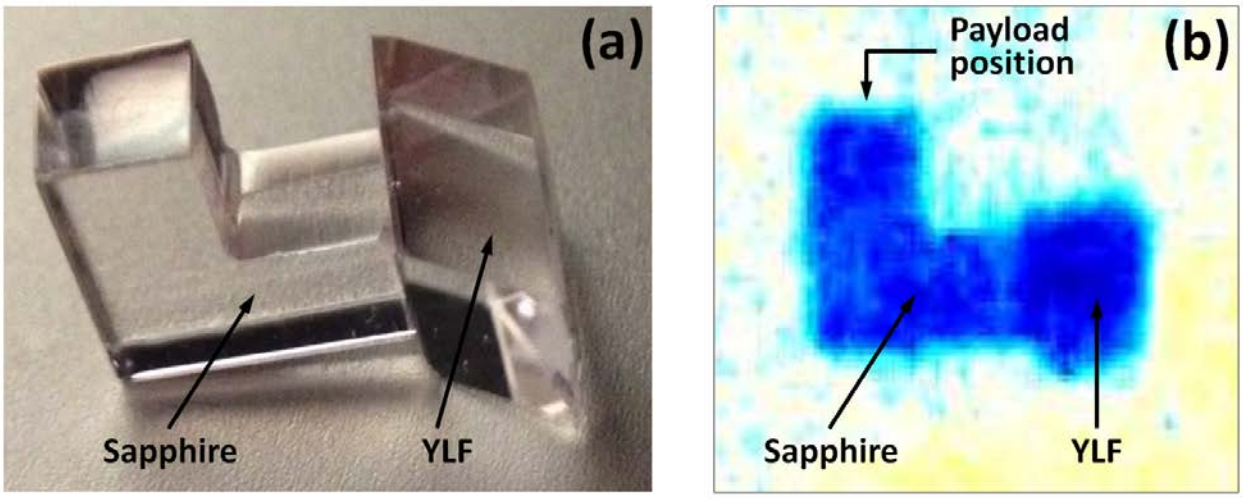

Figure 29: Experimental analysis of a thermal link constructed from sapphire. (a) Kinked sapphire waveguide van-der-Waals-bonded to a YLF crystal; (b) Temperature distribution across YLF crystal and sapphire thermal link. Figure adapted from (Melgaard, Seletskiy et al. 2014).

7. CONCLUSIONS AND OUTLOOK

The performance of optical refrigeration has dramatically improved over the last several years. Lanthanide-based optical refrigeration now shows cooling from room temperature to the neighborhood of 100 K with a cooling efficiency such that the cooling power is about 1% of the input power. Optical refrigeration has become the only solid-state technology that can cool to cryogenic temperatures. The recent discovery of optical refrigeration in CdS semiconductors shows that there are several families of materials that have good prospects for cryogenic optical refrigeration. In contrast, thermoelectric cooling (based on the Peltier effect) is the currently

dominant solid-state cooling technology, and it can cool from room temperature to only about 170 K.

As discussed in this article, there are well-defined paths forward for lowering the operating temperatures and increasing the cooling efficiencies of lanthanide-based optical refrigerators. Both experiments and calculations indicate that improving the purity of YLF:Yb^{3+} crystals will lead to optical refrigeration to temperatures below the boiling point of liquid nitrogen, 77 K. The needed purity level should be achievable by removing impurities in the starting materials with chelate-assisted solvent extraction. To further increase the cooling efficiency, one can dope the cooling crystal with a lanthanide ion that has a smaller energy first excited state. Doping ions such as Tm^{3+} and Ho^{3+} will provide nearly double the cooling efficiency, and using Dy^{3+} ions should nearly triple the cooling efficiency compared to Yb^{3+}. Additionally, by "recycling" the waste fluorescence, the cooling efficiency may be increased by about another factor of two (Sheik-Bahae and Epstein 2007, Sheik-Bahae and Epstein 2009).

Even with the demonstrated operating temperatures and efficiencies, the current generation of lanthanide-based optical cooling materials has significant potentials in a number of important areas. For some cooling applications the elimination of vibrations is so important that optical refrigeration is extremely attractive. High-performance infrared cameras and night-vision systems require cooling, but are sensitive to vibrations that blur images. This is especially true for satellite-borne systems where even slight vibrations can cause severe image degradation. Another potential early application of optical refrigeration is gamma-ray spectroscopy. High-energy-resolution is needed to identify nuclear isotopes for medical and national-security applications. High-purity germanium (HPGe) gamma-ray spectrometers can provide required energy resolution when the germanium crystals are cooled to near 100 K. However, even minor

vibrations generate variable capacitance and electronic noise that significantly blurs the spectral resolution (Upp, Keyser et al. 2005). There are niche application areas where the complete lack of vibrations of optical refrigerators may be critical. For example ultra-stable optical cavities for metrology need cooling to 124 K but cannot tolerate vibrations (Kessler, Hagemann et al. 2012). Another example is electron microscopy for studying cryogenically cooled samples (Shirazi, Kopylov et al. 2012).

While there are important applications for optical refrigerators using the current generations of lanthanide-doped materials, the potential uses for optical refrigeration expands greatly as the operating temperatures are lowered and the cooing efficiency grows. Furthermore, with large-scale deployment, the cost of optical refrigerators should drop, since there is nothing inherently costly about any of their components.

REFERENCES

Anashkina, E. and O. Antipov (2010). "Electronic (population) lensing versus thermal lensing in Yb:YAG and Nd:YAG laser rods and disks." Journal of the Optical Society of America B **27**(3): 363-369.

Anderson, M. H., J. R. Ensher, M. R. Matthews, C. E. Wieman and E. A. Cornell (1995). "Observation of Bose-Einstein Condensation in a Dilute Atomic Vapor." Science **269**(5221): 198-201.

Antipov, O. L., D. V. Bredikhin, O. N. Eremeykin, A. P. Savikin, E. V. Ivakin and A. V. Sukhadolau (2006). "Electronic mechanism for refractive-index changes in intensively pumped Yb:YAG laser crystals." Optics Letters **31**(6): 763-765.

Auzel, F. and F. Pellé (1997). "Bottleneck in multiphonon nonradiative transitions." Physical Review B **55**(17): 11006-11009.

Bao, S., P. J. Newman, A. Voelkel, Z. Zhou and D. R. MacFarlane (1995). "Electrochemical purification and GFAAS analysis of heavy metal fluoride glass." Journal of Non-Crystalline Solids **184**(0): 194-199.

Bensalah, A., Y. Guyot, M. Ito, A. Brenier, H. Sato, T. Fukuda and G. Boulon (2004). "Growth of Yb^{3+}-doped $YLiF_4$ laser crystal by the Czochralski method. Attempt of Yb^{3+} energy level assignment and estimation of the laser potentiality." Optical Materials **26**(4): 375-383.

Bigotta, S., A. Di Lieto, D. Parisi, A. Toncelli and M. Tonelli (2007). "Single fluoride crystals as materials for laser cooling applications." Proc. SPIE **6461**: 64610E-64611.

Bigotta, S., D. Parisi, L. Bonelli, A. Toncelli, A. D. Lieto and M. Tonelli (2006). "Laser cooling of Yb^{3+}-doped BaY_2F_8 single crystal." Optical Materials **28**(11): 1321-1324.

Bigotta, S., D. Parisi, L. Bonelli, A. Toncelli, M. Tonelli and A. Di Lieto (2006). "Spectroscopic and laser cooling results on Yb^{3+}-doped BaY_2F_8 single crystal." Journal of Applied Physics **100**(1).

Bigotta, S., D. Parisi, L. Bonelli, A. Toncelli, M. Tonelli and A. Di Lieto (2006). "Spectroscopic and laser cooling results on Yb^{3+}-doped BaY_2F_8 single crystal." Journal of Applied Physics **100**(1): 013109-013107.

Boccara, A. C., W. Jackson, N. M. Amer and D. Fournier (1980). "Sensitive photothermal deflection technique for measuring absorption in optically thin media." Optics Letters **5**(9): 377-379.

Bowman, S. R., N. W. Jenking, S. R. O'Connor and B. J. Feldman (2002). "Sensitivity and stability of a radiation-balanced laser system." Quantum Electronics, IEEE Journal of **38**(10): 1339-1348.

Bowman, S. R. and C. E. Mungan (2000). "New materials for optical cooling." Applied Physics B **71**(6): 807-811.

Bowman, S. R., S. P. O'Connor, S. Biswal, N. J. Condon and A. Rosenberg (2010). "Minimizing Heat Generation in Solid-State Lasers." Quantum Electronics, IEEE Journal of **46**(7): 1076-1085.

Buchanan, R. A., K. A. Wickersheim, J. J. Pearson and G. F. Herrmann (1967). "Energy Levels of Yb^{3+} in Gallium and Aluminum Garnets. I. Spectra." Physical Review **159**(2): 245-251.

Charles P. Poole, J. (2004). Encyclopedic Dictionary of Condensed Matter Physics. San Diego, CA, Elsevier.

Chodos, A. (2006). "This Month in Physics History - January 1938: Discovery of Superfluidity." APS News. **15:** 2.

Cohen-Tannoudji, C. N. and W. D. Phillips (1990). "New Mechanisms for Laser Cooling." Physics Today(October): 33-40.

Condon, N. J., S. R. Bowman, S. P. O'Connor, R. S. Quimby and C. E. Mungan (2009). "Optical cooling in Er^{3+}:KPb_2Cl_5." Opt. Express **17**(7): 5466-5472.

Condon, N. J., S. R. Bowman, S. P. O'Connor and M. J. Myers (2010). "Heat loads in erbium-doped laser materials." Optical Materials **32**(9): 1050-1054.

Condon, N. J., S. O'Connor and S. R. Bowman (2006). "Growth and characterization of single-crystal Er^{3+}:KPb_2Cl_5 as a mid-infrared laser material." Journal of Crystal Growth **291**(2): 472-478.

DeLoach, L. D., S. A. Payne, L. L. Chase, L. K. Smith, W. L. Kway and W. F. Krupke (1993). "Evaluation of absorption and emission properties of Yb^{3+} doped crystals for laser applications." Quantum Electronics, IEEE Journal of **29**(4): 1179-1191.

Dexter, D. L. (1953). "A Theory of Sensitized Luminescence in Solids." The Journal of Chemical Physics **21**(5): 836-850.

Di Bartolo, B. (2010). Optical Interactions in Solids. Hackensack, NJ, World Scientific Publishing Co. Pte. Ltd.

Dieke, G. H. and H. M. Crosswhite (1963). "The Spectra of the Doubly and Triply Ionized Rare Earths." Applied Optics **2**(7): 675-686.

Djeu, N. and W. T. Whitney (1981). "Laser Cooling by Spontaneous Anti-Stokes Scattering." Physical Review Letters **46**(4): 236-239.

Dobrovinskaya, E. R., L. A. Lytvynov and V. Pishchik (2009). Sapphire: Material, Manufacturing, Applications, Springer.

Edwards, B. C., J. E. Anderson, R. I. Epstein, G. L. Mills and A. J. Mord (1999). "Demonstration of a solid-state optical cooler: An approach to cryogenic refrigeration." Journal of Applied Physics **86**(11): 6489-6493.

Edwards, B. C., M. I. Buchwald and R. I. Epstein (1998). "Development of the Los Alamos solid-state optical refrigerator." Review of Scientific Instruments **69**(5): 2050-2055.

Epstein, R. I., J. J. Brown, B. C. Edwards and A. Gibbs (2001). "Measurements of optical refrigeration in ytterbium-doped crystals." Journal of Applied Physics **90**(9): 4815-4819.

Epstein, R. I., M. I. Buchwald, B. C. Edwards, T. R. Gosnell and C. E. Mungan (1995). "Observation of laser-induced fluorescent cooling of a solid." Nature **377**(6549): 500-503.

Epstein, R. I. and M. Sheik-Bahae (2009). "Optical Refrigeration in Solids: Fundamentals and Overview." Optical Refrigeration. Weinheim, Wiley-VCH**:** 1-32.

Fajardo, J. C., G. H. Sigel Jr, B. C. Edwards, R. I. Epstein, T. R. Gosnell and C. E. Mungan (1997). "Electrochemical purification of heavy metal fluoride glasses for laser-induced fluorescent cooling applications." Journal of Non-Crystalline Solids **213–214**(0): 95-100.

Fernandez, J., A. J. Garcia-Adeva and R. Balda (2006). "Anti-Stokes Laser Cooling in Bulk Erbium-Doped Materials." Physical Review Letters **97**(3): 033001.

Fernández, J., A. J. García-Adeva and R. Balda (2012). "Anti-Stokes laser-induced cooling in rare-earth doped low phonon materials." Optical Materials **34**(3): 579-590.

Fernández, J., A. Mendioroz, A. J. García, R. Balda and J. L. Adam (2000). "Anti-Stokes laser-induced internal cooling of Yb^{3+}-doped glasses." Physical Review B **62**(5): 3213-3217.

Fernández, J., A. Mendioroz, A. J. García, R. Balda and J. L. Adam (2001). "Laser-induced internal cooling of Yb^{3+}-doped fluoride-based glasses." Journal of Alloys and Compounds **323–324**(0): 239-244.

Fernández, J., A. Mendioroz, A. J. García, R. Balda, J. L. Adam and M. A. Arriandiaga (2001). "On the origin of anti-Stokes laser-induced cooling of Yb^{3+}-doped glass." Optical Materials **16**(1–2): 173-179.

Fernandez, J. R., A. Mendioroz, R. Balda, M. Voda, M. Al-Saleh, A. J. Garcia-Adeva, J.-L. Adam and J. Lucas (2002). "Origin of laser-induced internal cooling of Yb^{3+} -doped systems." Proc. SPIE **4645**: 135.

France, P. W., S. F. Carter and J. M. Parker (1986). "Oxidation states of 3d transition metals in ZrF_4 glasses." Phys. Chem. Glasses **27**: 32.

Gabriel, A. and A. D. Pelton (1985). "Phase diagram measurements and thermodynamic analysis of the $PbCl_2$–NaCl, $PbCl_2$–KCl, and $PbCl_2$–KCl–NaCl systems." Canadian Journal of Chemistry **63**(11): 3276-3282.

Gainov, V. V., R. I. Shaidullin and O. A. Ryabushkin (2010). "Temperature measurements in the core of active optical fibers under lasing conditions." Instruments and Experimental Techniques **53**(6): 853-859.

Gan, F. (1995). "Optical properties of fluoride glasses: a review." Journal of Non-Crystalline Solids **184**(0): 9-20.

Garcia-Adeva, A. J. (2008). "Spectroscopy, upconversion dynamics, and applications of -doped low-phonon materials." Journal of Luminescence **128**(5–6): 697-702.

Garcia-Adeva, A. J., R. Balda and J. Fernandez (2009). "Laser cooling of Er^{3+}-doped low-phonon materials: Current status and outlook." Optical Materials **31**(7): 1075-1081.

Garcia-Adeva, A. J., R. Balda and J. Fernández (2007). "Recent advances in laser-induced cooling in rare-earth doped low phonon materials." Proc. SPIE **6469**: 64690F-1.

General Electric (1982). Fluid Flow Data Book, Section 410.2., Genium Publishing.

Ghasemkhani, M., A. R. Albrecht, S. D. Melgaard, D. V. Seletskiy, J. Cederberg and M. Sheik-Bahae (2014). "Intracavity Optical Refrigeration to 130K Using High-Power Vertical External-Cavity Surface-Emitting Lasers (VECSELs)." Laser Refrigeration of Solids VII, OPTO Photonics West. San Francisco, CA**:** Paper 9000-4.

Gill, J. C. (1975). "The establishment of thermal equilibrium in paramagnetic crystals." Reports on Progress in Physics **38**(1): 91.

Gilmore, G. and J. D. Hemingway (1998). Practical Gamma-Ray Spectrometry. New York, John Wiley & Sons Inc.

Goldner, P. and M. Mortier (2001). "Effect of rare earth impurities on fluorescent cooling in ZBLAN glass." Journal of Non-Crystalline Solids **284**(1–3): 249-254.

Gorrie, J. (1851). "Improved process for the artificial production of ice." U.S. Patent # 8080A.

Gosnell, T. R. (1999). "Laser cooling of a solid by 65 K starting from room temperature." Opt. Lett. **24**(15): 1041-1043.

Green, M. A. (2003). "The integration of liquid cryogen cooling and cryocoolers with superconducting electronic systems." Lawrence Berkeley National Laboratory, Report #LBNL-53068.

Guiheen, J. V., C. D. Haines, G. H. Sigel, R. I. Epstein, J. Thiede and W. M. Patterson (2006). "Yb^{3+} and Tm^{3+}-doped fluoroaluminate classes for anti-Stokes cooling." Physics and Chemistry of Glasses - European Journal of Glass Science and Technology Part B **47**(2): 167-176.

Hänsch, T. W. and A. L. Schawlow (1975). "Cooling of gases by laser radiation." Optics Communications **13**(1): 68-69.

Heeg, B., M. D. Stone, A. Khizhnyak, G. Rumbles, G. Mills and P. A. DeBarber (2004). "Experimental demonstration of intracavity solid-state laser cooling of Yb^{3+}:ZrF_4-BaF_2-LaF_3-AlF_3-NaF glass." Physical Review A **70**(2): 021401.

Hehlen, M. P. (2009). "Design and fabrication of rare-earth-doped laser cooling materials." Optical Refrigeration: Science and Applications of Laser Cooling of Solids. Epstein, R.I. and Sheik-Bahae, M. (eds), Wiley, p. 37-74.

Hehlen, M. P. (2010). "Crystal-field effects in fluoride crystals for optical refrigeration." Proc. SPIE **7614**: 761404.

Hehlen, M. P., M. G. Brik and K. W. Krämer (2013). "50^{th} anniversary of the Judd–Ofelt theory: An experimentalist's view of the formalism and its application." Journal of Luminescence **136**(0): 221-239.

Hehlen, M. P., R. I. Epstein and H. Inoue (2007). "Model of laser cooling in the Yb^{3+}-doped fluorozirconate glass ZBLAN." Physical Review B **75**(14): 144302.

Hoyt, C. W. (2003). Laser cooling in thulium-doped solids. Ph.D., The University of New Mexico.

Hoyt, C. W., M. P. Hasselbeck, M. Sheik-Bahae, R. I. Epstein, S. Greenfield, J. Thiede, J. Distel and J. Valencia (2003). "Advances in laser cooling of thulium-doped glass." Journal of the Optical Society of America B: Optical Physics **20**(5): 1066-1074.

Hoyt, C. W., M. Sheik-Bahae, R. I. Epstein, B. C. Edwards and J. E. Anderson (2000). "Observation of Anti-Stokes Fluorescence Cooling in Thulium-Doped Glass." Physical Review Letters **85**(17): 3600-3603.

Izotova, O. Y. and V. B. Aleksandrov (1970). "Crystal structure of $BaTm_2F_8$." Doklady Akademii Nauk SSSR **192**(5): 1037-1039.

Jenkins, N. W., S. R. Bowman, S. O'Connor, S. K. Searles and J. Ganem (2003). "Spectroscopic characterization of Er-doped KPb_2Cl_5 laser crystals." Optical Materials **22**(4): 311-320.

Jewell, J. M., C. Askins and I. D. Aggarwal (1991). "Interferometric method for concurrent measurement of thermo-optic and thermal expansion coefficients." Applied Optics **30**(25): 3656-3660.

Judkoff, R. and F. Sokol (1981). "Performance of a selective-surface Trombe wall in a small commercial building." Boulder, CO, Solar Energy Research Institute. Report #TP-721-1158.

Kamber, L., P. Egger, B. Trusch, R. Giovanoli and J. Hulliger (1998). "High temperature phase segregation of a new host for Er^{3+} upconversion: $Cs_3Tl_2Cl_9$." Journal of Materials Chemistry **8**(5): 1259-1262.

Kastler, A. (1950). "Quelques suggestions concernant la production optique et la detection optique d'une inegalite de population des niveaux de quantification spatiale des atomes. Application a l'experience de Stern et Gerlach et a la resonance magnetique." J. Phys. Radium **11**: 255-265.

Kessler, T., C. Hagemann, C. Grebing, T. Legero, U. Sterr, F. Riehle, M. J. Martin, L. Chen and J. Ye (2012). "A sub-40-mHz-linewidth laser based on a silicon single-crystal optical cavity." Nat Photon **6**(10): 687-692.

Kim, J. and M. Kaviany (2009). "Ab initio calculations of f-orbital electron-phonon interaction in laser cooling." Physical Review B **79**(5): 054103.

Knoll, G. F. (2000). Radiation Detection and Measurement. New York, John Wiley & Sons Inc.

Kohmoto, T., Y. Fukuda, M. Kunitomo and K. Isoda (2000). "Observation of ultrafast spin-lattice relaxation in Tm^{2+}-doped CaF_2 and SrF_2 crystals by optical means." Physical Review B **62**(1): 579-583.

Kushida, T. and J. E. Geusic (1968). "Optical Refrigeration in Nd-Doped Yttrium Aluminum Garnet." Physical Review Letters **21**(16): 1172-1175.

Landau, L. (1946). "On the Thermodynamics of Photoluminescence." J. Phys. (Moscow) **10**: 503-506.

Lei, G., J. E. Anderson, M. I. Buchwald, B. C. Edwards and R. I. Epstein (1998). "Determination of spectral linewidths by Voigt profiles in Yb^{3+}-doped fluorozirconate glasses." Physical Review B **57**(13): 7673-7678.

Lenard, P., F. Schmidt and R. Tomascheck (1928). Handbuch der Experimentalphysik, 1. Teil. Leipzig, Akademische Verlagsgesellschaft.

Li, D., J. Zhang and Q. Xiong (2013). "Laser cooling of CdS nanobelts: Thickness matters." Opt. Express **21**(16): 19302-19310.

Lima, S. M., J. A. Sampaio, T. Catunda, A. C. Bento, L. C. M. Miranda and M. L. Baesso (2000). "Mode-mismatched thermal lens spectrometry for thermo-optical properties measurement in optical glasses: a review." Journal of Non-Crystalline Solids **273**(1–3): 215-227.

Luo, X., M. D. Eisaman and T. R. Gosnell (1998). "Laser cooling of a solid by 21 K starting from room temperature." Opt. Lett. **23**(8): 639-641.

Lupei, A., V. Lupei, C. Presura, V. N. Enaki and A. Petraru (1999). "Electron-phonon coupling effects on Yb^{3+} spectra in several laser crystals." Journal of Physics: Condensed Matter **11**(18): 3769.

MacFarlane, D. R., J. Javorniczky and P. J. Newman (1999). "Electrochemical studies of rare earths in fluoride melts." Journal of Non-Crystalline Solids **256**: 36-41.

MacFarlane, D. R., Z. Zhou and P. J. Newman (2004). "Differential pulse voltammetry studies of heavy metal fluoride melts." Journal of Applied Electrochemistry **34**(2): 197-204.

Mahdavinejad, M. and K. Javanrudi (2012). "Assessment of Ancient Fridges: A Sustainable Method to Storage Ice in Hot-Arid Climates." Asian Culture and History **4**(2): 133-139.

Malta, O. L. (1995). "The theory of vibronic transitions in rare earth compounds." Journal of Physics and Chemistry of Solids **56**(8): 1053-1062.

Martin, R. M. and R. S. Quimby (2006). "Experimental evidence of the validity of the McCumber theory relating emission and absorption for rare-earth glasses." J. Opt. Soc. Am. B **23**(9): 1770-1775.

Martin, R. M. and R. S. Quimby (2007). "Deviations from the reciprocity theory of McCumber at low temperature in Nd^{3+}-doped glasses." Applied Physics Letters **90**(22): 221104-221103.

Mason, J. J. and T. A. Brendel (1982). "Maxorb - A New Selective Surface On Nickel." Proc. SPIE **324**: 139.

McCumber, D. E. (1964). "Einstein Relations Connecting Broadband Emission and Absorption Spectra." Physical Review **136**(4A): A954-A957.

Melgaard, S., D. Seletskiy, M. Sheik-Bahae, S. Bigotta, A. Di Lieto, M. Tonelli and R. Epstein (2010). "Spectroscopy of Yb-doped YLF crystals for laser cooling." Proc. SPIE **7614**: 761407-1.

Melgaard, S. D. (2013). Cryogenic Optical Refrigeration: Laser cooling of solids below 123K. Ph.D., University of New Mexico.

Melgaard, S. D., D. V. Seletskiy, A. Di Lieto, M. Tonelli and M. Sheik-Bahae (2013). "Optical refrigeration progress: cooling below NIST cryogenic temperature of 123K." Proc. SPIE **8638**: 863804-1.

Melgaard, S. D., D. V. Seletskiy, A. Di Lieto, M. Tonelli and M. Sheik-Bahae (2013). "Optical refrigeration to 119 K, below National Institute of Standards and Technology cryogenic temperature." Opt. Lett. **38**(9): 1588-1590.

Melgaard, S. D., D. V. Seletskiy, D. Sills, R. I. Epstein and M. Sheik-Bahae (2014). "Device applications for cryogenic optical refrigeration." Laser Refrigeration of Solids VII, OPTO Photonics West. San Francisco, CA, Paper 9000-1.

Mendioroz, A., J. Fernández, M. Voda, M. Al-Saleh, R. Balda and A. J. García-Adeva (2002). "Anti-Stokes laser cooling in Yb^{3+}-doped KPb_2Cl_5 crystal." Optics Letters **27**(17): 1525-1527.

Merkulov, A. A., L. I. Isaenko, V. M. Pashkov, V. G. Mazur, A. V. Virovets and D. Y. Naumov (2005). "Crystal structure of KPb_2Cl_5 and KPb_2Br_5." Journal of Structural Chemistry **46**(1): 103-108.

Messias, D. N., T. Catunda, J. D. Myers and M. J. Myers (2007). "Nonlinear electronic line shape determination in Yb^{3+}-doped phosphate glass." Optics Letters **32**(6): 665-667.

Mills, G. L., A. J. Mord and P. A. Slaymaker (2002). "Design and Predicted Performance of an Optical Cryocooler for a Focal Plane Application." Cryocoolers 11. R. G. Ross, Jr., Kluwer Academic / Plenum Publishers, p. 613-620.

Mungan, C. E. (2005). "Radiation thermodynamics with applications to lasing and fluorescent cooling." American Journal of Physics **73**(4): 315-322.

Mungan, C. E., M. I. Buchwald, B. C. Edwards, R. I. Epstein and T. R. Gosnell (1997). "Internal laser cooling of Yb^{3+}-doped glass measured between 100 and 300 K." Applied Physics Letters **71**(11): 1458-1460.

Mungan, C. E., M. I. Buchwald, B. C. Edwards, R. I. Epstein and T. R. Gosnell (1997). "Laser Cooling of a Solid by 16 K Starting from Room Temperature." Physical Review Letters **78**(6): 1030-1033.

Mungan, C. E. and T. R. Gosnell (1999). "Laser Cooling of Solids." Advances In Atomic, Molecular, and Optical Physics. B. Benjamin and W. Herbert, Academic Press. **40:** 161-228.

Murtagh, M. T., G. H. Sigel Jr, J. C. Fajardo, B. C. Edwards and R. I. Epstein (1999). "Compositional investigation of Yb^{3+}-doped heavy metal fluoride glasses for laser-induced fluorescent cooling applications." Journal of Non-Crystalline Solids **256–257**(0): 207-211.

Murtagh, M. T., G. H. Sigel Jr, J. C. Fajardo, B. C. Edwards and R. I. Epstein (1999). "Laser-induced fluorescent cooling of rare-earth-doped fluoride glasses." Journal of Non-Crystalline Solids **253**(1–3): 50-57.

Nast, T., C. Barnes and R. Wedel (1976). "Development and orbital operation of a two-stage solid cryogen cooler for infrared detector cooling." 11th Thermophysics Conference, American Institute of Aeronautics and Astronautics.

Nemova, G. and R. Kashyap (2010). "Laser cooling of solids." Reports on Progress in Physics **73**(8): 086501.

Nostrand, M. C., R. H. Page, S. A. Payne, L. I. Isaenko and A. P. Yelisseyev (2001). "Optical properties of Dy^{3+}- and Nd^{3+}-doped KPb_2Cl_5." Journal of the Optical Society of America B **18**(3): 264-276.

Orlovskii, Y. V., T. T. Basiev, I. N. Vorob'ev, E. O. Orlovskaya, N. P. Barnes and S. B. Mirov (2002). "Temperature dependencies of excited states lifetimes and relaxation rates of 3–5 phonon (4–6 μm) transitions in the YAG, LuAG and YLF crystals doped with trivalent holmium, thulium, and erbium." Optical Materials **18**(4): 355-365.

Parker, J., D. Mar, S. Von der Porten, J. Hankinson, K. Byram, C. Lee, M. K. Mayeda, R. Haskell, Q. Yang, S. Greenfield and R. Epstein (2009). "Thermal links for the implementation of an optical refrigerator." Journal of Applied Physics **105**(1): 013116-013111.

Parker, J. M. (1989). "Fluoride Glasses." Annual Review of Materials Science **19**(1): 21-41.

Passilly, N., E. Haouas, V. Ménard, R. Moncorgé and K. Aı¨t-Ameur (2006). "Population lensing effect in Cr:LiSAF probed by Z-scan technique." Optics Communications **260**(2): 703-707.

Patterson, W., S. Bigotta, M. Sheik-Bahae, D. Parisi, M. Tonelli and R. Epstein (2008). "Anti-Stokes luminescence cooling of Tm^{3+} doped BaY_2F_8." Opt. Express **16**(3): 1704-1710.

Patterson, W., M. P. Hasselbeck, M. Sheik-Bahae, S. Bigotta, D. Parisi, A. Toncelli, M. Tonelli, R. I. Epstein and J. Thiede (2004). "Observation of optical refrigeration in Tm^{3+}:BaY_2F_8." Conference on Lasers and Electro-Optics (CLEO).

Patterson, W. M., D. V. Seletskiy, M. Sheik-Bahae, R. I. Epstein and M. P. Hehlen (2010). "Measurement of solid-state optical refrigeration by two-band differential luminescence thermometry." J. Opt. Soc. Am. B **27**(3): 611-618.

Patterson, W. M., M. Sheik-Bahae, R. I. Epstein and M. P. Hehlen (2010). "Model of laser-induced temperature changes in solid-state optical refrigerators." Journal of Applied Physics **107**(6): 063108-063109.

Patterson, W. M., P. C. Stark, T. M. Yoshida, M. Sheik-Bahae and M. P. Hehlen (2011). "Preparation and Characterization of High-Purity Metal Fluorides for Photonic Applications." Journal of the American Ceramic Society **94**(9): 2896-2901.

Peijzel, P. S., A. Meijerink, R. T. Wegh, M. F. Reid and G. W. Burdick (2005). "A complete $4f^n$ energy level diagram for all trivalent lanthanide ions." J. Sol. St. Chem. **178**: 448-453.

Petrushkin, S. V. and V. V. Samartsev (2009). Laser Cooling of Solids. Cambridge, UK, Cambridge International Science Publishing Ltd.

Pringsheim, P. (1929). "Zwei Bemerkungen über den Unterschied von Lumineszenz- und Temperaturstrahlung." Z. Physik **57**: 739-746.

Quimby, R. S. (2002). "Range of validity of McCumber theory in relating absorption and emission cross sections." Journal of Applied Physics **92**(1): 180-187.

Rayner, A., M. E. J. Friese, A. G. Truscott, N. R. Heckenberg and H. Rubinsztein-dunlop (2001). "Laser cooling of a solid from ambient temperature." Journal of Modern Optics **48**(1): 103-114.

Rayner, A., N. R. Heckenberg and H. Rubinsztein-Dunlop (2003). "Condensed-phase optical refrigeration." Journal of the Optical Society of America B: Optical Physics **20**(5): 1037-1053.

Rayner, A., M. Hirsch, N. R. Heckenberg and H. Rubinsztein-Dunlop (2001). "Distributed Laser Refrigeration." Appl. Opt. **40**(30): 5423-5429.

Riseberg, L. A. and H. W. Moos (1968). "Multiphonon Orbit-Lattice Relaxation of Excited States of Rare-Earth Ions in Crystals." Physical Review **174**(2): 429-438.

Rogalski, A. (2005). "HgCdTe infrared detector material: history, status and outlook." Reports on Progress in Physics **68**(10): 2267.

Rogalski, A. (2011). Infrared Detectors. CRC Press, Boca Raton.

Ruan, X. L. and M. Kaviany (2006). "Advances in Laser Cooling of Solids." Journal of Heat Transfer **129**(1): 3-10.

Ruan, X. L., S. C. Rand and M. Kaviany (2007). "Entropy and efficiency in laser cooling of solids." Physical Review B **75**(21): 214304.

Salazar, A., A. Sánchez-Lavega and J. Fernández (1993). "Thermal diffusivity measurements on solids using collinear mirage detection." Journal of Applied Physics **74**(3): 1539-1547.

Scholle, K., S. Lamrini, P. Koopmann and P. Fuhrberg (2010). "2 µm Laser Sources and Their Possible Applications." Frontiers in Guided Wave Optics and Optoelectronics, Bishnu Pal (ed.).

Schreier, F. (1992). "The Voigt and complex error function: A comparison of computational methods." Journal of Quantitative Spectroscopy and Radiative Transfer **48**(5–6): 743-762.

Schultz, M. K., R. M. Keyser, R. C. Trammell and D. L. Upp (2007). "Improvement of spectral resolution in the presence of periodic noise and microphonics for hyper-pure germanium detector gamma-ray spectrometry using a new digital filter." Journal of Radioanalytical and Nuclear Chemistry **271**(1): 101-106.

Seletskiy, D., M. P. Hasselbeck, M. Sheik-Bahae, R. I. Epstein, S. Bigotta and M. Tonelli (2008). "Cooling of Yb:YLF using cavity enhanced resonant absorption." Proc. SPIE **6907**: 69070B.

Seletskiy, D. V., M. P. Hasselbeck and M. Sheik-Bahae (2010). "Resonant cavity-enhanced absorption for optical refrigeration." Applied Physics Letters **96**(18): 181106-181103.

Seletskiy, D. V., S. D. Melgaard, S. Bigotta, A. Di Lieto, M. Tonelli, R. I. Epstein and M. Sheik-Bahae (2009). "Demonstration of an optical cryocooler." Conference on Lasers and Electro-Optics and Conference on Quantum Electronics and Laser Science (CLEO/QELS).

Seletskiy, D. V., S. D. Melgaard, S. Bigotta, A. Di Lieto, M. Tonelli and M. Sheik-Bahae (2010). "Laser cooling of solids to cryogenic temperatures." Nat Photon **4**(3): 161-164.

Seletskiy, D. V., S. D. Melgaard, A. Di Lieto, M. Tonelli and M. Sheik-Bahae (2010). "Laser cooling of a semiconductor load to 165 K." Opt. Express **18**(17): 18061-18066.

Seletskiy, D. V., S. D. Melgaard, R. I. Epstein, A. Di Lieto, M. Tonelli and M. Sheik-Bahae (2011). "Local laser cooling of Yb:YLF to 110 K." Opt. Express **19**(19): 18229-18236.

Seletskiy, D. V., S. D. Melgaard, R. I. Epstein, A. Di Lieto, M. Tonelli and M. Sheik-Bahae (2013). "Precise determination of minimum achievable temperature for solid-state optical refrigeration." Journal of Luminescence **133**(0): 5-9.

Sheik-Bahae, M. and R. I. Epstein (2007). "Optical refrigeration." Nature Photonics **1**(12): 693-699.

Sheik-Bahae, M. and R. I. Epstein (2009). "Laser cooling of solids." Laser & Photonics Reviews **3**(1-2): 67-84.

Sheik-Bahae, M., C. W. Hoyt, M. Ebrahimzadeh, R. I. Epstein and B. C. Edwards (2000). "High power optical parametric oscillators for optical refrigeration in solids." Nonlinear Optics: Materials, Fundamentals, and Applications, 2000. Technical Digest.

Sheik-Bahae, M., C. W. Hoyt, B. Imangholi, R. I. Epstein, B. C. Edwards, A. Gibbs and J. E. Anderson (2001). "Advances in laser cooling of solids." Quantum Electronics and Laser Science Conference (QELS '01), Technical Digest.

Shirazi, R., O. Kopylov, A. Kovacs and B. E. Kardynał (2012). "Temperature dependent recombination dynamics in InP/ZnS colloidal nanocrystals." Applied Physics Letters **101**(9): -.

Siegman, A. E. (1986). Lasers. Mill Valley, CA, University Science Books.

Silva, J. R., L. H. C. Andrade, S. M. Lima, M. P. Hehlen, Y. Guyot, A. N. Medina, L. C. Malacarne, M. L. Baesso and N. G. C. Astrath (2013). "Laser-induced lensing effects in solid-state optical refrigerators." Applied Physics Letters **102**(14): 141910-141914.

Silva, J. R., L. C. Malacarne, M. L. Baesso, S. M. Lima, L. H. C. Andrade, C. Jacinto, M. P. Hehlen and N. G. C. Astrath (2013). "Modeling the population lens effect in thermal lens spectrometry." Opt. Lett. **38**(4): 422-424.

Sui, G. Z., X. P. Li, L. H. Cheng, J. S. Zhang, J. S. Sun, H. Y. Zhong, Y. Tian, S. B. Fu and B. J. Chen (2013). "Laser cooling with optical temperature sensing in Er^{3+}-doped tellurite-germanate glasses." Applied Physics B **110**(4): 471-476.

Takahashi, S. (1992). "Prospects for ultra-low loss using fluoride glass optical fiber: a review." Journal of Non-Crystalline Solids **140**(0): 172-178.

Thiede, J., J. Distel, S. R. Greenfield and R. I. Epstein (2005). "Cooling to 208 K by optical refrigeration." Applied Physics Letters **86**(15): 154107-154103.

Toncelli, A., M. Tonelli, A. Cassanho and H. P. Jenssen (1999). "Spectroscopy and dynamic measurements of a Tm,Dy:BaY_2F_8 crystal." Journal of Luminescence **82**(4): 291-298.

Tran, D., G. Sigel and B. Bendow (1984). "Heavy metal fluoride glasses and fibers: A review." Lightwave Technology, Journal of **2**(5): 566-586.

Upp, D. L., R. M. Keyser and T. R. Twomey (2005). "New cooling methods for HPGE detectors and associated electronics." Journal of Radioanalytical and Nuclear Chemistry **264**(1): 121-126.

van Delft, D. and P. Kes (2010). "The discovery of superconductivity." Physics Today(September): 38-43.

Veprik, A. M., V. I. Babitsky, N. Pundak and S. V. Riabzev (2009). "Suppression of cryocooler-induced microphonics in infrared imagers." Cryogenics **49**(8): 449-454.

Voda, M., M. Al-Saleh, G. Lobera, R. Balda and J. Fernández (2004). "Crystal growth of rare-earth-doped ternary potassium lead chloride single crystals by the Bridgman method." Optical Materials **26**(4): 359-363.

Walsh, B. M., N. P. Barnes and B. Di Bartolo (1998). "Branching ratios, cross sections, and radiative lifetimes of rare earth ions in solids: Application to Tm3+ and Ho3+ ions in $LiYF_4$." Journal of Applied Physics **83**(5): 2772-2787.

Yen, W. M., W. C. Scott and A. L. Schawlow (1964). "Phonon-Induced Relaxation in Excited Optical States of Trivalent Praseodymium in LaF_3." Physical Review **136**(1A): A271-A283.

Zagarola, M. V., J. J. Breedlove, C. S. Kirkconnell, J. T. Russo and T. Chiang (2009). "Demonstration of a Two-Stage Turbo-Brayton Cryocooler for Space Applications." Cryocoolers 15, Boulder, CO, International Cryocooler Conference.

Zhang, J., D. Li, R. Chen and Q. Xiong (2013). "Laser cooling of a semiconductor by 40 kelvin." Nature **493**(7433): 504-508.

Zhou, Z., P. J. Newman and D. R. MacFarlane (1993). "Electroanalytical methods for transition metal analysis in heavy metal fluoride melts." Journal of Non-Crystalline Solids **161**(0): 36-40.

Zhou, Z., P. J. Newman and D. R. MacFarlane (1993). "Electrochemistry at a rotating disc electrode in heavy metal fluoride melts." Journal of Non-Crystalline Solids **161**(0): 27-31.

Zhou, Z., P. J. Newman, D. K. Y. Wong and D. R. MacFarlane (1992). "Electrochemical purification of fluoride melts." Journal of Non-Crystalline Solids **140**(0): 297-300.